

**STRUCTURE AND FUNCTION OF THE MYCOBACTERIAL  
MECHANOSENSITIVE CHANNEL OF LARGE  
CONDUCTANCE, MSCL**

Thesis by

Nadia Herrera

In Partial Fulfillment of the Requirements for the  
Degree of

Doctor of Philosophy

**Caltech**

California Institute of Technology

Pasadena, California

2017

(Defended May 4, 2017)

© 2017

Nadia Herrera

All Rights Reserved

## Acknowledgements

First and foremost, I would like to thank my advisor, Professor Douglas Rees. I owe many thanks to Doug for taking a chance on an undergraduate student in the summer of 2010. Though these opportunities are routine endeavors for many investigators at Caltech, for me, it was a life changing event that put me here today. After that summer, Doug allowed me to develop a feasible curiosity for membrane proteins, especially since my summer project yielded crystals! This was something that I had thought was an incredibly challenging and almost borderline impossible goal. One of the best pieces of advice Doug gave me was the following: membrane proteins are just like soluble proteins, with some detergent added. That mentality set me to pursue challenging projects without limits. Doug always knew what advice I needed during our meetings, be it scientific discussions or simply motivational anecdotes. His support and guidance over the years has made me a better academic, scientist, and person. I look forward to joining him in the ranks as a professor one day, and mentoring students with the same style as Doug mentored me.

I would also like to deliver my gratitude to my three committee members - Dianne Newman, Pamela Björkman and Harry Gray. Their time and advice over the past six years was invaluable and led to the pursuit of very exciting ideas over the years. Our yearly discussions were always stimulating and drove my research to avenues I never thought possible. Most importantly, our discussions encouraged me to continue developing scientific curiosity outside of my chosen field of interest. In particular, our discussions about microbiology inspired me to

direct my research aims towards studies of mycobacteria, which allowed me to discover an entirely new field of study. These studies are now the foundation of my research aspirations both in my postdoctoral studies and, hopefully, in my own lab someday. Thank you all for your support all these years.

My fellow Rees Peeps: Chinenye Idigo, Jeffrey Lai, Allen Lee, Jens Kaiser, Troy Walton, Chris Gandhi, Chengcheng Fan, Phong Nguyen, Aron Kamajaya, Qiwen Li, Gabriele Meloni, Pavle Nikolovski, Justin Moser, Tiffany Jager, Phoebe Ray, Welison Floriano, *et al.* Thank you for providing a wonderful work environment that led us to great discussions about science - along with coffee runs, boba runs and plant growing competitions (Phong always won!)! The friendly environment that everyone sustained made the Rees Lab an extremely enjoyable place to be in for six years. Thank you for all of the friendships and talks about both life and protein structure. I look forward to seeing all of you succeed in your future endeavors.

I would also like to deliver a very special acknowledgement to my undergraduate research mentor at the University of Texas at El Paso, Professor Ricardo A. Bernal. I remember the first conversation I had with him, I was an unassuming undergraduate student full of curiosity about science in dire need of direction. Initially, I asked him to volunteer in his lab as a dishwasher, just to get to know the lab environment and to earn a letter of recommendation from him for medical school applications. Please do not get startled at this; my interests never lined up with the pursuit of a medical degree. Rather, this was the only path that was presented to me as an option for pursuing a scientific career by the

extremely busy counselors who were tasked with advising an incoming class of thousands of freshmen. Ricardo had a better plan, he told me he was going to challenge himself to show me how rewarding a career in scientific research could be in the time I had left as an undergraduate. Up until this very day, I couldn't agree with him more. Thank you, Ricardo, for guiding me when I needed the most direction and getting me started on this wonderful journey.

Throughout the long time in graduate school, an integral component of happiness has been my wonderful friends at Caltech. Through the years many have come and gone, but just a few have remained constant. I would like to thank, Alysia Ahmed, Sofi Quinodoz, and Chengcheng Fan for being there for me through the all of the joyous and the arduous times of graduate school. Thank you for your friendship and great memories. Our impromptu shopping runs, coffee walks, lunch breaks, and early morning gym classes kept me strong through all the challenges put in my path. You all are such inspirations; I look forward to continuing to see both of you excel in your futures.

To my wonderful fiancé, Raymond Liu, thank you for the wonderful journey we have had this far. I am really excited for our future together! I look forward to continuing our life together and striving for our goals as scientists who aim to run our own labs one day. The adventures we have had together have been countless and full of life-long cherished memories. Out of all of them, there is one that I will consider our boldest one: the one of adopting a feathered, loud, and adorable *Aratinga solstitialis (pseudodomesticus)*. Ravi! Ravi is very loud, and all he wants is love and affection. Thank you for allowing Ravi to make us his flock

and helping him finally perch with his forever family. For the curious reader, a small figure of this creature is right underneath this paragraph.



Figure i – *Aratinga solstitialis (pseudodomeesticus)* in favorite habitat, the play gym. Image captures the creature consuming their favorite treat, an almond in shell.

Finally, and most importantly, I want to thank my family: Leticia Herrera, Fernando Herrera, Luis Herrera, Tania Herrera, and Iker Herrera. You are all my rock and my foundation. You have been there throughout my life (Except Iker – you are five, kid. Fun fact: you were born on the day I started graduate school!) and you were the most supportive and understanding when I decided to break the status quo and pursue graduate school. I dedicate this hard work to all of you, and I will not let you down. I know the journey has just begun, and I will continue to work very hard to make you all proud. I love you all.

## Table of Contents

<b>Title</b> .....	<b>i</b>
<b>Copyright Page</b> .....	<b>ii</b>
<b>Acknowledgements</b> .....	<b>iii</b>
<b>List of Figures and Tables</b> .....	<b>ix</b>
<b>1. Abstract</b> .....	<b>1</b>
<b>2. Introduction</b> .....	<b>3</b>
<b>2.1 Mechanosensation- ubiquitous in nature</b> .....	<b>3</b>
<b>2.2 Discovery of MS channels in bacteria</b> .....	<b>3</b>
<b>2.3 MS channels in bacteria</b> .....	<b>5</b>
<b>2.4 MscL X-ray crystallography structure analysis</b> .....	<b>6</b>
<b>2.5 The inner membrane has a role in tension physiology</b> .....	<b>9</b>
<b>2.6 Mycobacterium smegmatis</b> .....	<b>11</b>
<b>2.7 Effect of mycobacterial developments on MtMscL study</b> .....	<b>14</b>
<b>2.8 Studying intermediate states of MtMscL</b> .....	<b>15</b>
<b>2.9 References</b> .....	<b>17</b>
<b>3. Structural and functional studies of C-terminal truncation in MtMscL</b> .....	<b>24</b>
<b>3.1 Introduction</b> .....	<b>24</b>
<b>3.2 Materials and methods</b> .....	<b>29</b>
3.2.1 Protein cloning, expression, and purification .....	29
3.2.2 Crystallization, heavy metal soaking and data collection .....	29
3.2.3 Electrophysiology patch clamp .....	30
3.2.4 Crystallography data processing .....	31
<b>3.3 Results</b> .....	<b>32</b>
3.3.1 Structure .....	32
3.3.2 Electrophysiology analysis .....	35
<b>3.4 Discussion</b> .....	<b>37</b>

3.5	References.....	56
<b>4.</b>	<b><i>Mycobacterium smegmatis</i> and MscL mediated antibiotic entry</b>	<b>60</b>
4.1	Introduction .....	60
4.2	Materials and methods .....	62
4.2.1	Recombineering plasmid construction .....	62
4.2.2	Allelic exchange .....	63
4.2.3	Protein expression .....	64
4.2.4	Protein expression of MscL using the acetamide promoter .....	65
4.2.5	Brightfield and fluorescent microscopy .....	65
4.2.6	Antibiotic resistance assay using <i>mscL</i> - bacteria .....	66
4.3	Results .....	67
4.3.1	Plasmid construction and allelic exchange .....	67
4.3.2	MscL expression in <i>Mycobacterium smegmatis</i> MC2155 <i>mscL</i> - ...	68
4.3.3	Antibiotic resistance assays using dihydrostreptomycin and spectinomycin .....	69
4.4	Discussion .....	71
4.5	References.....	82
<b>5.</b>	<b>Discussion and future directions .....</b>	<b>85</b>
5.1	<i>Mycobacterium smegmatis</i> .....	85
5.1.1	Developments on mycobacterial target study .....	85
5.1.2	Mycobacterial cell walls and proteins .....	86
5.1.3	Mechanosensitive channels in <i>Mycobacterium smegmatis</i> .....	86
5.2	<b>MscL Structural Studies .....</b>	<b>89</b>
5.2.1	MscL structures to date .....	89
5.2.2	Limitations of MtMscL $\Delta$ C Crystals .....	91
5.2.3	The open state of MscL .....	92
5.2.4	Means of studying the open state of MscL .....	96
5.3	References.....	99

## List of Figures and Tables

Figure 1- Alignment of MscL channel sequences. ....	43
Figure 2- Structures.....	44
Figure 3- Rotation function maps .....	45
Figure 4- MtMscL $\Delta C$ crystal packing and gold density .....	46
Figure 5- Alignment with monomers from other MscL channel structures.....	47
Figure 6- Cartoon diagram of MtMscL $\Delta C$ .....	49
Figure 7- Micelle density around MtMscL $\Delta C$ .....	51
Figure 8 - Traces of MscL homologues using patch clamp analysis	53
Table 1- MscS : MscL midpoint ratios .....	54
Figure 8- Comparison of crystal packing of MtMscL $\Delta C$ and KcsA ..	55
Figure 1- Plasmids pNH01 and pNH02 layout. ....	73
Figure 2- Schematic layout of allelic exchange .....	74
Figure 3- Validation of engineered strains.....	75
Figure 4- Bright field and fluorescent microscopy analysis of MC2155 <i>mscL</i> - .....	77
Figure 5- Growth curves with dihydrostreptomycin in <i>M. smegmatis</i> and <i>E. coli</i> . ....	79
Figure 6- Analysis of growth across dilution gradients of MC2155 and MC2155 <i>mscL</i> -.....	80
Table of primers used in this study:.....	81
Table of plasmids made for this study:.....	81
Figure 1- Alignment of MscS sequences identified in <i>M. smegmatis</i> .	98

# 1 Abstract

MscL is a ubiquitous channel found in bacterial membranes. It provides a protective response to osmotic downshock by opening and closing in response to tension in the membrane. A number of studies have aimed to develop a mechanism for the gating of MscL in *E. coli*, but structural details describing the process have remained elusive. A few structures of non-conducting states of MscL have been solved using X-ray crystallography, *Mycobacterium tuberculosis* (Mt) MscL and *Staphylococcus aureus* (Sa) MscL with a C-terminal domain truncation. In addition, the structure of the *E. coli* (Ec) MscL C-terminal cytoplasmic domain has been solved.

The goals of the studies presented in this thesis are as follows: (i) capturing a C-terminal domain truncation of MtMscL using X-ray crystallography, and (ii) analyzing the functional regulation of MscL channels in mycobacteria. To achieve the latter goal, we generated a knockout of the *mscL* gene in a fast-growing mycobacteria species, *Mycobacterium smegmatis*. This strain was used to analyze the role of MscL in the cell during antibiotic entry. Structural studies of MtMscL are focused on identifying the role of the C-terminal domain by studying a channel with a truncation at the C-terminal domain. The motivation for this goal comes from the structure of SaMscL, which showed that truncation of the C-terminal domain resulted in crystallizing the protein as a tetramer, an alternative oligomeric state to the pentameric state observed for the MtMscL structure. Studies on an MtMscL C-terminal domain truncation aimed to further establish that correlation. This protein was overexpressed in *E. coli* BL21 DE3 *mscL*<sup>-</sup>, purified, and crystallized by sitting drop vapor diffusion. Native crystals diffracted to 6.5

Å, and heavy atom derivative crystals diffracted to 5.8 Å. The structure of the MtMscL C-terminal truncation has been solved, and is presented in this thesis. Our studies on the structure show that the pentameric state of the channel remains intact upon truncation of the C-terminal domain. To analyze the function of our mutant, we utilized patch clamp electrophysiology studies using our expression strain as the giant spheroplast platform. The findings from the electrophysiology studies indicate that MtMscL C-terminal domain truncation results in a channel that has gating tension requirements similar to EcMscL, whereas full-length MtMscL has much higher gating tension requirements than our construct. In addition, the role of MscL in mycobacterial antibiotic susceptibility is being tested in *Mycobacterium smegmatis*. We have created a strain of *M. smegmatis* with the *mscL* gene knocked out, MC2155 *mscL*- and we have observed that upon deletion of *mscL* an increase in tolerance to spectinomycin is observed in our knockout strain.

## 2 Introduction

### 2.1 *Mechanosensation- ubiquitous in nature*

Mechanical stimuli drive living organisms ubiquitously by triggering mechanosensitive channels in cell membranes, resulting in varying responses to respond to their environmental surroundings. In plants, the ability to sense and transduce mechanical stimuli into signals results in gravitropism; in animals, it results in hearing and touch; and in bacteria and archaea it results in osmoregulation (1-4). *Arabidopsis thaliana* use the mechanosensitive channel of large conductance-like proteins to maintain the structure of their plastids and to sense gravity (3,4). Likewise, mammals use both transient receptor potential channels and piezo channels to sense pain and pressure, to feel temperature, to taste, and for vision (5-7). Bacteria and archaea utilize a network of mechanosensitive channels of varying conductance to alleviate turgor pressure when faced with tension in the lipid bilayer caused by osmotic stress (8-10). Of the three examples provided, bacterial channels have been the most thoroughly studied.

### 2.2 *Discovery of MS channels in bacteria*

Bacteria are generally categorized into two major groups, gram negative and gram positive; based on a staining procedure developed by Hans Christian Gram in 1884. Gram negative cells stain with safranin and have three layers, an outer

membrane, peptidoglycan layer, and an inner membrane; gram positive cells stain with crystal violet and have two layers, a peptidoglycan layer and an inner membrane. The outer layers of both types of bacteria are relatively permeable to small molecules and water, however, the inner membrane layer of both types of bacteria are not, as it is a continuous lipid bilayer that has different proteins embedded within that regulate what enters or leaves the cell (11). When bacteria face osmotic downshock, the resulting influx of water into the cell causes swelling that increases tension in the inner cell membrane. Tension buildup triggers the activation of mechanosensitive channels in the inner membrane to prevent cell lysis. A channel is able to achieve this by opening pores on the membrane by which solutes can be released to alleviate tension. Bacteria have several types of MS channels, and those with a conductance between 0.1nS and 3nS were detected using patch clamp electrophysiology and classified as such based on their conductance (8). As such, three major groups were identified, the MS channels of mini, small, and large conductance. The mechanosensitive channels of mini conductance (MscM) have a conductance of approximately 0.1nS, the mechanosensitive channels of small conductance (MscS) (originally named YggB, YgdB, and KefA, to name a few) have a conductivity ranging from 0.5-1nS, and the mechanosensitive channel of large conductance (MscL) has a conductivity greater or equal to 3nS (8,9,12,13). Of these channels, MscL opens the largest non-selective gate by which the cell can release enough contents to alleviate turgor pressure; consequently, MscL essentially serves as an emergency release valve when a cell undergoes osmotic downshock (9,14,15). The area of study for mechanosensitive channels was initiated when the Kung group made the discovery of the *mscL* gene in

1994. The analysis showed MscL as a 136 amino acid protein that formed a higher ordered oligomer in the membrane (15). This paved the path for detailed studies on bacterial mechanosensation and transduction in bacteria, which ultimately led to discovery of the other mechanosensitive channels in other bacteria and ultimately, other organisms entirely.

### 2.3 MS channels in bacteria

Despite the apparent simplicity of the MS channels in bacteria, findings from these systems can be applied to formulating understanding from bacterial MS channels to higher organism MS channels (1-4). To this date, the majority of the physiological studies on bacterial MS channels have been conducted in *E. coli*. Typically, to understand a protein's detailed mechanism, it is essential to analyze its structure, which is usually determined using X-ray crystallography. Structural studies of MscS from different bacterial homologues, including *E. coli*, have been completed with structures for both open and closed states of the channel (16). Despite considerable effort, however, detailed structures of the inner membrane domains of bacterial MscL have only been solved for the *M. tuberculosis*, *S. aureus* MscL (MtMscL and SaMscL, respectively) (17,18). Whereas physiological studies on SaMscL result in rescue phenotypes in a live/dead plating assay no studies of a related nature have been conducted in MtMscL (18). Though the sequences are related, with EcMscL, SaMscL, and MtMscL containing 136, 120, and 156 amino acid residues, respectively, and high percentage sequence identity (37-51%), the rescue phenotype has not yet been observed when assaying MtMscL in *E. coli* cells (19,20). A major component of this may

be that the tension required to gate MtMscL in *E. coli* is close to the lytic limits of the membrane (21). Mycobacteria have a unique membrane that consists of a waxy outer layer and a lipid membrane that varies in lipid composition from *E. coli*, as such, the gating tension required to gate MtMscL in *E. coli* membranes is beyond that which can be accumulated prior to rupture. Despite this caveat, X-ray crystallography structures of MscL from Mycobacteria has resulted in formulating many biochemical and biophysical studies to study the mechanism of MscL, by applying the structural findings to EcMscL and studying it in *E. coli*.

#### 2.4 MscL X-ray crystallography structure analysis

A total of three structures of MscL have been solved using X-ray crystallography, 2-D electron microscopy crystallography, and low angle rotary shadowing EM (17-19,22,23). The structures have resulted in an initial picture that paints a heterologous overview of channel characteristics across different oligomers of MscL. Characterized attributes include oligomeric state, rescue phenotypes in a downshock assay and assessment of conductance states. The X-ray crystallography work was done using MtMscL, SaMscL with a truncation in the C-terminus and the cytoplasmic C-terminal domain of EcMscL, and the C-terminal domain of EcMscL (17-19). The EM structural determination was done on EcMscL.

MtMscL was the first structure to arise for MscL; it was solved at a 3.5 Å resolution and revealed the architecture of the channel, consisting of a pentameric channel (17). Each monomer contains two transmembrane domains that cover a closed pore and a C-terminal domain that stretches into the cytoplasm (17). The finer details in

the channel revealed an N-terminal  $\alpha$ -helix located on the cytoplasmic side of the membrane. Next to this helix is the first transmembrane helix (TM1), which lines the permeation pathway of the channel. Following TM1 is a periplasmic loop that joins TM1 and a second transmembrane helix, TM2, that lines the exterior of the channel. Following TM2 is a short loop that leads to the C-terminal cytoplasmic helix bundle that forms a coiled-coil domain with the other C-terminal helices in the pentamer.

The TM1 and TM2 helices are not simply adjoined by the polypeptide chain; the crystal structure revealed a vast network of interactions between these subunits. For instance, TM1 of one subunit interacts with two other TM1 regions of adjacent subunits in the pentamer; these regions cross at an angle of  $-41^\circ$ . TM1 also interacts with TM2 from its own subunit with a crossing angle of about  $134^\circ$ , and TM2 from an adjacent subunit with a crossing angle of  $-175^\circ$ . Furthermore, the N-terminal helix of a given subunit is inserted in between the TM1 and TM2 from a given adjacent subunit in the cytoplasmic interface. In the pore region of the channel lies a narrow permeation pathway that is hydrophobic in nature, residues Ile 17 and Val 21 line this pore and it is around 2 Å in diameter. This opening, however, is not large enough to allow for the passage of water, as a minimum diameter of 9 Å has to be reached before water can pass the channel, and around 13 Å is the minimum diameter for ions (24). Overall, this classifies this structure as a non-conducting state.

In 2009, the Rees group reported an X-ray crystallography structure of a C-terminal truncation of SaMscL at a resolution of 3.8 Å (18). A striking difference in this structure was that it crystallized as a tetramer with a shorter height and a wider diameter. The N-terminal region in this construct does not conform to ordered secondary structure,

and appears as a loop in the protein model. The TM1 and TM2 inner membrane domains remain helical, similar to the MtMscL structure. Further details show that TM1 of SaMscL has an equal number of residues as the TM1 of MtMscL, however, the TM2 of SaMscL is longer, by four residues, and the loop connecting the TM regions is seven residues longer than MtMscL. In this structure, TM1 lines the permeation pathway, and interacts with other TM1s in the same manner that was observed in MtMscL; the main difference lies in the tilt angle, which is around  $-63^\circ$ . As in MtMscL, TM2 in SaMscL interacts with TM1 and adjacent TM2 subunits, however, the angles differ, one is around  $111^\circ$  and the other is  $-191^\circ$ , respectively. The pore region in this structure is larger in diameter, with a measured distance of 6 Å at the constriction point, lined by Val 21. Though larger, this pore diameter is still not large enough to allow for the passage of water, and this structure is not considered to be in a conducting state.

The most recent X-ray crystallography structure is that of the EcMscL C-terminal domain. This structure was solved to 1.45 Å resolution and crystallized as a pentameric helical coiled-coil bundle (19). The detailed structure exemplifies the knob into hole packing of hydrophobic residues that are formed in a coiled coil; this is often observed in other proteins with similar secondary structures. The pentameric state observed supports oligomeric state predictions made by molecular dynamics and those observed by low angle rotary shadowing EM analysis on the structure of the full length EcMscL (23,25). This structure, however, contradicts studies that observe the EcMscL as a hexameric complex, such as the 2D-EM study published by Saint, et. al in 1998. The technique used in this study, negative stain electron microscopy, typically does not provide enough molecular details with a small target such as MscL which is only 75

kilodaltons. With such a small target, ambiguities in data acquired are inevitable. Oligomeric state determination aside, EcMscL remains the best-characterized homologue of MscL.

## 2.5 *The inner membrane has a role in tension physiology*

Physiological studies on MscL have illuminated the regions of the protein responsible for defining its main function, its ability to rescue a cell from osmotic downshock (8,9,12). These studies have been thoroughly informed by the X-ray crystal structure observations in MtMscL, but none of them have actually assayed the function of MtMscL. Most studies have been done with homologues of MscL for which the full-length X-ray crystallography structure has not been determined, such as *S. aureus*, *E. coli*, *Lactococcus lactis*, and *Bacillus subtilis*. Interestingly, when MscL was first discovered, *M. tuberculosis* was not in the initial survey of candidate sequences (39). Part of the reasoning behind this survey missing *M. tuberculosis* MscL likely comes from the fact that the homologues identified are endogenous to well-studied bacterial species, such as *E. coli*. As such, the use of the MtMscL structure was only to inform structural implications from alignments of MtMscL and EcMscL amino acid sequences. By aligning the protein sequences to each other, strategic construction of MscL constructs could be made to answer targeted questions about the gating mechanism of the channel.

A main limitation in using the Mt homologue of MscL in the studies was not only that the host species is pathogenic, but also stemmed from the observation that when electrophysiological studies of MtMscL were done in *E. coli* giant spheroplasts, the

tension required to gain conductance from the channel surpassed the lytic limits of the *E. coli* inner membrane (40). Furthermore, our studies found that *E. coli* with a genetic knockout of *mscL* could not be rescued from an osmotic downshock by MtMscL overexpression in the cell. This raised an interesting and difficult problem that was left untouched until 2013, when the Blount group further addressed the observation.

At first glance, a major difference between *E. coli* and *M. tuberculosis* can be attributed to the waxy outer layer of *M. tuberculosis* giving it more rigidity, and thus, more resistance to cell lysis by osmotic shock. The studies conducted by the Blount group showed that contrary to intuition, that is not the difference that makes the difference for MtMscL function. In their studies, they determined that the difference stems from the lipid composition of the *M. tuberculosis* membrane. The *E. coli* inner cell wall is predominantly composed of 75-85% phosphatidylethanolamine (PE), 10-20% phosphatidylglycerol (PG), and 5-15% cardiolipin (CL) (41). *M. tuberculosis* has a similar composition in the inner membrane, including similar levels of PE and CL; the difference lies in the inclusion of a different lipid, phosphatidylinositol (36), which composes about 15% of the inner membrane (42,43). Addition of PI to MtMscL in proteoliposomes resulted in characterization of MtMscL with similar gating properties and gating tensions as EcMscL, characterized by gating ratios of MscL: MscS, and unitary conductance (44). The implications of this study shed light on the importance of studying a system in its endogenous host. The ability to do this in MtMscL, however, is rendered quite difficult as *M. tuberculosis* is a human pathogen that is only studied under stringent levels of biosafety-leveled laboratories. To circumvent this limitation, a

bacterial species, *Mycobacterium smegmatis* has been developed to efficiently address questions from *M. tuberculosis* that could not be studied efficiently in *E. coli* before.

## 2.6 *Mycobacterium smegmatis*

The *Mycobacteria* are a genus of Actinobacteria that is in the Mycobacteriaceae family. Many of the strains in this family of bacteria, such as *Mycobacterium tuberculosis* and *Mycobacterium lepreae*, are responsible for devastating human pathogenesis. These bacteria are rather difficult to culture, and were initially cultured on armadillo and mouse footpads as those are organisms susceptible to mycobacterial infections (45). Recent developments in the field have fostered the discovery of an artificial medium that can yield growth of *Mycobacterium tuberculosis*, however, it takes incredibly long times to culture - in the range of 10-20 days for seed cultures, and 15 days for propagating cultures, making the study of individual components largely difficult and time consuming, yet possible.

Development in the *Mycobacteria* field was enhanced further, when the genome of the H37Rv *M. tuberculosis* was published in 1998. The genome revealed a vast number of targets for study that had gone previously unnoticed (46). Various targets of interest were identified from the genome, and studies were followed through with experiments that attempted to utilize existing systems for recombinant protein overexpression in *E. coli*. This attempt, unfortunately, resulted in limited studies, as most of the overexpressed products had low yields or produced inclusion bodies, rendering functional and structural studies impossible for a vast majority of the genes identified (47,48). There are a number of explanations as to why the protein did not

express in *E. coli*, the most prominent being that the mycobacterial genome is far more GC rich than the *E. coli* genome, presenting an initial challenge in expressing many targets (46). To circumvent these limitations, the field moved towards surveying a vast array of organisms for their ability to express *M. tuberculosis* proteins. Those organisms included insect cells using the baculovirus infection and expression system and *Streptomyces* recombinant protein expression systems. Unfortunately, neither of these yielded results that were efficient or sufficient. Meanwhile, developments on a non-pathogenic mycobacterial strain were being undertaken, and in no time, *M. smegmatis* was rendered useful to express a wide range of *M. tuberculosis* proteins which had not been previously possible (49).

Since the strain was discovered, *Mycobacterium smegmatis* has become a widely-used strain in mycobacterial protein studies. It has the advantage that it is a fast growing mycobacterial strain that originates in soil, and it is not pathogenic. Initial limitations of *M. smegmatis* were that the isolated strain could not be transformed with plasmid DNA. Studies that set out to identify a strain of *M. smegmatis* allowing DNA electroporation followed, and it was only a matter of time before a strain that allowed for plasmid transformation by electroporation was isolated; that strain is *M. smegmatis* MC2155 (50). Upon isolation, a number of systems were developed for the bacteria that allowed for DNA manipulation and protein expression in this system. Since then *Mycobacterium smegmatis* has allowed the field to shed light on a number of *M. tuberculosis* questions, in particular by allowing for overexpression of proteins that play essential roles in mediating antibiotic resistance in *M. tuberculosis* (51,52). Many methods for protein overexpression have been developed for this purpose in MC2155,

examples of the systems include acetamidase promoters, tetracycline-induction, T7 promoters, L-lactamase promoters, and arabinose promoters (49). These systems extend their utility to the production of selenomethionine labeled protein, which allows for the circumvention of the phasing problem in crystallography studies by replacing the sulfur in the methionines of a protein with selenium (53,54). In addition to creating a suitable strain for *M. tuberculosis* protein overexpression, *M. smegmatis* has also become a system for developing genetic engineering in mycobacteria (55).

Gene manipulation in *M. tuberculosis* was challenging since long cultivation times and low fidelity of the outcomes with use of allelic exchange did not allow for efficient construction of the strains necessary for undertaking many studies (56,57). In fact, experiments that undertook the challenge only yielded a rate of 20% effectiveness, making the process quite complicated and low throughput (57). To improve this outcome, a handful of approaches were attempted. Those approaches used specialized transduction shuttle plasmids, non-replicating vectors, and long linear DNA fragments to target genes; but they did not yield high efficiency and they required multiple steps that made the process increasingly difficult to complete (51,58,59). An alternate method of manipulating genes is based solely on looking at the means of bacterial gene manipulation by the bacterial pathogens, bacteriophages.

In *E. coli*, the  $\lambda$ red bacteriophage system has been thoroughly studied and developed to produce high fidelity genetic gene manipulations.  $\lambda$ red proteins are able to incorporate bacteriophage genetic material into a bacterial genome, and they do so by using their ability to recognize specific strands of DNA with high fidelity, which remains uncompromised despite artifacts in the DNA such as gaps (60,61). In order to use the

$\lambda red$  system in *E. coli*, proteins must be expressed in the host cell. Ironically enough, these proteins cannot be expressed in *M. smegmatis*, or any of the mycobacteria for that matter, and this is likely attributable to the large difference in GC content between the genomes. After some time, it was discovered that *M. smegmatis* bacteriophage Che9C encodes for a group of gene products which showed faint sequence similarity to the genes used for recombination  $\lambda red$ . Despite the similarity being low, in the 30-40% range, a test of the gene products revealed mycobacterial recombinase proteins that could be expressed in mycobacteria (55). After careful biochemical characterization of the gene products, van Kessel *et al.* were able to identify a system for gene manipulation for both slow and fast growing mycobacteria that had high efficiency and were rather simple to implement.

## 2.7 Effect of mycobacterial developments on MtMscL study

Developments in mycobacteria protein expression allowed for development of studies to analyze MtMscL. A gene product containing 75% similarity to MtMscL has been identified in the *M. smegmatis* MC2155 genome, as well as four MscS homologues. Production of the MscL protein in the cell has been verified with proteomic mass spectrometry studies of the mycobacterial membrane. Expression of MscL is indicative that, with adequate gene manipulation, this organism could be used to study MtMscL with physiological assays. Ultimately, it is of interest to see the role of MtMscL in a cell wall that is close to its native cell wall, and this bacterial strain provides an initial step in that direction.

The role of MtMscL and mycobacterial MscL proteins are being analyzed in *M. smegmatis*. The mechanosensitive channels in *M. smegmatis* have been knocked out of a well-studied strain, MC2155, and the resulting strain, MC2155 *mscL*-, is currently being analyzed to study the effects of the mutation on the cell. Initial antibiotic resistance assays indicate that there is a potential trend, where the deletion of the *mscL* gene results in slightly increased resistance to a common antibiotic used against mycobacteria, dihydrostreptomycin. A physiological downshock assay is being developed to study the effects of *mscL* gene deletions in mycobacteria, and current work is underway to establish a working assay. To further establish the findings, a series of complementation studies where *mscL* is replaced in the genome of MC2155 *mscL*- are needed. In this case, *mscL* would be inserted in an alternative appropriate site in the genome.

## 2.8 Studying intermediate states of MtMscL

In many channels, the cytoplasmic domain is essential for function as it mediates interactions with the cellular milieu (66). In MscL, the C-terminal domain has not been found to have a significant role in gating, supporting observations which find that the gating trigger for the channel is within the TM domains that sense stressors in the membrane upon tension application (9,67). The C-terminal domain of EcMscL has been either truncated, or destabilized by replacing conserved leucines with small polar residues, and both approaches agree in their conclusion that channel function remains intact (66). An observation in the latter studies indicated that EcMscL without the C-

terminal domain, was able to adopt multiple conducting states in patch clamp experiments, something that had not been otherwise observed (66). These results pointed to a key observation, which indicates that MscL undergoes intermediate states during gating before reaching the fully open state.

The ability to display multiple gating suggests that the channel likely undergoes multiple conformations before reaching the fully open state. This hypothesis is supported by a previous structure of SaMscL, in which the C-terminal domain truncation resulted in an intermediate state of MscL. This structure also showed that truncation of the C-terminal domain resulted in a tetrameric MscL structure. Collectively, the structure suggests that the role of the C-terminal domain may be involved in oligomerization and intermediate state formation in SaMscL. To establish the observations as a trend of MscL, it is necessary to solve the structure in another homologue of MscL. Given that the structure of full-length MtMscL has been solved, targeting a truncation of the C-terminal domain for structural studies is of interest. By undertaking this task, we are completing the first study to observe multiple mutations and resulting states in a single homologue of MscL. This thesis will outline the work that has been done on determining the structure and the function of a C-terminal truncation of MtMscL.

## 2.9 References

1. Kung, C. (2005) A possible unifying principle for mechanosensation. *Nature* **436**, 647-654
2. Kloda, A., and Martinac, B. (2001) Mechanosensitive channels in archaea. *Cell Biochem Biophys* **34**, 349-381
3. Haswell, E. S., and Meyerowitz, E. M. (2006) MscS-like proteins control plastid size and shape in *Arabidopsis thaliana*. *Curr Biol* **16**, 1-11
4. Haswell, E. S., Peyronnet, R., Barbier-Brygoo, H., Meyerowitz, E. M., and Frachisse, J. M. (2008) Two MscS homologs provide mechanosensitive channel activities in the *Arabidopsis* root. *Curr Biol* **18**, 730-734
5. Ramsey, I. S., Delling, M., and Clapham, D. E. (2006) An introduction to TRP channels. *Annual Review of Physiology* **68**, 619-647
6. Coste, B., Mathur, J., Schmidt, M., Earley, T. J., Ranade, S., Petrus, M. J., Dubin, A. E., and Patapoutian, A. (2010) Piezo1 and Piezo2 are essential components of distinct mechanically activated cation channels. *Science* **330**, 55-60
7. Coste, B., Xiao, B., Santos, J. S., Syeda, R., Grandl, J., Spencer, K. S., Kim, S. E., Schmidt, M., Mathur, J., Dubin, A. E., Montal, M., and Patapoutian, A. (2012) Piezo proteins are pore-forming subunits of mechanically activated channels. *Nature* **483**, 176-181
8. Martinac, B., Buechner, M., Delcour, A. H., Adler, J., and Kung, C. (1987) Pressure-sensitive ion channel in *Escherichia coli*. *Proc Natl Acad Sci U S A* **84**, 2297-2301
9. Sukharev, S. I., Martinac, B., Arshavsky, V. Y., and Kung, C. (1993) Two types of mechanosensitive channels in the *Escherichia coli* cell envelope: solubilization and functional reconstitution. *Biophys J* **65**, 177-183
10. Sukharev, S. I., Blount, P., Martinac, B., and Kung, C. (1997) Mechanosensitive channels of *Escherichia coli*: the MscL gene, protein, and activities. *Annu Rev Physiol* **59**, 633-657

11. Silhavy, T. J., Kahne, D., and Walker, S. (2010) The bacterial cell envelope. *Cold Spring Harb Perspect Biol* **2**, a000414
12. Levina, N., Totemeyer, S., Stokes, N. R., Louis, P., Jones, M. A., and Booth, I. R. (1999) Protection of *Escherichia coli* cells against extreme turgor by activation of MscS and MscL mechanosensitive channels: identification of genes required for MscS activity. *EMBO J* **18**, 1730-1737
13. Booth, I. R., and Blount, P. (2012) The MscS and MscL families of mechanosensitive channels act as microbial emergency release valves. *J Bacteriol* **194**, 4802-4809
14. Blount, P., Sukharev, S. I., Moe, P. C., Nagle, S. K., and Kung, C. (1996) Towards an understanding of the structural and functional properties of MscL, a mechanosensitive channel in bacteria. *Biol Cell* **87**, 1-8
15. Sukharev, S. I., Blount, P., Martinac, B., Blattner, F. R., and Kung, C. (1994) A large-conductance mechanosensitive channel in *E. coli* encoded by *mscL* alone. *Nature* **368**, 265-268
16. Lai, J. Y., Poon, Y. S., Kaiser, J. T., and Rees, D. C. (2013) Open and shut: crystal structures of the dodecylmaltoside solubilized mechanosensitive channel of small conductance from *Escherichia coli* and *Helicobacter pylori* at 4.4 Å and 4.1 Å resolutions. *Protein Sci* **22**, 502-509
17. Chang, G., Spencer, R. H., Lee, A. T., Barclay, M. T., and Rees, D. C. (1998) Structure of the MscL homolog from *Mycobacterium tuberculosis*: a gated mechanosensitive ion channel. *Science* **282**, 2220-2226
18. Liu, Z., Gandhi, C. S., and Rees, D. C. (2009) Structure of a tetrameric MscL in an expanded intermediate state. *Nature* **461**, 120-124
19. Walton, T. A., and Rees, D. C. (2013) Structure and stability of the C-terminal helical bundle of the *E. coli* mechanosensitive channel of large conductance. *Protein Sci* **22**, 1592-1601
20. Malashkevich, V. N., Kammerer, R. A., Efimov, V. P., Schulthess, T., and Engel, J. (1996) The crystal structure of a five-stranded coiled coil in COMP: a prototype ion channel? *Science* **274**, 761-765

21. Kung, C., Martinac, B., and Sukharev, S. (2010) Mechanosensitive channels in microbes. *Annu Rev Microbiol* **64**, 313-329
22. Saint, N., Lacapere, J. J., Gu, L. Q., Ghazi, A., Martinac, B., and Rigaud, J. L. (1998) A hexameric transmembrane pore revealed by two-dimensional crystallization of the large mechanosensitive ion channel (MscL) of *Escherichia coli*. *J Biol Chem* **273**, 14667-14670
23. Yoshimura, K., Usukura, J., and Sokabe, M. (2008) Gating-associated conformational changes in the mechanosensitive channel MscL. *Proc Natl Acad Sci U S A* **105**, 4033-4038
24. Beckstein, O., Tai, K., and Sansom, M. S. (2004) Not ions alone: barriers to ion permeation in nanopores and channels. *J Am Chem Soc* **126**, 14694-14695
25. Sukharev, S., Betanzos, M., Chiang, C. S., and Guy, H. R. (2001) The gating mechanism of the large mechanosensitive channel MscL. *Nature* **409**, 720-724
26. Ajouz, B., Berrier, C., Garrigues, A., Besnard, M., and Ghazi, A. (1998) Release of thioredoxin via the mechanosensitive channel MscL during osmotic downshock of *Escherichia coli* cells. *J Biol Chem* **273**, 26670-26674
27. Kouwen, T. R., Antelmann, H., van der Ploeg, R., Denham, E. L., Hecker, M., and van Dijl, J. M. (2009) MscL of *Bacillus subtilis* prevents selective release of cytoplasmic proteins in a hypotonic environment. *Proteomics* **9**, 1033-1043
28. Basle, A., Iyer, R., and Delcour, A. H. (2004) Subconductance states in OmpF gating. *Biochim Biophys Acta* **1664**, 100-107
29. Cowan, S. W., Schirmer, T., Rummel, G., Steiert, M., Ghosh, R., Pauptit, R. A., Jansonius, J. N., and Rosenbusch, J. P. (1992) Crystal structures explain functional properties of two *E. coli* porins. *Nature* **358**, 727-733
30. Hille, B. (1968) Pharmacological modifications of the sodium channels of frog nerve. *J Gen Physiol* **51**, 199-219
31. Cruickshank, C. C., Minchin, R. F., Le Dain, A. C., and Martinac, B. (1997) Estimation of the pore size of the large-conductance mechanosensitive ion channel of *Escherichia coli*. *Biophys J* **73**, 1925-1931

32. Sukharev, S. I., Sigurdson, W. J., Kung, C., and Sachs, F. (1999) Energetic and spatial parameters for gating of the bacterial large conductance mechanosensitive channel, MscL. *J Gen Physiol* **113**, 525-540
33. van den Bogaart, G., Krasnikov, V., and Poolman, B. (2007) Dual-color fluorescence-burst analysis to probe protein efflux through the mechanosensitive channel MscL. *Biophys J* **92**, 1233-1240
34. Mika, J. T., Birkner, J. P., Poolman, B., and Kocer, A. (2013) On the role of individual subunits in MscL gating: "all for one, one for all?". *Faseb J* **27**, 882-892
35. Sukharev, S., Durell, S. R., and Guy, H. R. (2001) Structural models of the MscL gating mechanism. *Biophys J* **81**, 917-936
36. Perozo, E., Cortes, D. M., Sompornpisut, P., Kloda, A., and Martinac, B. (2002) Open channel structure of MscL and the gating mechanism of mechanosensitive channels. *Nature* **418**, 942-948
37. Wang, Y., Liu, Y., Deberg, H. A., Nomura, T., Hoffman, M. T., Rohde, P. R., Schulten, K., Martinac, B., and Selvin, P. R. (2014) Single molecule FRET reveals pore size and opening mechanism of a mechano-sensitive ion channel. *Elife* **3**, e01834
38. Ornatska, M., Jones, S. E., Naik, R. R., Stone, M. O., and Tsukruk, V. V. (2003) Biomolecular stress-sensitive gauges: surface-mediated immobilization of mechanosensitive membrane protein. *J Am Chem Soc* **125**, 12722-12723
39. Moe, P. C., Blount, P., and Kung, C. (1998) Functional and structural conservation in the mechanosensitive channel MscL implicates elements crucial for mechanosensation. *Mol Microbiol* **28**, 583-592
40. Moe, P. C., Levin, G., and Blount, P. (2000) Correlating a protein structure with function of a bacterial mechanosensitive channel. *J Biol Chem* **275**, 31121-31127
41. Raetz, C. R. (1978) Enzymology, genetics, and regulation of membrane phospholipid synthesis in *Escherichia coli*. *Microbiol Rev* **42**, 614-659
42. Jackson, M., Crick, D. C., and Brennan, P. J. (2000) Phosphatidylinositol is an essential phospholipid of mycobacteria. *J Biol Chem* **275**, 30092-30099
43. Haites, R. E., Morita, Y. S., McConville, M. J., and Billman-Jacobe, H. (2005) Function of phosphatidylinositol in mycobacteria. *J Biol Chem* **280**, 10981-10987

44. Zhong, D., and Blount, P. (2014) Electrostatics at the membrane define MscL channel mechanosensitivity and kinetics. *Faseb J* **28**, 5234-5241
45. Snapper, S. B., Lugosi, L., Jekkel, A., Melton, R. E., Kieser, T., Bloom, B. R., and Jacobs, W. R., Jr. (1988) Lysogeny and transformation in mycobacteria: stable expression of foreign genes. *Proc Natl Acad Sci U S A* **85**, 6987-6991
46. Cole, S. T., Brosch, R., Parkhill, J., Garnier, T., Churcher, C., Harris, D., Gordon, S. V., Eiglmeier, K., Gas, S., Barry, C. E., 3rd, Tekaia, F., Badcock, K., Basham, D., Brown, D., Chillingworth, T., Connor, R., Davies, R., Devlin, K., Feltwell, T., Gentles, S., Hamlin, N., Holroyd, S., Hornsby, T., Jagels, K., Krogh, A., McLean, J., Moule, S., Murphy, L., Oliver, K., Osborne, J., Quail, M. A., Rajandream, M. A., Rogers, J., Rutter, S., Seeger, K., Skelton, J., Squares, R., Squares, S., Sulston, J. E., Taylor, K., Whitehead, S., and Barrell, B. G. (1998) Deciphering the biology of *Mycobacterium tuberculosis* from the complete genome sequence. *Nature* **393**, 537-544
47. Baneyx, F. (1999) Recombinant protein expression in *Escherichia coli*. *Curr Opin Biotechnol* **10**, 411-421
48. Goldstone, R. M., Moreland, N. J., Bashiri, G., Baker, E. N., and Shaun Lott, J. (2008) A new Gateway vector and expression protocol for fast and efficient recombinant protein expression in *Mycobacterium smegmatis*. *Protein Expr Purif* **57**, 81-87
49. Bashiri, G., and Baker, E. N. (2015) Production of recombinant proteins in *Mycobacterium smegmatis* for structural and functional studies. *Protein Sci* **24**, 1-10
50. Snapper, S. B., Melton, R. E., Mustafa, S., Kieser, T., and Jacobs, W. R., Jr. (1990) Isolation and characterization of efficient plasmid transformation mutants of *Mycobacterium smegmatis*. *Mol Microbiol* **4**, 1911-1919
51. Husson, R. N., James, B. E., and Young, R. A. (1990) Gene replacement and expression of foreign DNA in mycobacteria. *J Bacteriol* **172**, 519-524
52. Martin, C., Timm, J., Rauzier, J., Gomez-Lus, R., Davies, J., and Gicquel, B. (1990) Transposition of an antibiotic resistance element in mycobacteria. *Nature* **345**, 739-743

53. Bashiri, G., Squire, C. J., Baker, E. N., and Moreland, N. J. (2007) Expression, purification and crystallization of native and selenomethionine labeled *Mycobacterium tuberculosis* FGD1 (Rv0407) using a *Mycobacterium smegmatis* expression system. *Protein Expr Purif* **54**, 38-44
54. Gokulan, K., O'Leary, S. E., Russell, W. K., Russell, D. H., Lalgondar, M., Begley, T. P., Ioerger, T. R., and Sacchettini, J. C. (2013) Crystal structure of *Mycobacterium tuberculosis* polyketide synthase 11 (PKS11) reveals intermediates in the synthesis of methyl-branched alkylpyrones. *J Biol Chem* **288**, 16484-16494
55. van Kessel, J. C., and Hatfull, G. F. (2007) Recombineering in *Mycobacterium tuberculosis*. *Nat Methods* **4**, 147-152
56. Kalpana, G. V., Bloom, B. R., and Jacobs, W. R., Jr. (1991) Insertional mutagenesis and illegitimate recombination in mycobacteria. *Proc Natl Acad Sci U S A* **88**, 5433-5437
57. Aldovini, A., Husson, R. N., and Young, R. A. (1993) The *uraA* locus and homologous recombination in *Mycobacterium bovis* BCG. *J Bacteriol* **175**, 7282-7289
58. Balasubramanian, V., Pavelka, M. S., Jr., Bardarov, S. S., Martin, J., Weisbrod, T. R., McAdam, R. A., Bloom, B. R., and Jacobs, W. R., Jr. (1996) Allelic exchange in *Mycobacterium tuberculosis* with long linear recombination substrates. *J Bacteriol* **178**, 273-279
59. Bardarov, S., Bardarov Jr, S., Jr., Pavelka Jr, M. S., Jr., Sambandamurthy, V., Larsen, M., Tufariello, J., Chan, J., Hatfull, G., and Jacobs Jr, W. R., Jr. (2002) Specialized transduction: an efficient method for generating marked and unmarked targeted gene disruptions in *Mycobacterium tuberculosis*, *M. bovis* BCG and *M. smegmatis*. *Microbiology* **148**, 3007-3017
60. Gottesman, M. M., Gottesman, M. E., Gottesman, S., and Gellert, M. (1974) Characterization of bacteriophage lambda reverse as an *Escherichia coli* phage carrying a unique set of host-derived recombination functions. *J Mol Biol* **88**, 471-487

61. Court, D. L., Sawitzke, J. A., and Thomason, L. C. (2002) Genetic engineering using homologous recombination. *Annu Rev Genet* **36**, 361-388
62. Ou, X., Blount, P., Hoffman, R. J., and Kung, C. (1998) One face of a transmembrane helix is crucial in mechanosensitive channel gating. *Proc Natl Acad Sci U S A* **95**, 11471-11475
63. Anishkin, A., Chiang, C. S., and Sukharev, S. (2005) Gain-of-function mutations reveal expanded intermediate states and a sequential action of two gates in MscL. *J Gen Physiol* **125**, 155-170
64. Li, Y., Wray, R., Eaton, C., and Blount, P. (2009) An open-pore structure of the mechanosensitive channel MscL derived by determining transmembrane domain interactions upon gating. *Faseb J* **23**, 2197-2204
65. Iscla, I., Eaton, C., Parker, J., Wray, R., Kovács, Z., and Blount, P. (2013) Improving the Design of a MscL-Based Triggered Nanovalve. *Biosensors* **3**, 171-184
66. Anishkin, A., Gendel, V., Sharifi, N. A., Chiang, C. S., Shirinian, L., Guy, H. R., and Sukharev, S. (2003) On the conformation of the COOH-terminal domain of the large mechanosensitive channel MscL. *J Gen Physiol* **121**, 227-244
67. Powl, A. M., East, J. M., and Lee, A. G. (2007) Different effects of lipid chain length on the two sides of a membrane and the lipid annulus of MscL. *Biophys J* **93**, 113-122

## 3 Structural and functional studies of C-terminal truncation in MtMscL

### 3.1 Introduction

Mechanical stimuli drive living organisms by triggering mechanosensitive channels in cell membranes, resulting in varying responses to respond to their environmental surroundings. Though they have been reported in other organisms, mechanosensitive channels have been most comprehensively studied in bacteria, where their main role is in osmoregulation (1-4). To regulate osmolarity, a network of mechanosensitive (MS) channels of varying conductance work together to alleviate turgor pressure when faced with increased tension in the lipid bilayer caused by osmotic stress (5-7). Bacterial MS channels are characterized by their conductance, ranging between 0.1 nS and 3 nS, as determined using patch clamp electrophysiology – these conductances are several orders of magnitude greater than ion-selective channels (5). Three major groups of MS channels have been identified, the MS channels of mini, small, and large conductance (5,6,8,9). The MS channel of mini conductance, MscM, has a conductance of ~ 0.1 nS; channels of small conductance, MscS, (including homologues such as YggB, YgdB, and KefA) have a conductivity ranging from 0.5-1 nS; and the channel of large conductance, MscL, has a conductivity greater or equal to 3 nS. Of these channels, MscL opens the largest non-selective gate by which the cell can release enough contents to alleviate turgor pressure. Consequently, MscL serves as an emergency release valve when a cell undergoes large osmotic downshock (6,10,11). A

considerable effort has been made to establish a molecular mechanism by which MscL gates, including patch clamp electrophysiology, molecular dynamics, and X-ray crystallography structural studies.

Structures of MscL homologues from *Mycobacterium tuberculosis*, *Staphylococcus aureus*, and *Methanosarcina acetivorans* have been solved using X-ray crystallography (MtMscL, SaMscL, and MaMscL respectively) (12-14). These homologues of MscL retain the following sequence identity, MtMscL to SaMscL 40.5%, MtMscL to EcMscL 35.2%, and MtMscL to MaMscL 29.2%, the alignment for these sequences is in Figure 1. MtMscL was solved at 3.5 Å resolution and revealed the architectural features of the channel; specifically, a symmetric pentameric oligomer arrangement where each monomer contains two transmembrane helices that surround a transmembrane pore and a C-terminal helix that faces cytoplasm (the structure is shown in Figure 2 A) (12). The finer details in the channel present an N-terminal helix located on the cytoplasmic side of the membrane; next to this helix is a transmembrane (TM) helix, TM1, that lines the permeation pathway of the channel. Following TM1 is a periplasmic loop that joins TM1 and a second TM helix, TM2, that lines the exterior of the channel; and finally, a short loop leads to the C-terminal cytoplasmic helix that forms a coiled-coil domain with the other C-termini helices in the pentamer. In the pore region of the channel lies a narrow permeation pathway that is a hydrophobic gate, framed by residues Ile 17 and Val 21. This opening is calculated to be ~ 3 Å in diameter, which is not large enough to allow for the passage of water. As a minimum of 9 Å in diameter has to be reached before water can pass the channel, and around 13 Å is the minimum

diameter for ions (14,15). Altogether, this classifies this structure as a non-conducting state.

Seeking to understand the role of the C-terminal domain in retaining the structure and function of the channel, a structure of a C-terminal truncation of SaMscL (SaMscL  $\Delta$ C) at a resolution of 3.8 Å was reported in 2009; the structure is shown in Figure 2 B (14). A striking difference in this structure is that it crystallized as a tetramer with a shorter height and wider diameter along the transmembrane domain. The N-terminal region in this construct does not conform to ordered secondary structure, but the TM1 and TM2 inner membrane domains remain similar to the MtMscL structure. The pore region in this structure is larger in diameter, with a measured diameter of ~6 Å at the hydrophobic gate, lined by Val 21 (14). Though larger, this pore diameter is still not large enough to allow for the passage of water, and this structure is to be in an expanded, non-conducting state. The most recent X-ray crystallography structures are those from MaMscL, which naturally lack a C-terminal domain (13). This structure was solved with the aid of a fused pentameric soluble protein scaffold, riboflavin synthase from *Methanocaldococcus jannaschii*. This addition made this channel slightly more difficult to gate, and therefore limited the reach of the expanded state. Two non-conducting states of the protein were solved to 3.5 Å and 4.1 Å, respectively (13). This homologue crystallized as a pentamer, and exhibited similar architectural arrangements between TM1 and TM2 in the two structures as MtMscL in the closed state and SaMscL in the expanded intermediate state.

The role of the C-terminal domain of MscL in *E. coli* MscL (EcMscL) gating has been thoroughly studied, and the consensus is that the channel does not lose function as

a result of C-terminal domain deletion. Instead, deletion of the C-terminal domain in EcMscL (EcMscL  $\Delta$ C) requires a greater amount of tension to gate in electrophysiology experiments,  $\sim$ -140 mm Hg, as opposed to  $\sim$ -70 mm Hg in full length EcMscL (7,16). In addition, electrophysiology studies have shown that EcMscL  $\Delta$ C fails to reach a fully expanded state, and stays locked in a conducting state for longer periods of time. Longer gating times result in increased loss of intracellular metabolites, such as ATP, to the downshock medium; making recover of the cell increasingly difficult (16). The role of the C-terminal domain in SaMscL is highlighted by electrophysiology studies in which SaMscL and SaMscL  $\Delta$ C were compared (14). These studies show that SaMscL  $\Delta$ C has clear and stable gating events, whereas full length SaMscL displays flickering events that are not fully defined or stable. In this case, deletion of the MscL C-terminal domain results in increased stability and length of gating events. Studies of EcMscL and SaMscL indicate that truncation of the C-terminal domain in MscL results in a trend, where increased tension is required to gate the channel and the channel remains in a gated position for longer periods of time. Though it is an apparent trend, the length of the C-terminal domain of MtMscL is 37 residues longer than that of SaMscL and 17 residues longer than that of EcMscL. It is possible that the difference in length establishes a different, or additional, roles for the C-terminal domain in MtMscL. It is particularly difficult to gate MtMscL in *E. coli* giant spheroplasts, due to a need for high tensions that are close to the lytic limits of the membrane. Gating MtMscL in *E. coli* spheroplasts requires tensions as high as -430 mm Hg, making the experiments difficult to replicate for sufficient data acquisition and analysis (17).

When aligning the MscL sequences from different homologues, the C-terminus remains highly conserved. Furthermore, the C-terminal domain of EcMscL crystallized as a helical pentameric assembly, much like the COMP oligomerization domain (18,19). This structure shows that the C-terminal of MscL is capable of forming a pentameric arrangement on its own, and therefore could have a role in mediating the oligomeric state of MscL (18). Studies using non-denaturing mass spectrometry show that removal of the C-terminal domain in SaMscL and MtMscL results in mixed oligomeric states, as a function of different detergents and different C-terminal domain truncations (20). In addition, oligomeric characterization by the addition of mass (OCAM), suggests that oligomeric state is influenced by detergents used to solubilize the protein (21).

In this study, we seek to establish the role of the C-terminal domain in oligomeric state and function of MtMscL. After screening various truncations, a variant of MtMscL truncated at residue 101, had the highest expression and crystallization ability and resulted the construct referred to as MtMscL  $\Delta$ C. Several constructs of MtMscL, including MtMscL  $\Delta$ C, have been reported to be pentameric across many different biochemical methods, indicating that it would be the best candidate to show the effects of C-terminal domain truncation (22). To this end, we solved the structure of an MtMscL  $\Delta$ C construct using X-ray crystallography. In addition, we assayed the function both MtMscL and MtMscL  $\Delta$ C using patch clamp electrophysiology in *E. coli* BL21 DE3 *mscL*-. This study presents the analysis of MtMscL gating in patch clamp experiments in *E. coli*, and aids in understanding the role of the C-terminal domain of MscL in channel gating tension thresholds.

## 3.2 Materials and methods

### 3.2.1 Protein cloning, expression, and purification

Using site directed mutagenesis, two mutations were introduced to MtMscL, one adding a tryptophan at the hexa-his tag linker, and the other adding a stop codon at residue 101. As MtMscL naturally lacks tryptophan, this residue was added to facilitate quantitation of this protein by the UV absorption at 280 nm. The product was inserted into a pET 19b vector carrying ampicillin resistance. This construct was transformed into *E. coli* BL21 DE3 *mscL*-, and protein was overexpressed using a final concentration of 1  $\mu$ M Isopropyl  $\beta$ -D-1-thiogalactopyranoside (IPTG) in Terrific-Broth medium. Cells were lysed using osmotic downshock, and cell walls were solubilized with 1% n-dodecyl- $\beta$ -D-maltopyranoside (DDM) overnight at 4 °C, as per Chang, *et al.* (12). Cellular debris was removed by ultracentrifugation using rotor JLA 16.250 at 31,500xg and protein was purified using Qiagen Superflow NiNTA beads, followed by source 30s anion exchange, and finalized with size exclusion through a Superdex s200 16/60. The purified protein was concentrated to 25mg/mL in 150 mM NaCl, 50 mM Tris HCl pH 7.5, 0.05% DDM.

### 3.2.2 Crystallization, heavy metal soaking and data collection

Crystallization trays were set up using both sitting drop and hanging drop vapor diffusion at 4 °C. MtMscL  $\Delta$ C crystallized in 0.1 M Tris HCl pH 8, 0.15 M CaCl<sub>2</sub>, 25% PEG 400, with a final concentration of 10% of 1 M glycine as an additive directly added to the crystallization drop. After 1.5 weeks, crystals typically grew to 0.4 x 0.3 x 0.1 mm<sup>3</sup> and were cryo-protected using PEG 400. Sodium aurothiosulfate was used as a heavy

atom derivative in the original MtMscL structure determination, and as such, a batch of crystals was soaked with 5 mM sodium aurothiosulfate for one week after crystals had reached full size. Following the soak, crystals were briefly crosslinked, using glutaraldehyde, for 5 minutes. Crystals were then harvested and cryoprotected with a mixture of 12.5% diethylene glycol, 25% ethylene glycol, 12.5 2-methyl-2,4-pentanediol, 12.5% glycerol, 12.5 1,2-propanediol, 12.5% nondetergent sulfobetaine, 3-(1-pyridino)-1-propane sulfonate from the Molecular Dimensions CryoProtX kit. All data was collected at SSRL BL 12-2, at wavelength 0.8974 Å (13.82 keV), distance 900 mm, on a Pilatus 6M detector.

### 3.2.3 Electrophysiology patch clamp (performed by Dr. Grigory Maksaev and Prof. Elizabeth Haswell, Washington University)

Giant spheroplasts were prepared using established protocols, with several modifications (23). Briefly, BL21 DE3 *E. coli*  $\Delta mscL$  containing the construct of interest was treated with cephalixin for 1.5 hours and induced with 1 mM IPTG (high IPTG) or 0.05 mM IPTG (low IPTG) for 30 minutes. Spheroplasts were then prepared at room temperature for 18-20 min. The spheroplast suspension was centrifuged through 7 mL of 1 M sucrose and re-suspended in 300  $\mu$ L 1 M sucrose. The aliquots were stored at -80 °C.

Patch-clamp experiments were carried out using a pipette buffer (200 mM KCl, 90 mM MgCl<sub>2</sub>, 5 mM CaCl<sub>2</sub>, 5 mM HEPES, pH 7.4) and a bath buffer (same as pipette with the addition of 450 mM sucrose). Excised inside-out patches from spheroplast membranes were treated with 5-second symmetric triangle pressure ramps of

amplitudes from -50 mm Hg to -250 mm Hg at -20 mV membrane potential, using pipettes with bubble number 4.5, as previously described (24). A high-speed pressure clamp system HSPC-1 (ALA Scientific) was utilized in the experiments. Data were acquired with Axopatch 200B amplifier and Digidata 1440 digitizer (Molecular Devices) at 20 kHz and filtered at 5 kHz. Data were further analyzed with pCLAMP 10.6 software suite (Molecular Devices).

The tension sensitivity of MscL channels was assessed as the ratio of the gating thresholds of MscL and endogenously expressed *EcMscS*, as described previously (10,25). Briefly, the  $P_{\text{MscL}} : P_{\text{MscS}}$  ratio was calculated as the ratio of the pressures at which the first MscL channel and the second MscS channels were gated. After that, the pressure applied to the patch was increased to reach MscL current saturation, when possible. Amplitudes of saturated (or peak at patch rupture) currents of MscL and MscS were used as an estimate for the relative expression ratio of the channels. Unitary conductances of MscL channels were corrected for the pipette access resistance.

#### 3.2.4 Crystallography data processing

Datasets were processed using XDS-GUI, scaled using AIMLESS in the CCP4i suite, molecular replacement was done using Phaser MR in CCP4i, and phase verification was done using MR-SAD in Phenix with the gold-derivative dataset. Structure refinement utilized REFMAC5 and Phenix.refine (26-29).

### 3.3 Results

#### 3.3.1 Structure

Although the MtMscL  $\Delta$ C construct crystallized readily, the crystals typically diffracted poorly, to  $\sim 9\text{\AA}$  resolution. After screening  $\sim 2000$  crystals, a crystal was found that diffracted to  $6.5\text{\AA}$  resolution. The diffraction data collected from this crystal was used for molecular replacement, using the pentameric MtMscL full-length structure with the C-terminal domain computationally truncated as the search model. Using this search model in Phaser MR, a TFZ score of 17.1 was obtained, which indicated that the structure obtained was likely correct. The asymmetric unit consists of two channels and a solvent content of  $\sim 75\%$ . The major crystal contacts involve the association of two pentamers through the periplasmic loops such that five-fold axes are aligned, similar contacts are found in the full-length MtMscL structure. This arrangement exhibits 522 symmetry, consistent with the self-rotation function calculated from the native data (shown in figure 3). Contacts involving the cytoplasmic region of MtMscL  $\Delta$ C are more poorly defined and presumably contribute to the low-resolution diffraction pattern. To verify the molecular replacement data, crystals were soaked with various heavy metal derivatives; after screening  $\sim 1000$  additional crystals, the most promising of these were the ones soaked in sodium aurothiosulfate, which diffracted to  $\sim 7\text{\AA}$ . The resolution was further improved by crosslinking the crystals for 5 minutes with glutaraldehyde; using this method the resolution could be improved from  $\sim 7\text{\AA}$  to  $5.5\text{\AA}$ . A dataset was collected on the best crystal at the Au edge and processed to  $5.8\text{\AA}$ . The data were used to search for the heavy atom positions using MR-SAD phasing in the AutoSol program in Phenix. The MR-SAD results identified 5 gold sites along the periplasmic

region of MtMscL at the same locations as observed for the full-length protein (shown in Figure 4 A). SAD phases were refined to a figure of merit of 0.57, and an overall CC score of 50.9. The sodium aurothiosulfate soaked crystal dataset revealed similar crystal packing to that observed for native datasets (shown in Figure 4 B), and this data was used for final model refinement. Diffraction patterns for these crystals have very intense reflections at low resolution, which rapidly weaken as the resolution increases. The lower resolution, 50 – 15 Å, contains information about the solvent around the protein, whereas higher resolution, 15 – 6 Å, contains information about the protein structure (30). Refinement was carried out from 12 – 5.8 Å, so as to minimize effects of solvent in density analysis for the protein. The refinement was largely based on moving secondary structure elements into the observed density; the fits of TM1 and TM2 to the density are shown in Figures 4 B and 4 C, respectively. Refinement completed using Phenix.refine, followed by jelly body refinement in Refmac5, and finalized with Phenix.refine. Our final  $R_{\text{work}} / R_{\text{free}}$  values are 0.28/0.29, respectively.

Our structure of MtMscL  $\Delta C$  confirms that despite the removal of the C-terminal helical bundle in MtMscL  $\Delta C$ , the channel adopts a pentameric channel that conserves secondary structure when compared to its MtMscL full length counterpart. The overall dimensions of MtMscL  $\Delta C$  are 43 Å in height and 46 Å in diameter (shown in Figure 5). When both MtMscL  $\Delta C$  and MtMscL structures are aligned, the root mean square deviation of  $\alpha$  helices, RMSD, is 1.2 Å; indicating little deviation in overall structure and arrangement. Upon further analysis, we looked at the transmembrane helices crossing angles. This allows us to understand the conformational similarities between the channels. The crossing angle between TM1 and TM2 of a monomer of MtMscL  $\Delta C$  is

130.2°, whereas for MtMscL it is 135.6 (shown in Figure 6 A). A 5° difference is too small to establish a major conformational change, instead it highlights the similarity between the crossing angles in these two channels. The crossing angle between TM1 and TM1 of an adjacent subunit, TM1', allows for the assessment of the helix arrangement around the pore of the channel. The TM1-TM1' crossing angle for MtMscL  $\Delta C$  is 39°, for MtMscL it is 42°, for SaMscL  $\Delta C$  it is 64°, for MaMscL closed it is 41°, and for MaMscL expanded it is 62°. These measurements show a trend, where the expanded state TM1-TM1' angle is ~60° and the TM1-TM1' angle of the closed states is ~40°. Lastly, the angle between TM1 and TM2 of an adjacent monomer, TM2', is generally conserved, with an RMSD of ~1 Å and a crossing angle of ~165-168° across all MscL structures (Figure 6 F). Collectively, the TM1-TM2, TM1-TM1', and TM1-TM2' crossing angle measurements show that there is no substantial structural rearrangement upon removal of the C-terminal domain in MtMscL.

Crystals of MtMscL  $\Delta C$  formed in a way such that most of the crystal contacts were made between the periplasmic loops of the channel, and the rest of the crystal contacts were ~20 Å or greater. The Matthew's coefficient of our data revealed that the crystals contained a high solvent content of 75%. To determine if we could attribute the solvent content to detergent in the crystal we calculated a map from 12-30 Å resolution; the density shows an array of density surrounding the channel in the crystal lattice along the transmembrane domain regions of the channel. This is particularly clear when we compare this map to a second map calculated from 5.5-12 Å resolution; this map highlights the protein electron density in the crystal. The maps are shown in Figure 7, where the low-resolution map is in gray and the high-resolution map is in green. Figures

7 A and 7 C show a solvent-based, continuous, large, and dense entity that has even coverage along the TM2 domains of MtMscL  $\Delta C$  and lines the outer part of the channel. Coverage along the TM2 domains of MtMscL  $\Delta C$ , along with the high amount of detergent in the protein used for crystallization, point to the possibility that the density may actually be the maltoside head group in the DDM molecules. We considered the measurement of a single molecule of DDM  $\sim 22$  Å and the distance between TM2 and the center of the continuous dense entity is 20-22 Å. The distance between TM2 from neighboring proteins in the crystal is  $\sim 44$ -42 Å throughout the length of the channel. Altogether, these observations point to the possibility that crystal contacts in those regions are likely mediated by detergent maltoside groups in certain regions of the crystal, as opposed to being composed of only protein mediated crystal contacts. These detergent mediated arrangements are clearly rendered in a map at a resolution from 12-30 Å, which consists of signal from the solvent region. This data suggests that the DDM lattice is an integral part of the crystal and is likely a major contributing factor to the diffraction limit of our crystals.

### 3.3.2 Electrophysiology analysis

To assay the function of our construct, our collaborators Dr. Grigory Maksaev and Prof. Elizabeth Haswell of Washington University used patch clamp electrophysiology. The challenge with previous electrophysiological studies of MtMscL expressed in *E. coli* was that the tension necessary to see gating of MtMscL was close

to the lytic tension of *E. coli* (17). A possible way to circumvent that limitation is increasing the level of channel expression in the cell, so that patches with a low probability of any single channel opening have a higher number of channels in the patch, resulting in an increased probability that at least one of the channels may open when tension is applied. Using this strategy, we are able to gather information on the electrophysiological properties of MtMscL and MtMscL  $\Delta C$  by varying the expression levels of our constructs in *E. coli* BL21 DE3 *mscL*<sup>-</sup>, by using different amounts of IPTG. When we analyze the low expressing profiles, those with less IPTG, it becomes increasingly difficult to record gating in our patches, in accordance with expectations.

Representative traces of patches, using high protein expression, are shown in Figure 8 for MtMscL full length, MtMscL  $\Delta C$ , and EcMscL full length. To assess our results, we compared the gating ratio of MscL to an endogenous reference, MscS. In our calculations, a larger ratio corresponds to higher tension requirements for MscL gating. In general, our experiments show that when channels are overexpressed, it is possible to observe consistent gating events of EcMscL, MtMscL, and MtMscL  $\Delta C$  (shown in Table 1). On the other hand, when both MtMscL and MtMscL  $\Delta C$  are expressed at very minimal levels, it is not possible to observe any gating activity for MtMscL, and one patch (N= 1) yielded gating activity for MtMscL  $\Delta C$ . When analyzing the averaged data, including all data from high and low expression patches (Table 1), we note that MtMscL  $\Delta C$  gates at a minimally greater tension than EcMscL, and both MtMscL  $\Delta C$  and EcMscL gate at lower tensions than MtMscL. The average gating ratios are 2.0 +/- 0.4, 2.8 +/- 0.62, and 1.8 +/- 0.1 for MtMscL  $\Delta C$ , MtMscL, and EcMscL respectively (Table 1). The averaged data, however, includes data from low protein

expression patches, which were not reliably consistent for MtMscL and MtMscL  $\Delta$ C. If we analyze only the high protein expression profiles, our margins of error, along with our variability in measurements are diminished. In these data, we note that the average gating ratios are  $1.9 \pm 0.2$ ,  $3.0 \pm .4$ , and  $1.6 \pm 0.1$  for MtMscL  $\Delta$ C, MtMscL, and EcMscL, respectively (Table 1). These studies indicate that MtMscL  $\Delta$ C gates at tensions more akin to EcMscL, while MtMscL gates at significantly higher tensions than all subjects tested. To further analyze the data from our experiments, we calculated the unitary conductance of our individual patches. The average unitary conductance (in nanoSiemens (nS)) across all patches is as follows: MtMscL  $2.7 \pm 0.2$  (N = 9), EcMscL  $3.5 \pm 0.1$  (N = 9), and MtMscL  $\Delta$ C  $3.25 \pm 0.2$  (N = 10). The average conductance measurements suggest that MtMscL  $\Delta$ C and EcMscL are closer in unitary conductance, and MtMscL is smaller than either of these constructs.

### 3.4 Discussion

In our studies, we have solved the structure of MtMscL  $\Delta$ C and shown that upon removal of the C-terminal domain, the oligomeric state and conformation are retained, in relation to MtMscL. When comparing the dimensions of the MscL homologues the height of the TM domain of MtMscL  $\Delta$ C is 43 Å tall, MtMscL is 48 Å, and SaMscL  $\Delta$ C is 30 Å; the width of the channel is 46 Å for MtMscL  $\Delta$ C, 47 Å for MtMscL, and 62 Å for SaMscL  $\Delta$ C (Figures 2 and 4). The differences in measurements are larger when comparing MtMscL  $\Delta$ C and SaMscL  $\Delta$ C; on the other hand, MtMscL has a difference of

only 4 Å in each dimension when compared to MtMscL  $\Delta$ C. Collectively, MtMscL is more similar to MtMscL full length than to SaMscL  $\Delta$ C.

To further investigate the structure of MtMscL  $\Delta$ C, we analyzed the helix crossing angle measurements across all the available structures for MscL. The helix crossing angles revealed that the angle between TM1 and TM2 of MtMscL  $\Delta$ C is 130.2°, for MtMscL full length it is 135.6°, for SaMscL  $\Delta$ C is 104.2°, for MaMscL closed it is 136.6°, and MaMscL expanded is 123.6° (Figure 6). A clear trend is observed between closed states of the pentameric channel structures retaining a TM1-TM2 crossing angle near  $\sim$  135°, whereas expanded states of MscL retain a smaller tilt angle between helices. In addition, alignment of TM1 for a single monomer of each MscL shows that there is a pivoting movement along TM2 that moves in a counter-clockwise fashion. MtMscL  $\Delta$ C more closely resembles the closed state structures, MtMscL and MaMscL closed than to the expanded intermediate structures, MaMscL expanded and SaMscL. MscL channels have an extensive hydrophobic residue network that remains intact upon movement, this network is found between TM1 and TM2' of an adjacent subunit, TM2'. When analyzing the angles between TM1 and TM2' for all of the MscL structures we see that they all lie in the range of 165-169°, indicating that all of these structures retain this interaction. Furthermore, measurements of the crossing angles between TM1 helices of adjacent subunits (TM1 and TM1') allow us to study the extent of the tilt in the helices that line the permeation pathway. Our measurements show that the angle between TM1 and TM1' for both MtMscL  $\Delta$ C, MtMscL and MaMscL closed is 30° - 41°, and the angle for SaMscL and MaMscL expanded is 56° - 62°. Collectively, these analyses indicate that we have two states of MscL depicted in the structures, a closed

state, shown by MtMscL  $\Delta$ C, MtMscL, and MaMscL closed; and an expanded non-conducting state, shown by SaMscL and MaMscL expanded.

To further understand how much MtMscL  $\Delta$ C related to any given state of MscL, a single monomer from each MtMscL  $\Delta$ C and other MscL structures were aligned. The RMSD was analyzed for each pairing. When MtMscL  $\Delta$ C is aligned with MtMscL full length the RMSD is 0.8Å, and when it is aligned with MaMscL closed the RMSD is 1.2Å. These measurements indicate that there is not much deviation in secondary structure arrangement between these channels. When MtMscL  $\Delta$ C is compared to MscL channels in an intermediate state, the RMSD is 5.9 Å when aligned to SaMscL  $\Delta$ C and 6.5 Å when aligned to MaMscL in an intermediate state. Based on our analysis, there is a large variation between both  $\Delta$ C homologues of MscL. In addition, the structures tend to belong to one of two states, closed (MtMscL, MaMscL closed, and MtMscL  $\Delta$ C) and an expanded intermediate (SaMscL  $\Delta$ C, and MaMscL expanded) (Figure 6). Our results are consistent with extensive biochemical data that reveals that MtMscL  $\Delta$ C is a pentamer, including by the methods of oligomeric characterization by the addition of mass (OCAM) method, and by native mass spectrometry (20,21). Furthermore, OCAM studies of EcMscL and SaMscL chimeras, where each domain in the protein was interchanged so as to establish unique combinations between the five domains of the protein revealed that the chimeras which formed tetramers did not involve the C-terminal domain, but rather the N-terminal domain of SaMscL, the loop of EcMscL, and TM2 of SaMscL (31).

We have shown that function of MtMscL can be analyzed using patch clamp electrophysiology when using *E. coli* BL21 DE3 *mscL*-. By using this system, it was

possible to control the amount of protein produced by the cell by utilizing IPTG as a titration agent, where addition of less IPTG resulted in lower protein expression, and vice versa. This system is different from those previously used, as it allows us to titrate the amount of protein expressed in the cell. Previous methods use a low expression vector, pB10, which does not allow for inducing high expression of the target of interest (17). Our method allows us to introduce sufficient amounts of protein in the cell membrane in order to increase our chances of observing a gating event, particularly when working with a channel that has a low probability of gating. The low expressing conditions tested show similar gating events as those shown when using the pB10 expression system used in other gating studies (17,25). In our high expression experiments, our results were consistent with our hypothesis that by increasing the number of channels in a patch, we had a higher instance of recoding channel activity in spheroplasts prepared from high-expressing conditions, and fewer instances in low-expressing conditions. Our analysis depends on utilizing the MscS channels in the cell as references for our gating calculations. Analysis of the MscS : MscL gating ratio of MtMscL, analysis of this ratio was only possible from data in our high protein expression patches. For MtMscL  $\Delta C$ , we were able to record only one patch at low IPTG concentrations, but multiple consistent patches were recorded with high expression patches. As such, the gating ratios of MtMscL, MtMscL  $\Delta C$  and EcMscL had smaller margins of error when using the high expression data. MtMscL  $\Delta C$  has an overall MscS : MscL gating ratio of  $\sim 2$ , which is closer to the EcMscL ratio of  $\sim 1.6$ . On the other hand, MtMscL full length has a gating ratio of 3, making it the highest ratio observed, and indicating it requires much greater tension to gate than MtMscL  $\Delta C$ . Our calculated

ratios are consistent with prior MscL electrophysiology studies on both MtMscL and EcMscL (17). Based on these results, we postulate that truncation of the C-terminal domain in MtMscL contributes to sustaining a high gating threshold for MtMscL, and therefore by removing it that threshold is reduced. Interestingly enough, this trend is opposite to trends observed when removing the C-terminal domain of EcMscL, and in SaMscL (14,16,32). Our results indicate that the C-terminal domain is not necessary for either oligomerization or gating of MtMscL. Given this, the gating events, as well as the oligomerization determinants, are found in the periplasmic loops and membrane-spanning regions of MtMscL. The role of the C-terminus, however, clearly plays a role in the detailed electrophysiology of the channel, as reflected in the gating tension and conductance. The C-terminal domain of MtMscL could undoubtedly play other functional roles, such as interacting with other proteins or taking the role of a filter so as to limit release of certain entities during gating of MscL.

Membrane protein X-ray crystallography studies are challenging due to the requirement to use detergent to keep hydrophobic portions of proteins covered by a micelle to maintain the protein in a liquid form. Micelle formation around the protein obstructs the covered regions from making crystal contacts to form a crystal lattice. In our data, we were able to resolve density around the protein that covers the TM2 helices in the membrane spanning region of MscL that likely represents the micelle arrangement. In the crystal packing, MtMscL  $\Delta$ C protein-protein contacts involving the periplasmic loops of interacting channels are clearly present, but lattice contacts involving the cytoplasmic regions of MscL are not evident, as these regions are separated by  $\sim 40$  Å from their nearest symmetry related molecule. Upon analysis of

low-resolution data from the crystal, the density resolved between protein subunits, appears to be an array of micelle-micelle interactions. This shows that the ordered solvent array must contribute to crystal packing, providing us with a rationale for the large gaps between protein subunits in the crystal packing. In fact, this may be a feature of membrane proteins forming Type II crystals, where the membrane spanning region is embedded in the micelle (33). Crystal packing with large gaps between protein lattices was also observed in the structure of KcsA (34). In this crystal packing arrangement, protein crystal contacts are made at the periplasmic loops of the channel, and the rest of the crystal packing consists of a sizeable gap found between protein lattices (34,35). In this case, the KcsA crystals had a high solvent content, 64%, similar to the solvent content in MtMscL  $\Delta C$  crystals. The packing is slightly tighter in KcsA, and the micellar lattices are  $\sim 30$  Å from each other, whereas in MtMscL  $\Delta C$  crystals the spacing is  $\sim 40$  Å (Figure 9). The difference in spacing is likely due to the detergent used to create the micelle, in the KcsA purification they utilized n-dodecyl-N, N-dimethylamine-N-oxide (LDAO), which has a smaller head group than DDM. In addition, a DDM micelle is estimated to be 72-149 kDa in mass, whereas an LDAO micelle is  $\sim 17$ -21.5 kDa (36,37). Altogether, there can be significant contributions from micellar arrangements in protein crystals grown with detergents, and this is a consideration that should be made when choosing detergents for protein extraction, purification, and crystallization.

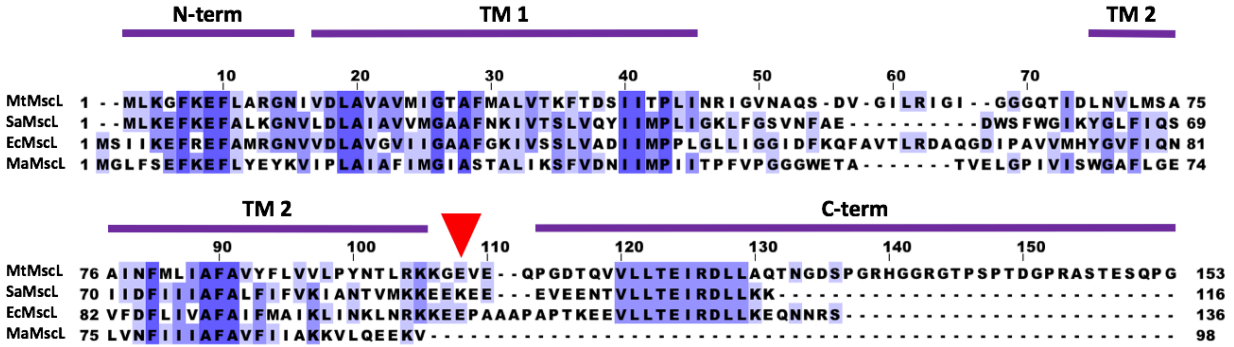
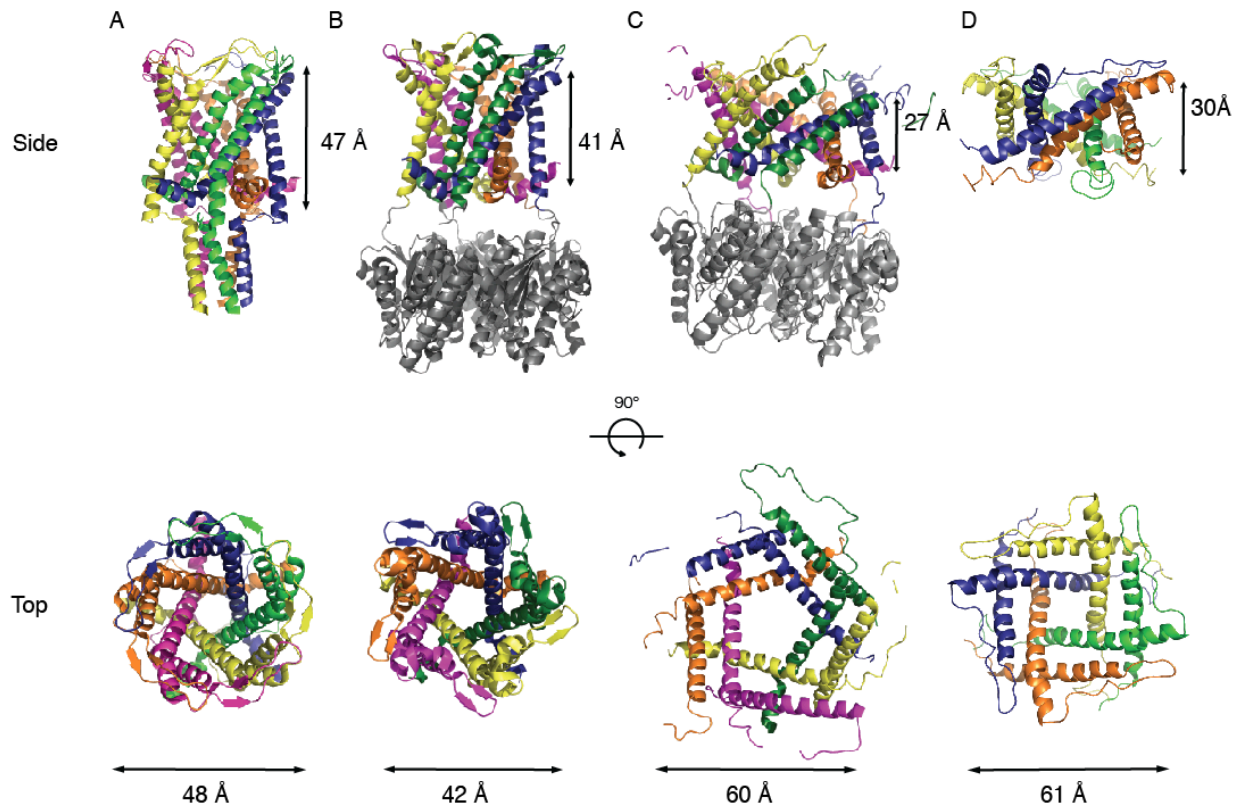


Figure 1- Alignment of MscL channel sequences.

Full-length sequences were aligned for MtMscL, SaMscL, EcMscL and MaMscL.

Sequence identity is as follows: MtMscL to SaMscL 40.5%, MtMscL to EcMscL 35.2%, and of MtMscL to MaMscL 29.2%. The red triangle over the sequence alignment depicts the location where the C terminus was cleaved for both MtMscL  $\Delta$ C and SaMscL  $\Delta$ C.

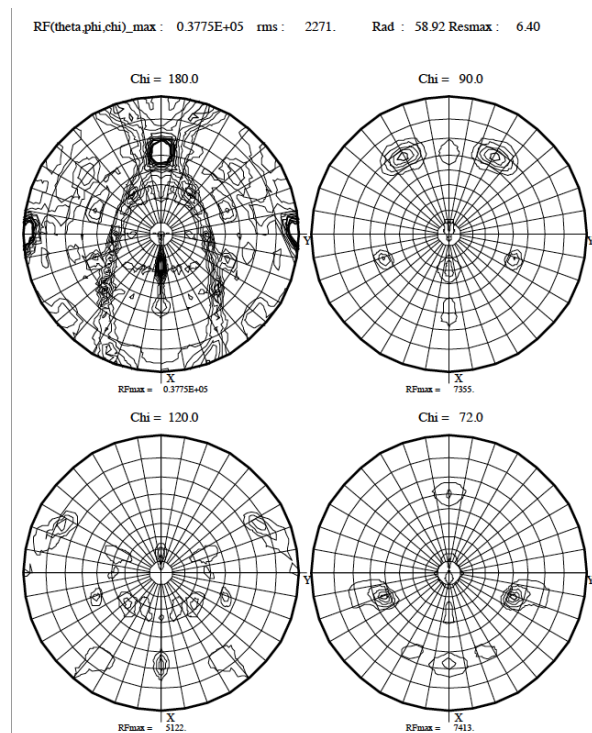
Colors represent sequence identity gradients.



*Figure 2- Structures*

Structure of bacterial MscL channels in closed and expanded conformations. MtMscL full length PDBID 2OAR (A), MaMscL closed PDB 4Y7K (B), MaMscL expanded PDBID 4Y7J (C), and SaMscL  $\Delta$ C PDBID 3HZQ (D) in cartoon diagram with channel height and diameter measurements. Monomers are colored in by subunit, and dimensions are labeled by the arrows around the protein cartoon. Side views in panels B and C include the MjRS protein (colored in grey) that was fused to MaMscL for crystallization.

A



B

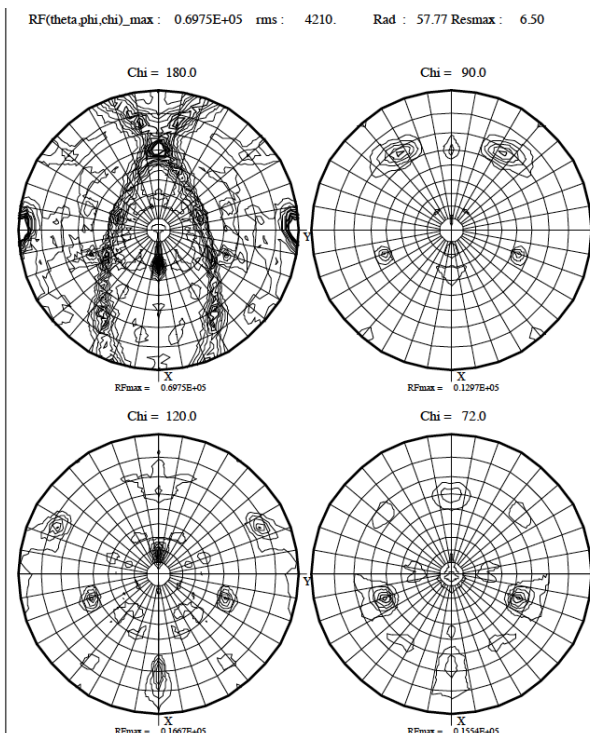


*Figure 3- Rotation function maps*

Rotation function calculations from native data of MtMscL  $\Delta$ C (panel A) and of MtMscL  $\Delta$ C soaked with sodium aurothiosulfate (panel B). The peaks highlight 522 symmetry in data from both crystals.

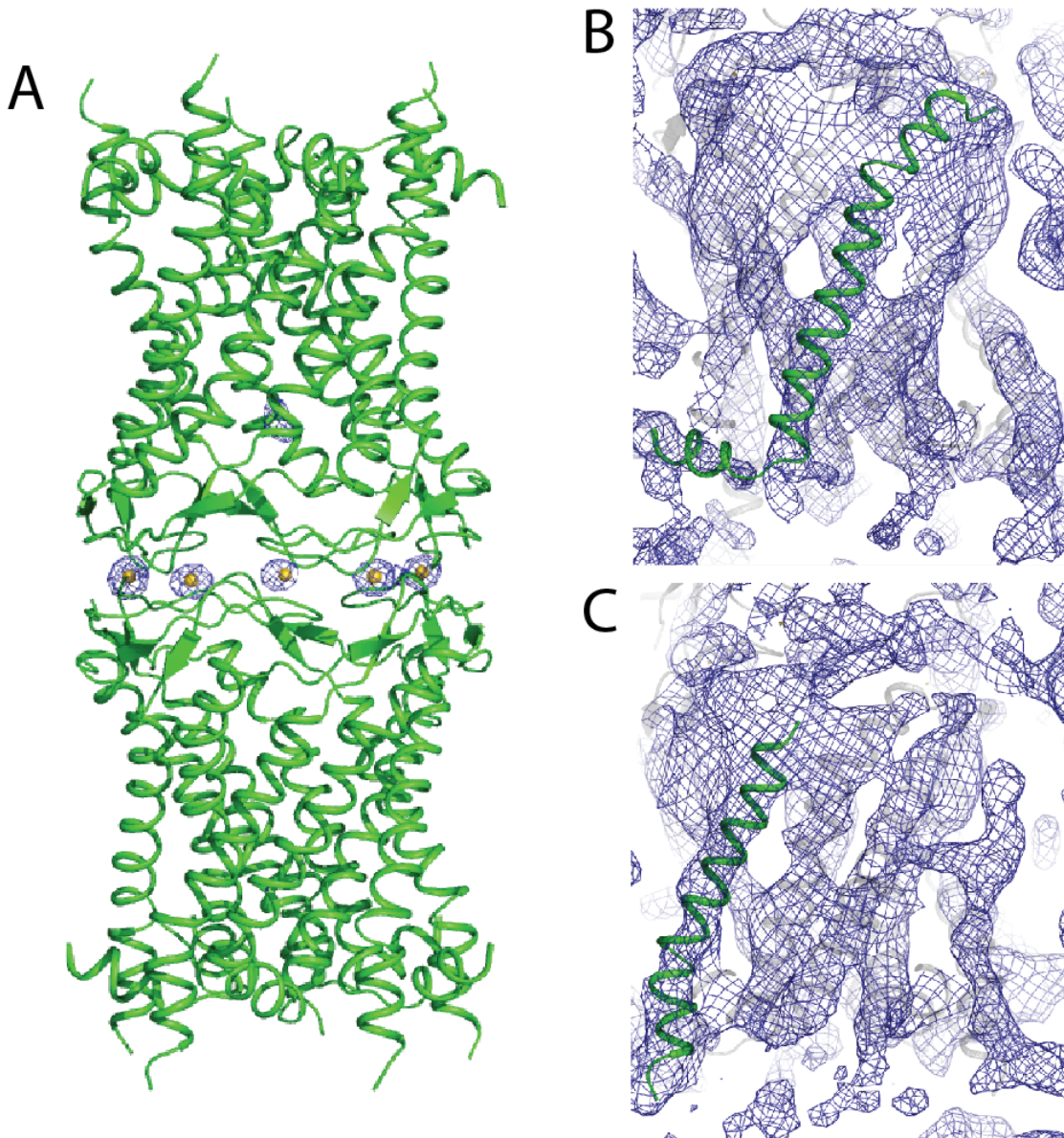


*Figure 4- MtMscL  $\Delta$ C crystal packing and gold density*

Panel A depicts density around the gold atoms bound in between the periplasmic loop crystal contacts, depicted as yellow spheres, surrounded by corresponding density.

Panels B and C show the fit of helices for TM1 and TM2, respectively, maps were contoured at a sigma of 1.

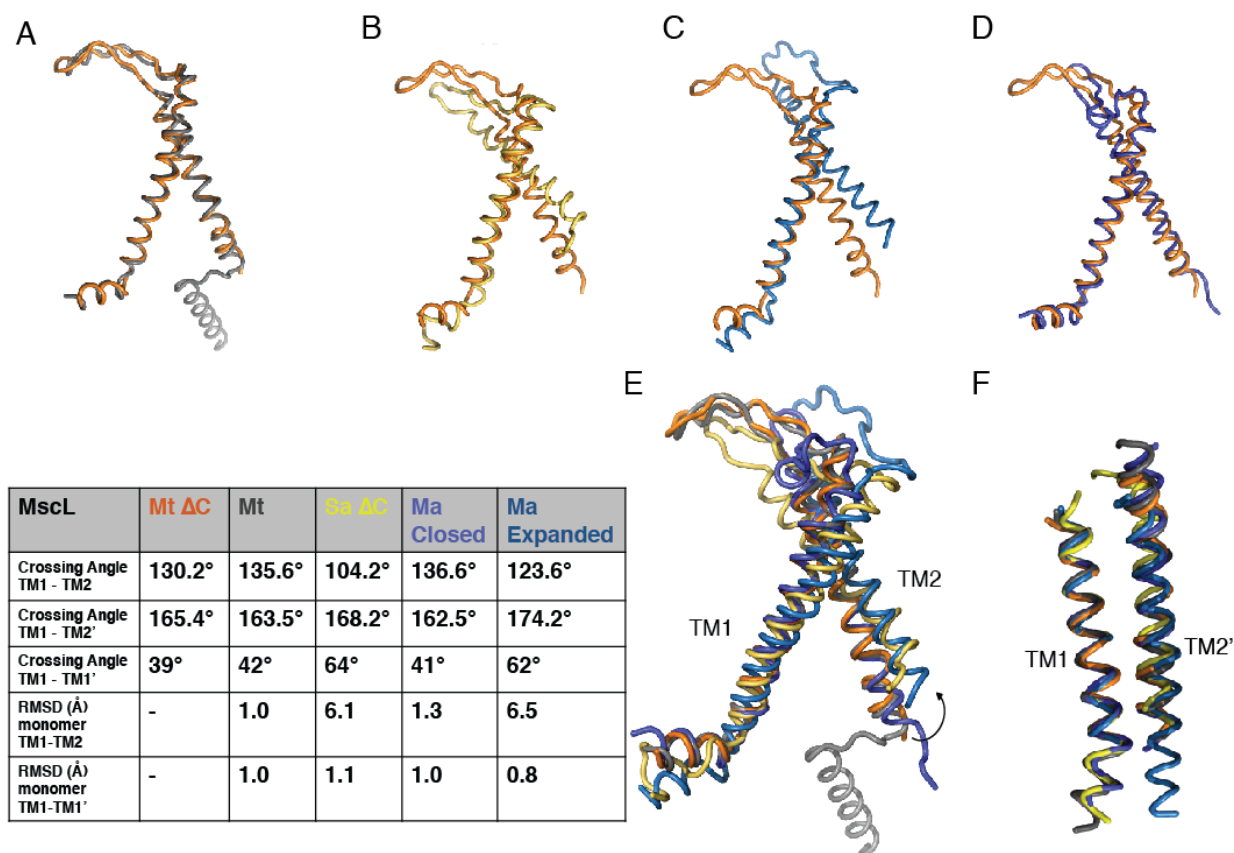
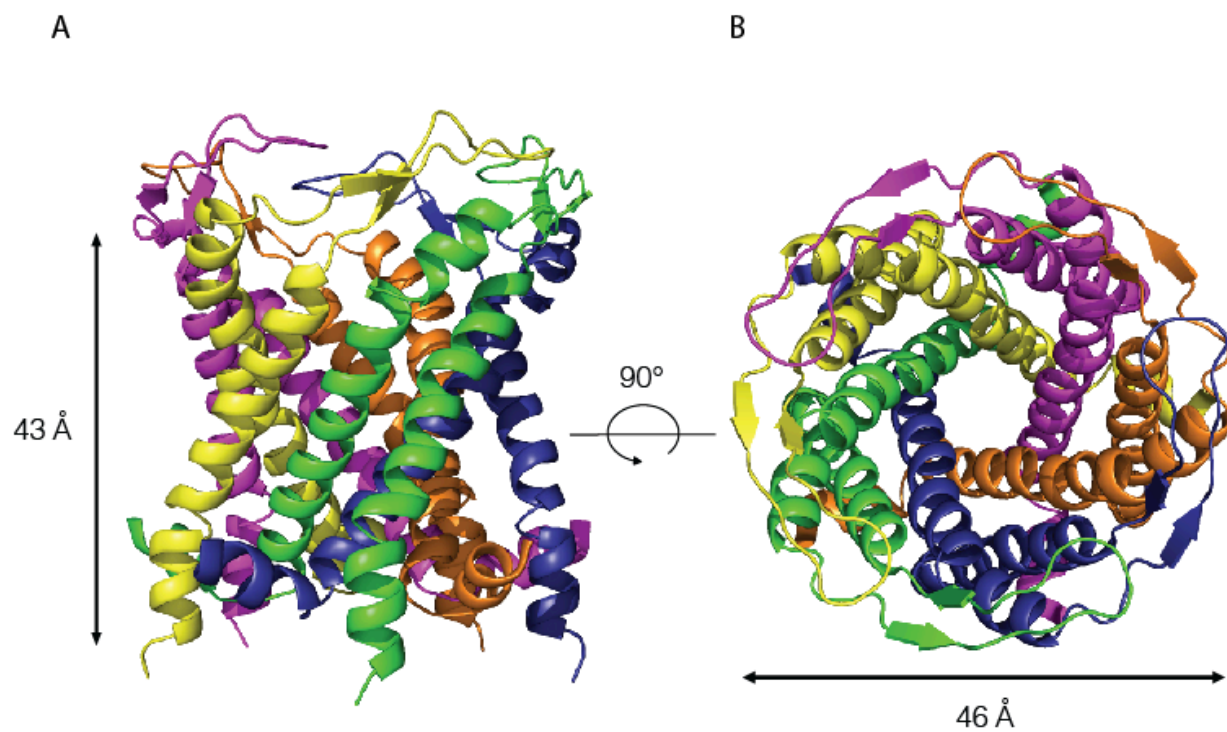


Figure 5- Alignment with monomers from other MscL channel structures

A TM1 from a single monomer in MtMscL  $\Delta C$  was aligned with other MscL structures solved to date. MtMscL  $\Delta C$  is depicted in orange, and it is aligned with MtMscL full length (A, grey), SaMscL  $\Delta C$  (B, yellow), MaMscL closed (C, purple), MaMscL expanded (D, blue). Alignment of all the sequences shows a consensus of movement from the closed states to the intermediate states as a movement that is predominant in TM2, as indicated by the arrow on panel E. The helix crossing angle observed in TM1 and TM2 further depicts the difference with a narrow angle corresponding to an intermediate state and a wider angle corresponding to closed states. The angle between TM1 and TM2' of all the channels remains constant, regardless of

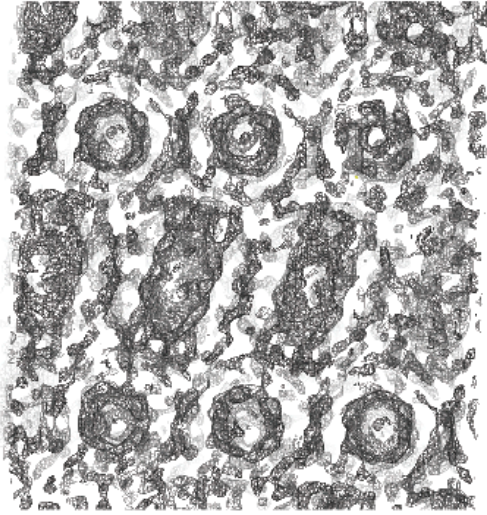
conformational state, as depicted in the alignment in panel F. Tilt angles, along with RMSD values are recoded in the table shown.



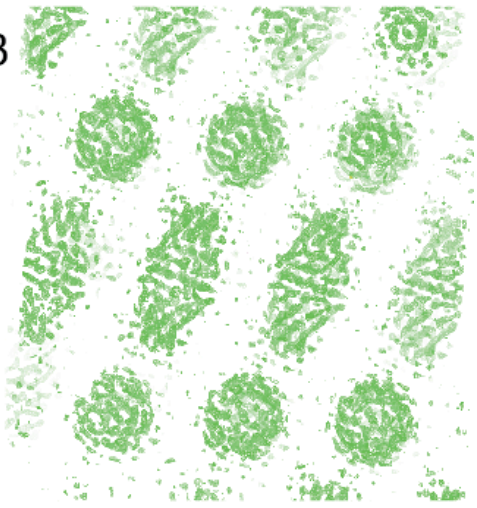
*Figure 6- Cartoon diagram of MtMscL  $\Delta C$*

The structure of MtMscL  $\Delta C$  is represented in cartoon format with the length and width labeled in panels A and B, respectively.

A



B



C

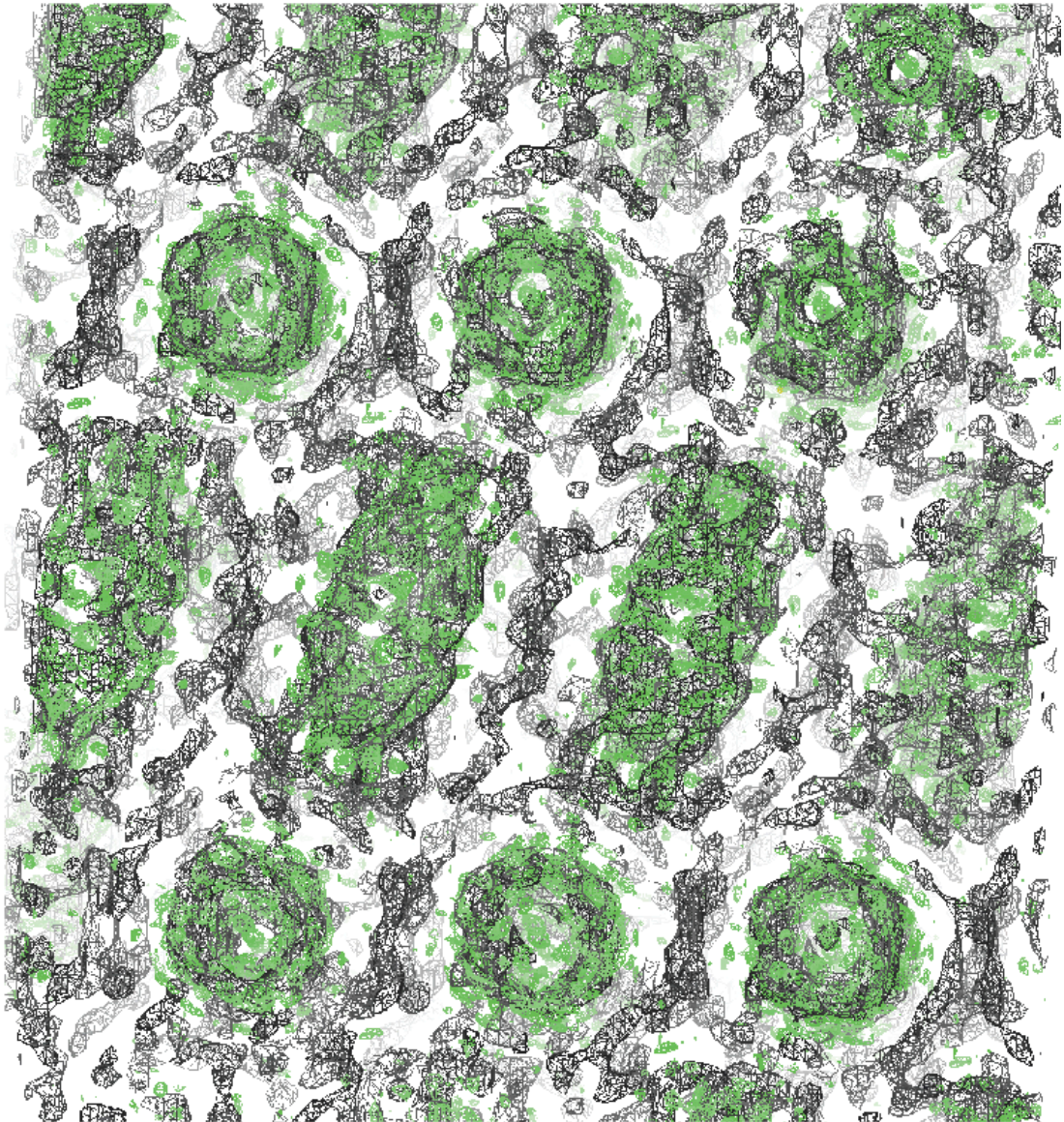
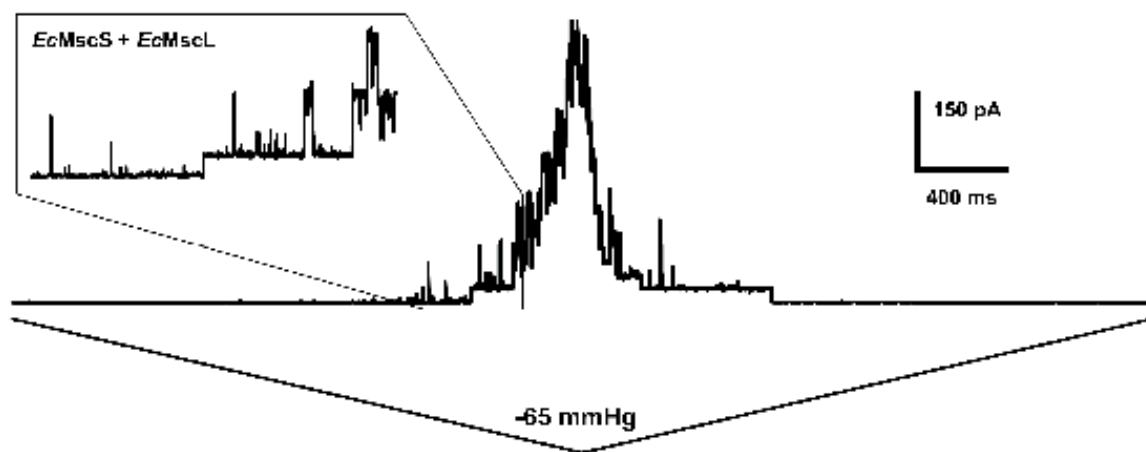


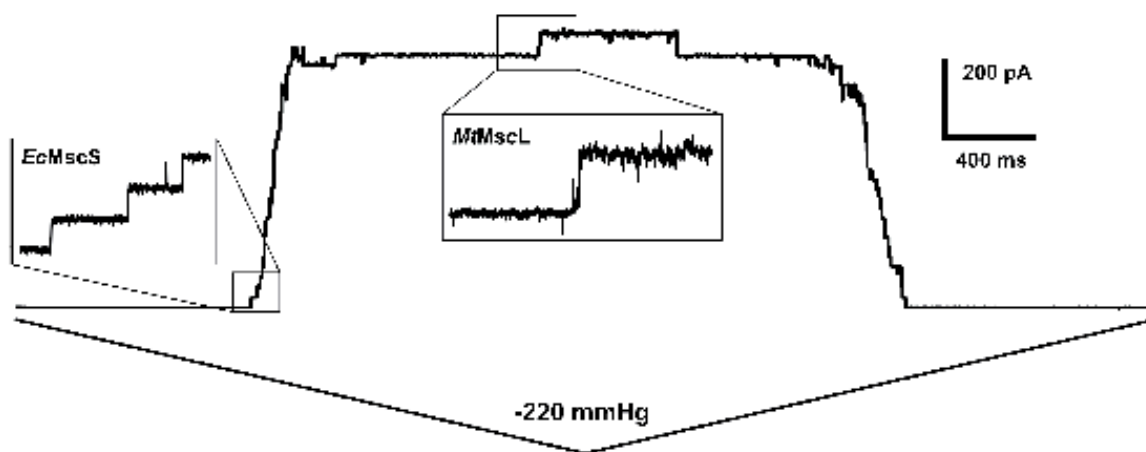
*Figure 7- Micelle density around MtMscL  $\Delta C$*

A map calculated from 12-30 Å resolution is rendered in panel A in gray, while the electron density map calculated from 5.5-12 Å solution is rendered in panel B in green. The merge of both maps is in panel C. Both maps have been contoured to a sigma of 1. The density around MtMscL  $\Delta C$  for the low-resolution shells appears as a continuous array of density, on the other hand, there is little density for solvent at the higher resolution shells, leaving only information about the protein in green. The gray density highlights the solvent in the crystal, reflecting the arrangements of the detergent micelles in the crystal. Due to high volume of detergent around the protein, this uneven array of solvent around the molecule is a likely contributor to low resolution diffraction of the data obtained from these crystals.

A



B



C

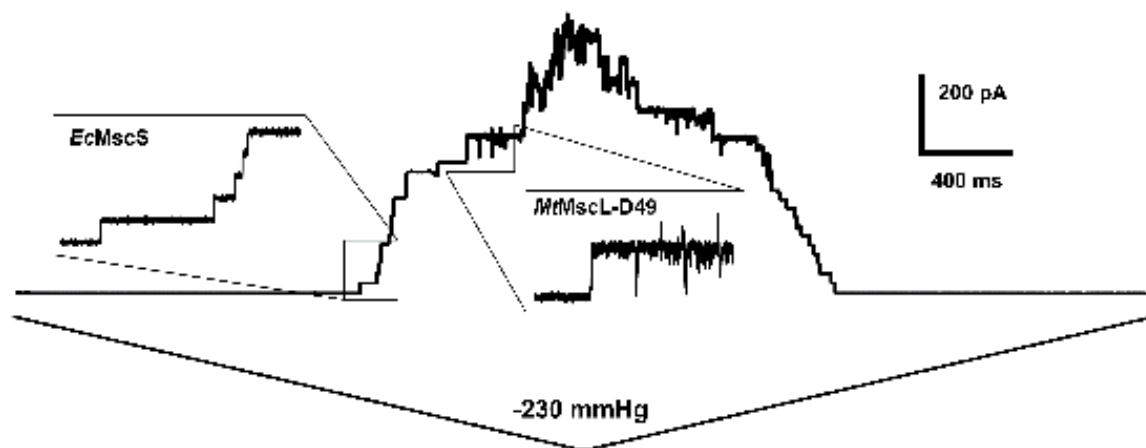


*Figure 8 - Traces of MscL homologues using patch clamp analysis*

Representative traces for EcMscL (A), MtMscL full length (B), and MtMscL  $\Delta C$  (C) in BL21 DE3  $\Delta mscL$  are shown. EcMscL reaches saturation at a tension of -65mm Hg, whereas MtMscL full length reaches saturation at a tension of -220mm Hg, and MtMscL  $\Delta C$  reaches saturation at a tension of -230mm Hg.

	MscS : MscL midpoints (all points)	MscS : MscL midpoints (high IPTG)	MscS : MscL midpoints (low IPTG)
<b>EcMscL full length</b>	1.78 ± 0.1 N = 5	1.6 ± 0.1 N = 2	1.9 ± 0.1 N = 3
<b>MtMscL ΔC</b>	2.1 ± 0.4 N = 7	1.9 ± 0.2 N = 6	2.9 N = 1
<b>MtMscL full length</b>	3.0 ± 0.4 N = 3	3.0 ± 0.4 N = 3	No data

*Table 1- MscS : MscL midpoint ratios*

Points for when half of the population of channels is gated relative to an endogenously expressed MscS population are documented for EcMscL, MtMscL full length, and MtMscL ΔC. Ratios were calculated for patches using both 1 mM final concentration of IPTG (high) and 0.05 mM final concentration of IPTG (low). EcMscL has an average ratio of 1.77, MtMscL ΔC has an average ratio of 2.06, and MtMscL has an average ratio of 2.78. The trend observed is that MtMscL full length has the highest ratio amongst the constructs tested. The number of patches from which the ratio was calculated is depicted by the N value next to it.

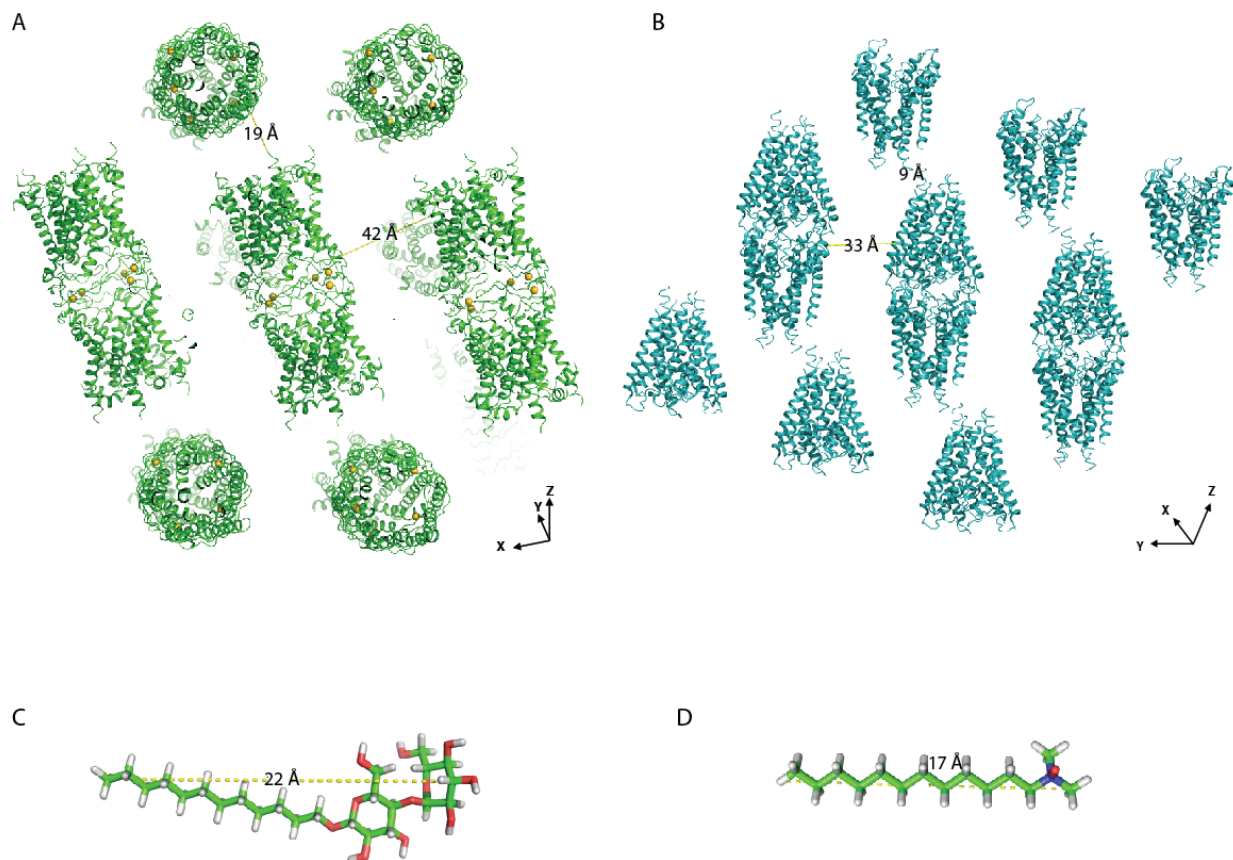


*Figure 8- Comparison of crystal packing of MtMscL  $\Delta C$  and KcsA*

Panel A depicts crystal packing of MtMscL  $\Delta C$  and measurements along two crystal contact sites. Panel B depicts crystal contacts in KcsA, PDBID 1JVM, along two contact sites that have gaps in packing, similar to the gaps observed in MscL  $\Delta C$ . The lower right hand corner of each panel displays the orientations of the unit cell axes at which these images were taken. Panels C and D depict a measurement from opposite carboxyl groups in a DDM and LDAO molecule, respectively.

### 3.5 References

1. Kung, C. (2005) A possible unifying principle for mechanosensation. *Nature* **436**, 647-654
2. Kloda, A., and Martinac, B. (2001) Mechanosensitive channels in archaea. *Cell Biochem Biophys* **34**, 349-381
3. Haswell, E. S., and Meyerowitz, E. M. (2006) MscS-like proteins control plastid size and shape in *Arabidopsis thaliana*. *Curr Biol* **16**, 1-11
4. Haswell, E. S., Peyronnet, R., Barbier-Brygoo, H., Meyerowitz, E. M., and Frachisse, J. M. (2008) Two MscS homologs provide mechanosensitive channel activities in the *Arabidopsis* root. *Curr Biol* **18**, 730-734
5. Martinac, B., Buechner, M., Delcour, A. H., Adler, J., and Kung, C. (1987) Pressure-sensitive ion channel in *Escherichia coli*. *Proc Natl Acad Sci U S A* **84**, 2297-2301
6. Sukharev, S. I., Martinac, B., Arshavsky, V. Y., and Kung, C. (1993) Two types of mechanosensitive channels in the *Escherichia coli* cell envelope: solubilization and functional reconstitution. *Biophys J* **65**, 177-183
7. Sukharev, S. I., Blount, P., Martinac, B., and Kung, C. (1997) Mechanosensitive channels of *Escherichia coli*: the MscL gene, protein, and activities. *Annu Rev Physiol* **59**, 633-657
8. Booth, I. R., and Blount, P. (2012) The MscS and MscL families of mechanosensitive channels act as microbial emergency release valves. *J Bacteriol* **194**, 4802-4809
9. Levina, N., Totemeyer, S., Stokes, N. R., Louis, P., Jones, M. A., and Booth, I. R. (1999) Protection of *Escherichia coli* cells against extreme turgor by activation of MscS and MscL mechanosensitive channels: identification of genes required for MscS activity. *EMBO J* **18**, 1730-1737
10. Blount, P., Sukharev, S. I., Moe, P. C., Nagle, S. K., and Kung, C. (1996) Towards an understanding of the structural and functional properties of MscL, a mechanosensitive channel in bacteria. *Biol Cell* **87**, 1-8

11. Sukharev, S. I., Blount, P., Martinac, B., Blattner, F. R., and Kung, C. (1994) A large-conductance mechanosensitive channel in *E. coli* encoded by *mscL* alone. *Nature* **368**, 265-268
12. Chang, G., Spencer, R. H., Lee, A. T., Barclay, M. T., and Rees, D. C. (1998) Structure of the MscL homolog from *Mycobacterium tuberculosis*: a gated mechanosensitive ion channel. *Science* **282**, 2220-2226
13. Li, J., Guo, J., Ou, X., Zhang, M., Li, Y., and Liu, Z. (2015) Mechanical coupling of the multiple structural elements of the large-conductance mechanosensitive channel during expansion. *Proc Natl Acad Sci U S A* **112**, 10726-10731
14. Liu, Z., Gandhi, C. S., and Rees, D. C. (2009) Structure of a tetrameric MscL in an expanded intermediate state. *Nature* **461**, 120-124
15. Beckstein, O., Tai, K., and Sansom, M. S. (2004) Not ions alone: barriers to ion permeation in nanopores and channels. *J Am Chem Soc* **126**, 14694-14695
16. Anishkin, A., Gendel, V., Sharifi, N. A., Chiang, C. S., Shirinian, L., Guy, H. R., and Sukharev, S. (2003) On the conformation of the COOH-terminal domain of the large mechanosensitive channel MscL. *J Gen Physiol* **121**, 227-244
17. Moe, P. C., Levin, G., and Blount, P. (2000) Correlating a protein structure with function of a bacterial mechanosensitive channel. *J Biol Chem* **275**, 31121-31127
18. Walton, T. A., and Rees, D. C. (2013) Structure and stability of the C-terminal helical bundle of the *E. coli* mechanosensitive channel of large conductance. *Protein Sci* **22**, 1592-1601
19. Malashkevich, V. N., Kammerer, R. A., Efimov, V. P., Schulthess, T., and Engel, J. (1996) The crystal structure of a five-stranded coiled coil in COMP: a prototype ion channel? *Science* **274**, 761-765
20. Reading, E., Walton, T. A., Liko, I., Marty, M. T., Laganowsky, A., Rees, D. C., and Robinson, C. V. (2015) The effect of detergent, temperature, and lipid on the oligomeric state of MscL constructs: insights from mass spectrometry. *Chem Biol* **22**, 593-603
21. Gandhi, C. S., Walton, T. A., and Rees, D. C. (2011) OCAM: a new tool for studying the oligomeric diversity of MscL channels. *Protein Sci* **20**, 313-326

22. Walton, T. A., Idigo, C. A., Herrera, N., and Rees, D. C. (2015) MsCL: channeling membrane tension. *Pflugers Arch* **467**, 15-25
23. Martinac, B., Rohde, P. R., Cranfield, C. G., and Nomura, T. (2013) Patch clamp electrophysiology for the study of bacterial ion channels in giant spheroplasts of *E. coli*. *Methods Mol Biol* **966**, 367-380
24. Schnorf, M., Potrykus, I., and Neuhaus, G. (1994) Microinjection technique: routine system for characterization of microcapillaries by bubble pressure measurement. *Exp Cell Res* **210**, 260-267
25. Blount, P., and Moe, P. C. (1999) Bacterial mechanosensitive channels: integrating physiology, structure and function. *Trends Microbiol* **7**, 420-424
26. Adams, P. D., Afonine, P. V., Bunkoczi, G., Chen, V. B., Davis, I. W., Echols, N., Headd, J. J., Hung, L. W., Kapral, G. J., Grosse-Kunstleve, R. W., McCoy, A. J., Moriarty, N. W., Oeffner, R., Read, R. J., Richardson, D. C., Richardson, J. S., Terwilliger, T. C., and Zwart, P. H. (2010) PHENIX: a comprehensive Python-based system for macromolecular structure solution. *Acta Crystallogr D Biol Crystallogr* **66**, 213-221
27. McCoy, A. J., Grosse-Kunstleve, R. W., Adams, P. D., Winn, M. D., Storoni, L. C., and Read, R. J. (2007) Phaser crystallographic software. *J Appl Crystallogr* **40**, 658-674
28. Terwilliger, T. C., Adams, P. D., Read, R. J., McCoy, A. J., Moriarty, N. W., Grosse-Kunstleve, R. W., Afonine, P. V., Zwart, P. H., and Hung, L. W. (2009) Decision-making in structure solution using Bayesian estimates of map quality: the PHENIX AutoSol wizard. *Acta Crystallogr D Biol Crystallogr* **65**, 582-601
29. Zwart, P. H. (2005) Anomalous signal indicators in protein crystallography. *Acta Crystallogr D Biol Crystallogr* **61**, 1437-1448
30. Brunger, A. T., Adams, P. D., Fromme, P., Fromme, R., Levitt, M., and Schroder, G. F. (2012) Improving the accuracy of macromolecular structure refinement at 7 Å resolution. *Structure* **20**, 957-966
31. Idigo, C. A. (2015) *Structural and Biophysical Characterization of Variants of the Mechanosensitive Channel of Large Conductance (MsCL)* Dissertation (Ph.D.), California Institute of Technology

32. Moe, P. C., Blount, P., and Kung, C. (1998) Functional and structural conservation in the mechanosensitive channel MscL implicates elements crucial for mechanosensation. *Mol Microbiol* **28**, 583-592
33. Michel, H. (1983) Crystallization of membrane-proteins. *Trends Biochem Sci* **8**, 56-59
34. Doyle, D. A., Morais Cabral, J., Pfuetzner, R. A., Kuo, A., Gulbis, J. M., Cohen, S. L., Chait, B. T., and MacKinnon, R. (1998) The structure of the potassium channel: molecular basis of K<sup>+</sup> conduction and selectivity. *Science* **280**, 69-77
35. Morais-Cabral, J. H., Zhou, Y., and MacKinnon, R. (2001) Energetic optimization of ion conduction rate by the K<sup>+</sup> selectivity filter. *Nature* **414**, 37-42
36. Strop, P., and Brunger, A. T. (2005) Refractive index-based determination of detergent concentration and its application to the study of membrane proteins. *Protein Sci* **14**, 2207-2211
37. Herrmann, K. W. (1962) Non-ionic—cationic micellar properties of dimethyldodecylamine oxide<sup>1</sup>. *The Journal of Physical Chemistry* **66**, 295-300

## 4 *Mycobacterium smegmatis* and MscL mediated antibiotic entry

### 4.1 Introduction

*Mycobacterium tuberculosis* continues to cause millions of deaths every year worldwide. This pathogen is notable for having become increasingly multi-drug resistant, making this pathogen difficult to eradicate with known antibiotics (1,2). In order to discover new antibiotics, it is necessary to understand the pathways of resistance in *M. tuberculosis*. That is not always a straightforward task though, as this organism has a slow growth rate and takes long periods of time to grow a culture. In recent years, a fast growing *Mycobacteria*, *Mycobacterium smegmatis*, has been identified as a model organism for use in studying mycobacterial proteins and function (3). Methods for facilitated genome engineering and protein expression have been developed in this system, making it an ideal candidate for studying targets from *M. tuberculosis* in a comparable cell strain. (4-6). As such, it is possible to analyze the role of individual proteins and their involvement with antibiotic activity in *Mycobacteria* to better elucidate pathways of intake, output and processing to ultimately develop antibiotics that more effectively target the *Mycobacteria*.

The mechanosensitive channel of large conductance (MscL) is a membrane embedded protein responsible for osmoregulation in bacteria. MscL has been thoroughly studied in *E. coli*, and recently it has also been identified as having a role in antibiotic entry into the cell (7). Antibiotics whose entry into the cell is increased upon MscL expression in *E. coli* are Viomycin, Spectinomycin, Nifuroxazide, and most

notably, Dihydrostreptomycin. A few of these antibiotics, Viomycin, Spectinomycin, and Dihydrostreptomycin, have activity against *M. tuberculosis* and *M. smegmatis*. Furthermore, streptomycin was developed as one of the first antibiotics used to treat *M. tuberculosis* (2,8-10). MscL is known to be expressed in the membrane *M. tuberculosis*, and it is relevant in the pathway of infection as *M. tuberculosis* undergoes various osmolarity changes in environment where osmoregulation likely plays a role (11,12). A number of proteomic mass spectrometry studies have shown that *M. tuberculosis* MscL (MtMscL) is expressed in the cell, and it has been specifically located in the cell membrane (12-14). Expression of MtMscL indicates that it is a gene that is readily produced in the cell during various phases of growth or stress. Due to the routine production of MscL, it is possible that it can mediate antibiotic entry into the cell.

A gene product containing 75% similarity to MtMscL has been identified in the *M. smegmatis mc2155* genome. The gene for MsMscL is in the same locus as a secondary porin MspC, which has been shown to be part of the porin network in *M. smegmatis* by which nutrients and antibiotics have been shown to gain access into the cell (15). Interestingly, MscL has also been shown to mediate antibiotic entry into *E. coli*, and is also a generally non-selective channel when releasing solutes from the cell to release tension on the cell wall (7,16). The native environment of *M. smegmatis* as a soil bacterium place it in a native environment that is susceptible to osmotic stress, and therefore also suggests a role for *M. smegmatis* MscL (MsMscL)-mediated osmoregulation, as it faces osmotic challenges that can be aided by MsMscL gating.

In this study, we have created a strain of *M. smegmatis* with the *mscL* gene knocked out, to generate strain MC2155 *mscL*-. We are utilizing the strain to study the

effects of antibiotic resistance with and without *mscL*. Our preliminary antibiotic resistance assays indicate that, upon comparison with wild-type MC2155, MC2155 *mscL*- exhibits a trend where deletion of the *mscL* gene results in slightly increased resistance to a common antibiotic used against mycobacteria, dihydrostreptomycin, and spectinomycin. To further establish the findings, a series of complementation studies, where MscL expression, both the *M. smegmatis* and the *M. tuberculosis* homolog, are being studied. In this case, expression of either Mt or Ms MscL is expected to return the cells to their decreased tolerance to antibiotics. Our studies suggest that not only nutrients but also some antibiotics enter the cell through an MscL mediated path.

## 4.2 Materials and methods

### 4.2.1 Recombineering plasmid construction

In order to create a double selection marker and suitable restriction sites for our insertions, we inserted the *galk* gene from plasmid pDB88 66bp upstream of the *SacB* selection cassette in pYUB1471, and then inserted an NdeI site at the end of the downstream target region to create plasmid pNH01 (6,17). 600bp regions encoding the sequences upstream and downstream of *mscL* in the *M. smegmatis* MC2155 genome were inserted at either end of the selection cassettes to create pNH02. All reactions were completed using Kapa Hifi polymerase with buffer A. Insertion of *galk* was completed by amplifying the vector backbone using primers pNH01GK\_F and pNH01GK\_R and *galk* with primers pGK\_F and pGK\_R. The products were purified

and ligated using the Clontech In-Fusion kit. Upstream and downstream regions of *mscL* were amplified from MC2155 genomic DNA using primers pMscLU\_F and pMscLU\_R for the upstream region, and primers pMscLD\_F and pMscLD\_R for the downstream region. The upstream region was inserted by digestion of pNH01 with NcoI, followed by purification and In-Fusion; thereafter the downstream region was inserted by digestion of pNH01 with NdeI and BamHI followed by purification and In-Fusion. pNH02 was amplified in *E. coli* cells, and linearized by restriction enzyme digestion with NdeI and BamHI.

#### 4.2.2 Allelic exchange

100 ng of linearized gene product from pNH02 was electroporated into *M. smegmatis* MC2155 expressing Che 60 and 61 proteins in the pJV53 plasmid, and made electrocompetent. Allelic exchange, also known as recombineering, was allowed to proceed for 4 hours at 37 °C. Thereafter, the cells were plated on selective media plates containing hygromycin (HygR 7H9). After 5 days, colonies were streaked onto both HygR and 2-deoxy- galactose + sucrose 7H9 medium (DS 7H9) plates. Colonies which survived on HygR but died on DS 7H9 medium plates were selected for unmarking. To unmark the cells, they were grown to log phase, OD<sub>600</sub> 1.0, and infected with bacteriophage pHAe 280 for 72 hours at 37 °C. Cells were then plated on DS 7H9 medium plates. Individual colonies were patched on HygR and DS 7H9 medium plates and colonies that survived on DS 7H9 plates but died on HygR 7H9 medium plates were selected. Unmarking was verified by colony PCR using primers pCPCR\_F and

pCPCR\_R, and by deep genome sequencing of extracted genomic DNA using the Illumina Hiseq 2500. Sequencing data was analyzed by aligning with Bowtie2, samtools, and visualized using IGV. The verified strain was named MC2155 *mscL*-.

#### 4.2.3 Protein expression

The inserts, MsMscL and MtMscL, were fused with a GFP marker at the C-terminal domain to allow for rapid protein expression by using fluorescence based detection. We amplified the GFP from a vector used in another study (18). The MtMscL insert was amplified from an existing MtMscL insert in pET19 (19) using primers pMtMscL\_F and pMTMscL\_R, and the MsMscL insert was amplified from genomic DNA using primers pMsMscL\_F and pMsMscL\_R. GFP was amplified using primers pGFPMtMscL\_F, pGFPMsMscL\_F and pGFP\_R and fused to MsMscL using primers pMsMscL\_F and pGFP\_R, and to MtMscL using primers pMtMscL\_F and pGFP\_R. Plasmid pMyNT (20) was digested with SphI and BamHI to create the insertion site for our insert and put into plasmid PMyNT using the infusion kit from Clontech to create pMsMscL GFP and pMtMscL GFP.

#### 4.2.4 Protein expression of MscL using the acetamide promoter

MC2155 *mscL*- cells were electroporated with 50 ng of pMsMscL GFP and pMtMscL GFP. After selecting for positive clones on HygR 7H9 plates, the cells were grown at 37 °C in 7H9 medium containing 0.5% glycerol, 0.02 % Tween, and 150 µg/mL hygromycin. After 42 hours, the cells were diluted 1:10000 into 7H9 medium containing the previously mentioned components and 0.2% sodium succinate. Once the cells reached an OD<sub>600 nm</sub> of 1-1.5, expression of the protein was induced using 0.2 % acetamide for 12 hours at 37 °C. Expressed and non-expressed cells were imaged under a fluorescent light to expose the GFP fluorescence in the cell at a wavelength of 488 nm and detected at 510 nm.

#### 4.2.5 Brightfield and fluorescent microscopy

Protein expression was analyzed by imaging the GFP fluorophore fused with each of our MscL constructs expressed in MC2155 *mscL*-. Following an expression experiment, 5 µL of cell culture was spread between a microscope slide and coverslip. Brightfield and fluorescence microscopy was performed on a Nikon eclipse NI-E microscope and images were taken with a Nikon DS Ri2 camera.

#### 4.2.6 Antibiotic resistance assay using *mscL*- bacteria

Two types of assays were conducted on *M. smegmatis*, one in liquid culture and another one on agar plates. For both assays, MC2155 and MC2155 *mscL*- cells were grown in a 3 mL 7H9 medium starter culture at 37 °C. In the liquid culture assay, a suitable starter culture was grown for both *M. smegmatis* (3 days) and *E. coli* (12 hours). 50 µL aliquots of these cultures were transferred to individual 3 mL cultures in 7H9 for *M. smegmatis*. Cultures for *M. smegmatis* contained a dihydrostreptomycin gradient of 0-25 µM, with concentrations of 0.1, 0.2, 0.4, 0.5, 0.6, and 1, followed by a gradient from 1-25 in steps of 5 µM. The experiments were all done at 37 °C in triplicate. These cells were grown for 24 hours and the cultures were transferred to a 96 well plate. OD<sub>600 nm</sub> was recorded using a Tecan plate reader. For the agar plate method, the OD<sub>600 nm</sub> of the MC2155 and MC2155 *mscL*- cultures was recorded and regularized using 7H9 medium. Once regularized, a series of eight serial dilutions was done with 7H9 medium, the dilutions were 1, 1/2, 1/4, 1/8, 1/16, 1/32, 1/64, and 1/128. These dilutions were plated in triplicates onto individual 7H9 agar plates containing 20 µg/mL of spectinomycin, nifuroxazide, and viomycin, and 0.5 µg/mL dihydrostreptomycin. The plates were incubated at 37 °C until colony growth was observed, typically after 3 days.

A series of control experiments using *E. coli* was done using Frag1 *E. coli* (*E. coli* WT) and MJF455 *E. coli* (*E. coli mscL*-). *E. coli* WT and *E. coli mscL*- starter cultures were grown in 5 mL LB medium for 12 hours at 37 °C. 50 µL aliquots of these cells were transferred to individual 5 mL LB cultures containing 0-70 µM dihydrostreptomycin at 37 °C. The cultures for *E. coli* contained a gradient of 0-70 µM in steps of 5 µM increasing

concentrations of dihydrostreptomycin. These cells were grown until they reached early exponential phase in the condition without antibiotic,  $OD_{600\text{ nm}}$  0.2, and transferred to a 96 well plate.  $OD_{600\text{ nm}}$  was recorded using a Tecan plate reader.

## 4.3 Results

### 4.3.1 Plasmid construction and allelic exchange

Sequence layouts for plasmid pNH01 and pNH02 are depicted in Figure 1 with relevant restriction digest sites shown on each map in Figure 1. These plasmids were used to follow the sequence of recombineering, summarized in Figure 2. In brief, we amplified flanking regions of *mscL* and inserted them into pNH01 to create pNH02. We amplified and linearized pNH02 to create a linear targeting vector for recombineering into MC2155 expressing Che 60-61, and we selected for cells which had been recombined by plating the recombineering reaction on HygR 7H9 agar for selection of recombined cells, as outlined in Figure 3. Successful recombineering appeared as individual colonies which grew on HygR 7H9 plates, thereafter individual colonies were patched onto HygR 7H9 agar and DS 7H9 agar. Successfully recombined colonies would grow on HygR 7H9 but not on DS 7H9 medium plates.

After selection of a suitable set of colonies, the unmarking infection with bacteriophage pHAE280 expressing resolvase was carried out. To select for unmarked cells, reactions were plated on DS 7H9 medium. After individual colonies were obtained, they were further patched on DS 7H9 and HygR 7H9. Unmarked colonies grew on DS

7H9 plates and failed to grow on HygR 7H9 plates. Four isolates which met these criteria were further analyzed using colony PCR; the results of our analysis are shown in Figure 3A. Using this method, we obtained a 75% yield of colonies that were unmarked after the resolvase reaction. A single unmarked strain and the wild-type lab strain were analyzed using deep genome sequencing; the alignment is depicted in Figure 3B. A library was prepared with extracted genomic DNA and used on an Illumina HiSeq 2500 sequencer, followed by alignment analysis. With our sequencing data, we compared Genbank sequence CP001663.1 with our lab strains, MC2155 and MC2155 *mscL*-. The MC2155 sequencing data yielded 9071376 reads; when aligned against the reference sequence the data yielded 90% alignment rate, with 84% of the sequences aligning one time, and 6% of the sequences aligning more than one time, and 10% of the sequences not aligning. The MC2155 *mscL*- data yielded 9036555 reads, and when compared to the reference sequence, we obtained a 90% alignment rate, with 84% of the sequences aligning one time, and 6% of the sequences aligning more than one time. 10% of the sequences were not aligned. The MC2155 *mscL*- strain was used to test expression of MscL from both *M. tuberculosis* and *M. smegmatis*.

#### 4.3.2 MscL expression in *Mycobacterium smegmatis* MC2155 *mscL*-

pMsMscL GFP and pMtMscL GFP were each electroporated into MC2155 *mscL*- and grown on HygR 7H9 plates. After 5 days, colonies were observed and transferred to liquid 7H9 medium with hygromycin added to seed a starter culture. The culture was then transferred to 7H9 expression medium, which has everything 7H9 includes but also

utilizes sodium succinate as a carbon source, in addition to the glycerol in the medium. Cultures were grown until they reached an OD<sub>600nm</sub> of 0.8-1.0, then they were split in half, with half induced by addition of acetamide to a final concentration of 0.2%; whereas the other half was left untouched. Cells were allowed to grow for an additional 12 hours, and then transferred to a coverslip for imaging analysis. Both MsMscL GFP and MtMscL GFP induced with acetamide showed fluorescent signal in the imaging analysis, whereas the half of the culture without acetamide addition did not show any fluorescent signal in the imaging analysis (Figure 4). Our results indicate that we are able to express MtMscL GFP and MsMscL using our MC2155 *mscL*- strain.

#### 4.3.3 Antibiotic resistance assays using dihydrostreptomycin and spectinomycin

We tested the growth of *M. smegmatis* in liquid cultures using dihydrostreptomycin. In our analysis, we determined that much lower concentrations of this antibiotic are required to eradicate *M. smegmatis* when compared to the concentrations required for *E. coli*. Our data assessing growth of bacteria in a liquid culture containing varying concentrations of antibiotics show that wild-type *E. coli* is susceptible to a minimum concentration of 25  $\mu$ M dihydrostreptomycin, whereas *M. smegmatis* MC2155 is susceptible to a minimum concentration of 1  $\mu$ M dihydrostreptomycin. When testing a range of antibiotic concentrations for testing, these limitations were taken into consideration, and as such, we designed different gradients for the analysis of each bacterial survivability study. In our initial *E. coli* studies, we found that wild-type *E. coli*, expressing endogenous levels of MscL, survives up to an

expected concentration of 25  $\mu\text{M}$ , with a sharp decrease in  $\text{OD}_{600\text{ nm}}$  readings in the culture grown at that concentration of dihydrostreptomycin. On the other hand, *E. coli mscL-* was able to survive antibiotic exposure up to 40  $\mu\text{M}$  dihydrostreptomycin, shown in Figure 5C. When the experiment was paralleled in *M. smegmatis*, wild-type MC2155, expressing endogenous levels of MscL survived up to 0.6  $\mu\text{M}$  concentration of dihydrostreptomycin ( $\text{OD}_{600\text{ nm}} = 0.08$ ), on the other hand, when MC2155 *mscL-* was exposed to the antibiotic, it was able to survive in up to 5  $\mu\text{M}$  of dihydrostreptomycin ( $\text{OD}_{600\text{ nm}} = 0.07$ ), as shown in Figure 5A. The difference is highlighted by analyzing the log of the  $\text{OD}_{600\text{ nm}}$ , which allows us to emphasize the differences amongst the lower  $\text{OD}_{600\text{ nm}}$  changes. In our logarithmic analysis, a larger difference is seen between the survivability of MC2155 and MC2155 *mscL-*. To analyze the effects of other antibiotics, we used 7H9 agar plates to study MC2155 and MC2155 *mscL-*. In these studies, we used serially diluted cells to analyze their survival rates in a plate containing various antibiotics. Out of our initial screen, only the 20  $\mu\text{g/mL}$  spectinomycin yielded a result with a difference shown between MC2155 and MC2155 *mscL-*. To survey the other antibiotics screened, alternate concentrations need to be surveyed in order to observe an effect. For the 20  $\mu\text{g/mL}$  spectinomycin plate, this concentration was shown to be sufficient to inhibit growth at low dilutions of *M. smegmatis*. In our results, we observe MC2155 growth inhibition at lower dilutions, whereas we see full growth in all dilutions of MC2155 *mscL-* cells, indicating that these cells have higher survival rates in this medium, as depicted in Figure 6. All cultures grew similarly on non-selective 7H9 medium. With our results, we are able to observe a trend where our MC2155 *mscL-* strain is resistant to antibiotic concentrations when compared to MC2155.

#### 4.4 Discussion

*Mycobacteria* have firm and thick outer membranes; in fact, they have the thickest known cell wall entity among bacteria (21). The thick membrane implies that mycobacteria are less permeable to environmental stresses, including antibiotics. This unique property makes them difficult to target when designing antibiotics, as they have to permeate the waxy outer cell layer of the cell wall. The outer membrane of mycobacteria has two distinct diffusion mechanisms, one mediated by interactions with lipids and characterized as hydrophobic and another mediated by the porins in the outer membrane and characterized as hydrophilic (22). A study observed that porin proteins of *Mycobacteria* are responsible for nutrient uptake and antibiotic entry into the cell (15,23).

Bacteria typically utilize their porin network to import nutrients, but it has been found that *E. coli* and *Salmonella* porins also play a significant role in the transport of beta-lactam antibiotics (24,25). Removal of the major porin in *M. smegmatis*, MspA, results in 16-fold increase to ampicillin and a 3-fold increase in resistance to rifampin (26). Interestingly, the outer membrane of *Mycobacteria* is less permeable than that of other gram-negative bacteria, and as such, porin mediated influx of antibiotics is a finding that can point to targets for antibiotic development. In our studies, we are studying a non-selective mechanosensitive channel embedded in the inner membrane of *Mycobacterium smegmatis*, which has not been considered as an antibiotic entry gate until recently. Our preliminary experiments have shown that when only this channel is deleted, the cells show increased resistance to two antibiotics, dihydrostreptomycin and spectinomycin. We will continue to use the tools we have developed to survey

MscL-mediated antibiotic resistance in finer detail. Ultimately, this system can be applied to other targets and will allow us to assay other mechanosensitive channels of *Mycobacteria* and their individual roles in antibiotic entry into the cell.

Furthermore, in these studies we provide a platform by which to study antibiotic resistance of *M. smegmatis*, with potential application of the findings to proteins from *M. tuberculosis*. We were able to express the membrane protein, MscL, from both *M. tuberculosis* and *M. smegmatis* in *M. smegmatis*, with a visible marker. Using this tool, we can design studies in which we can study the effect of different antibiotics between both channels. In addition, this setup enables us to study loss of function and gain of function mutants of the channel. Ultimately, this expression system can be used to purify this membrane-embedded protein from a native membrane, which will result in purification with native lipids bound with a consequent increased stability and improved crystallization of these protein targets.

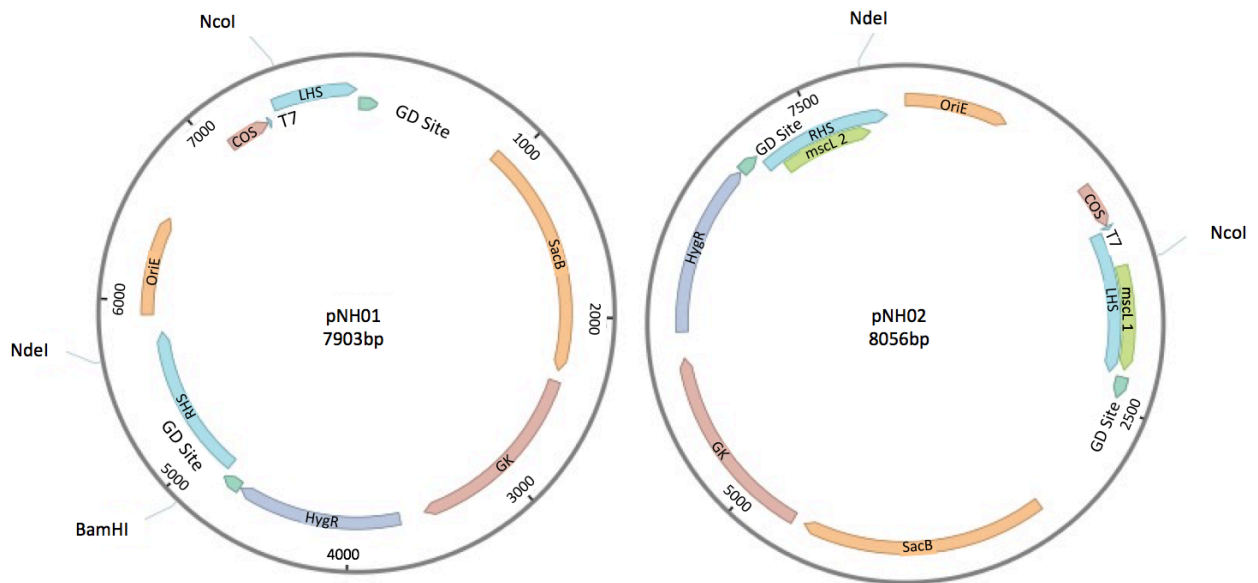
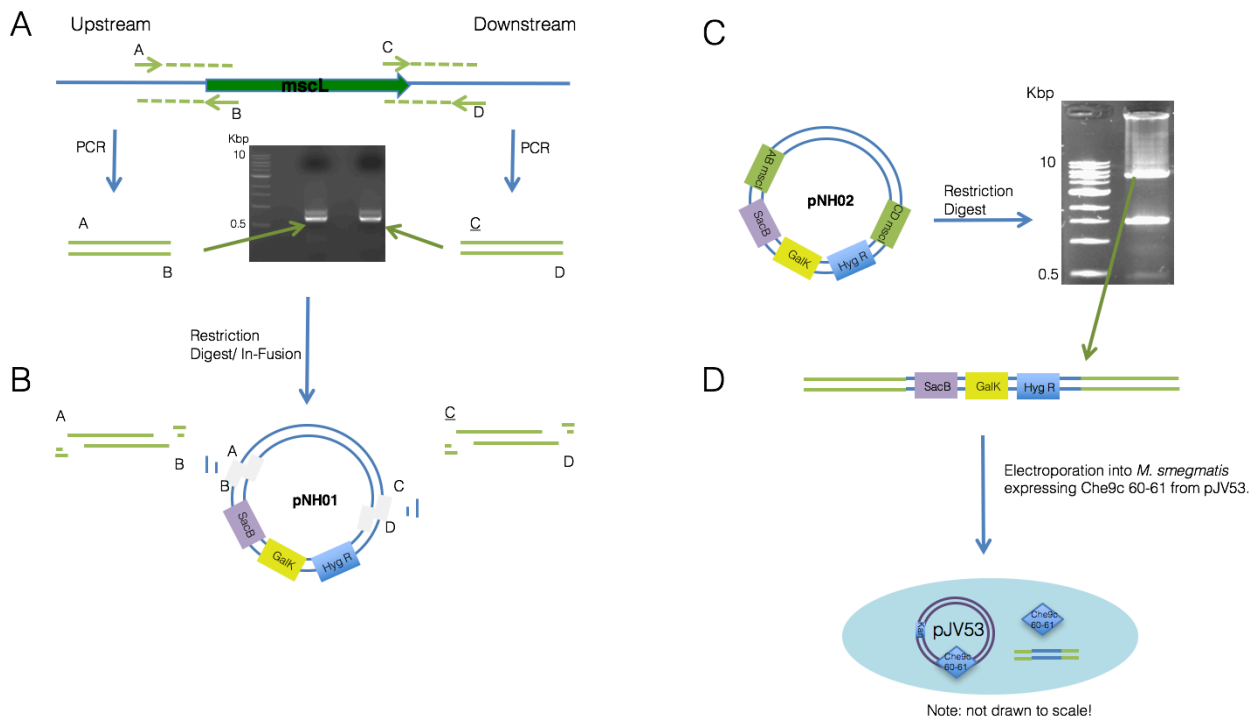


Figure 1- Plasmids pNH01 and pNH02 layout.

pNH01 was made as a template for inserting target flanking regions with three selection markers. pNH02 contains the flanking regions of *mscL* and was used for allelic exchange.



*Figure 2- Schematic layout of allelic exchange*

Design of the amplicons for the flanking regions used to target the gene of interest, *mscL*, is presented in panel A. The regions are 600 bp, this is shown on the agarose gel in the inlet of panel A, and is pointed out by a green arrow. The amplified flanking regions are then inserted into pNH01 by restriction digest and in-fusion reactions, as depicted in panel B. The ligated product, pNH02, is then digested to produce a linear targeting DNA for allelic exchange, depicted in panel C. The linearized DNA was purified from an agarose gel after digestion, shown by the green arrow in panel D. Finally, the linear substrate is electroporated into *M. smegmatis* expressing the pJV53 products Che 60-61, and allelic exchange is allowed to proceed for four hours at 37 °C.

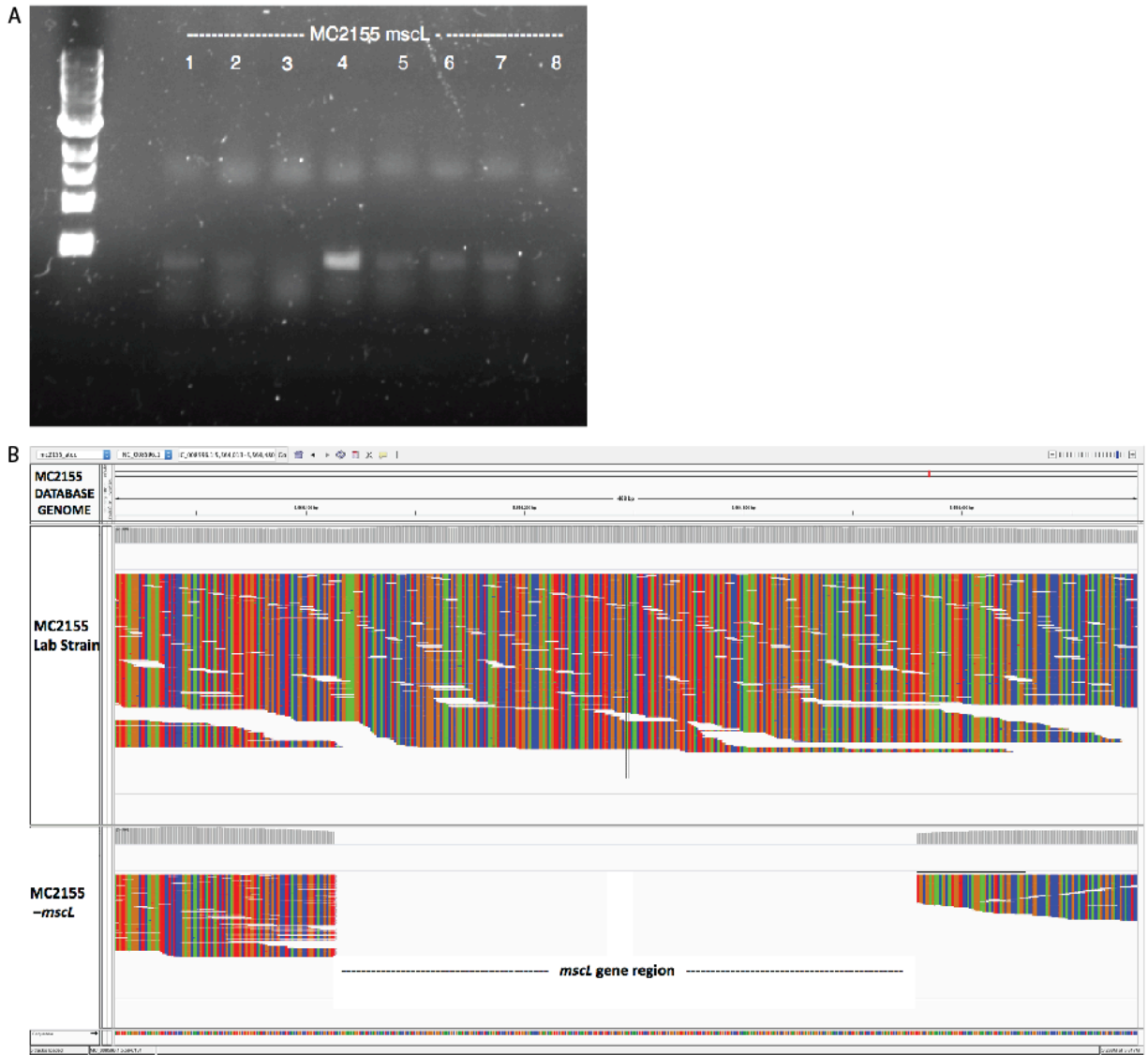


*Figure 3- Validation of engineered strains*

In panel A, PCR verification of unmarked gene deletion for *mscL* in MC2155, shown in an agarose gel. Eight colonies were sequenced using colony PCR; positive clones amplified a region that is unique to the unmarked sequence and 449bp long, amplification is strongest in colony 4, and observed for colonies 1,2, 4, 5, 6, 7. In panel B, we show verification of colony 4 by deep genome sequencing. The *mscL* gene region

contains many reads for the MC2155 lab strain, but no reads were aligned for the MC2155 *mscL*- strain.

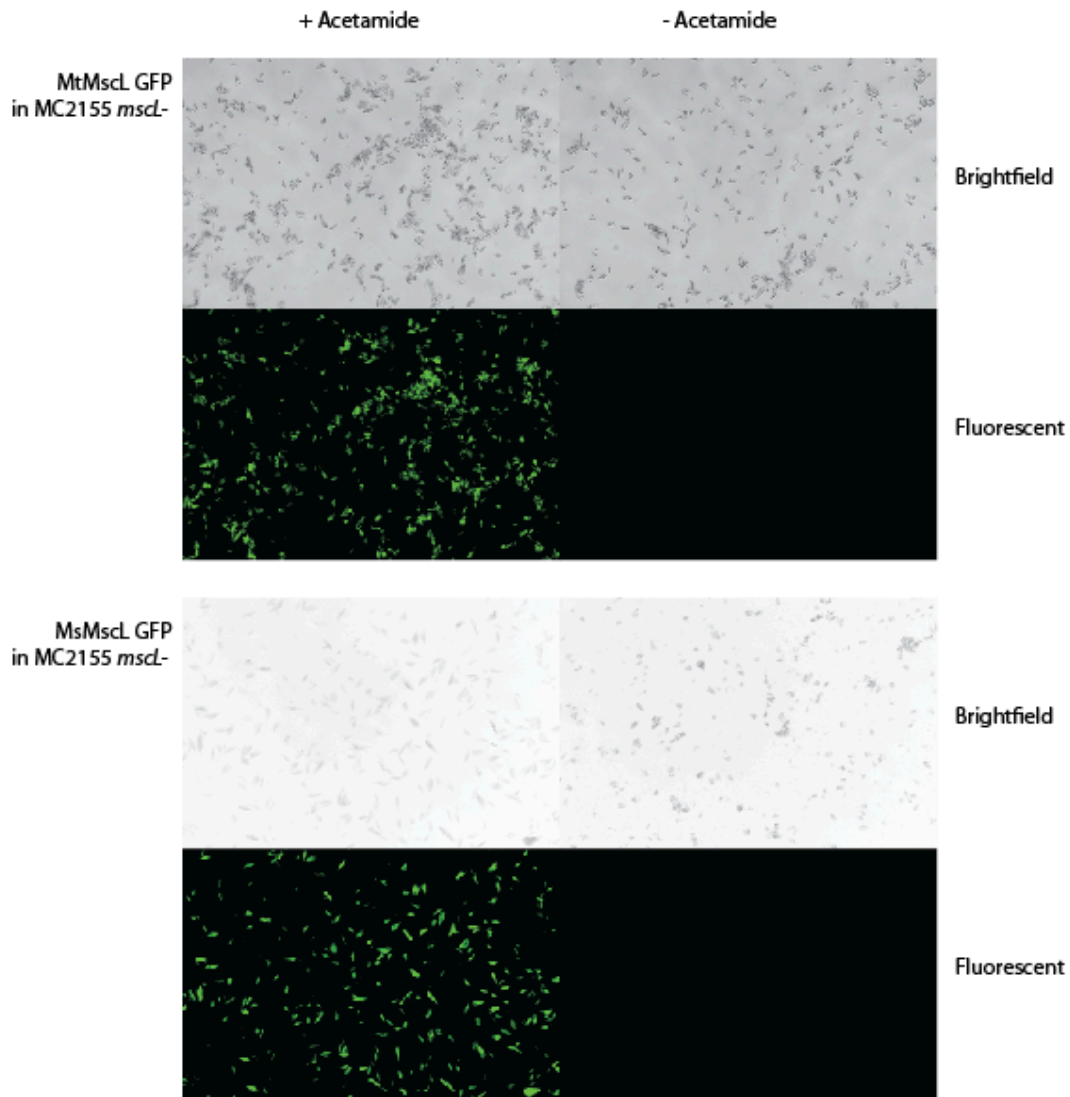
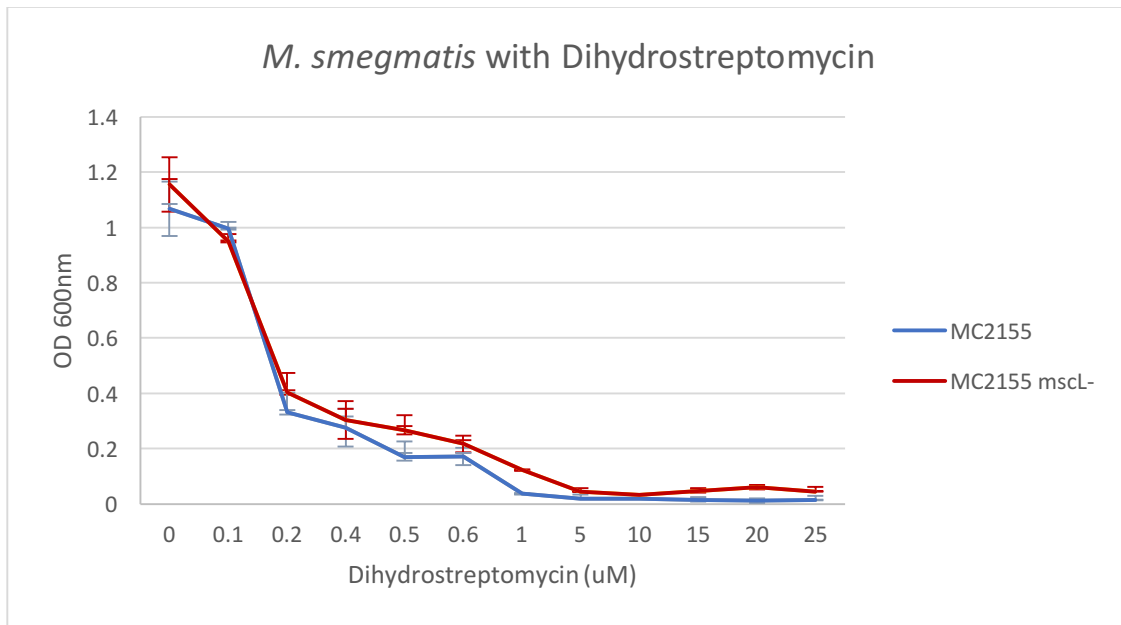


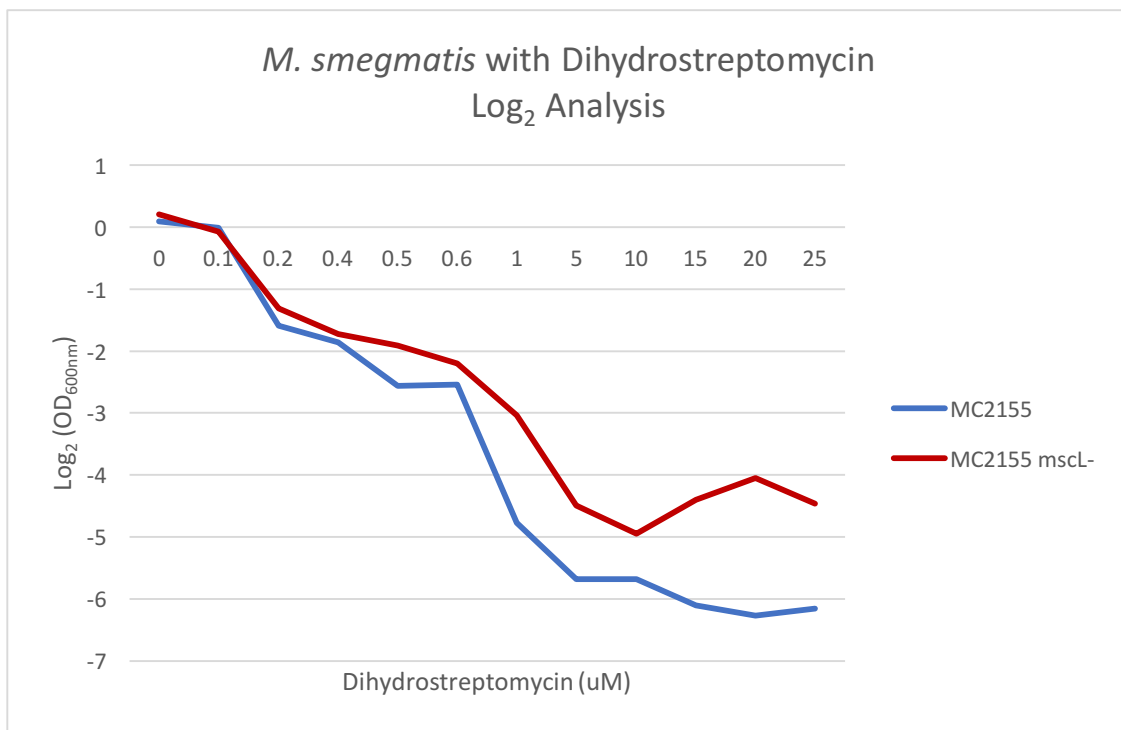
Figure 4- Bright field and fluorescent microscopy analysis of MC2155 *mscL-*

MC2155 and MC2155 *mscL-* expressing Ms and Mt MscL GFP using an acetamidase promoter are shown. In the top panel, MtMscL GFP shows a fluorescent signal upon addition of acetamide to the medium. Likewise, on the bottom panel, MsMscL GFP shows a fluorescent signal upon addition of acetamide to the medium.

A



B



C

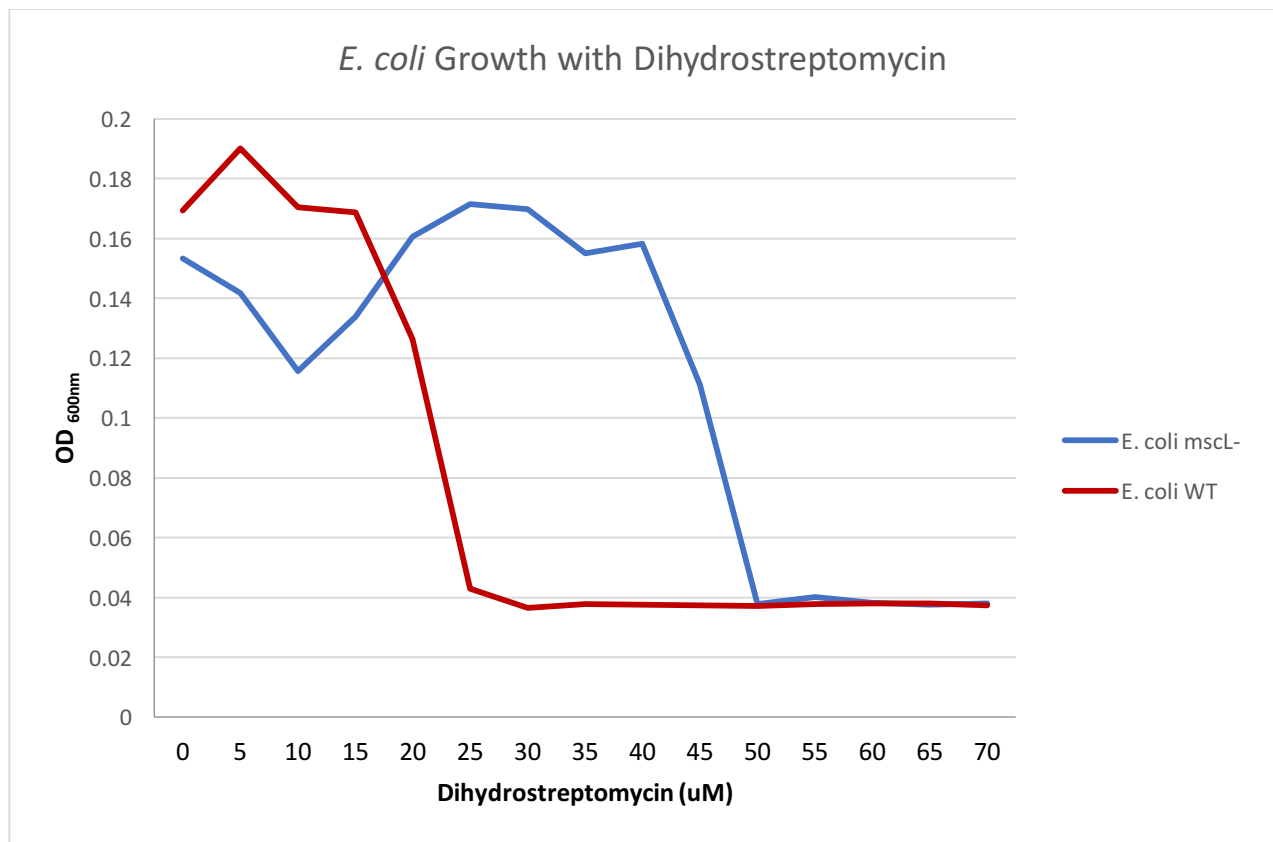
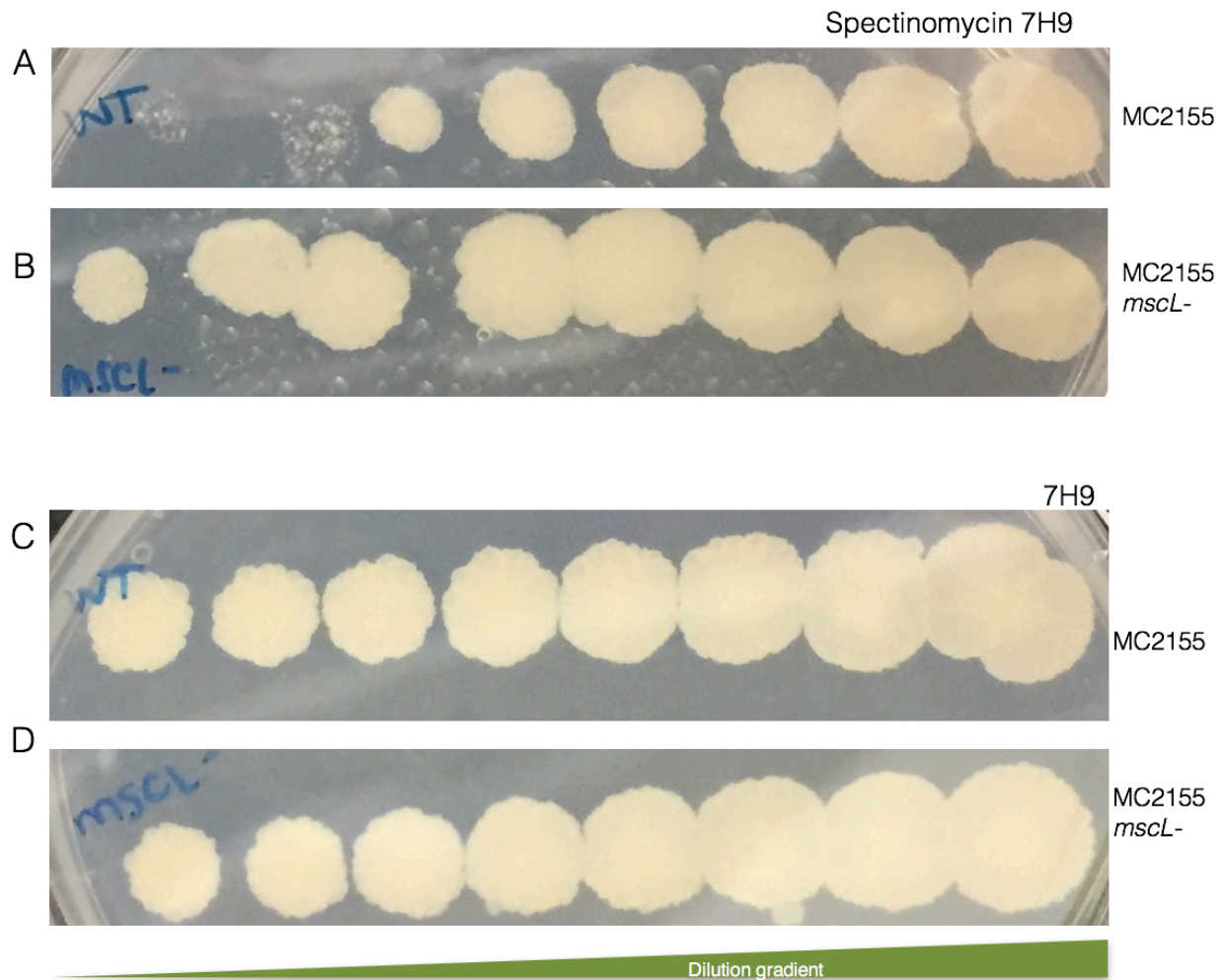


Figure 5- Growth curves with dihydrostreptomycin in *M. smegmatis* and *E. coli*.

Panels A and B show the growth curve analysis for *M. smegmatis*. MC2155 is depicted by the blue line and MC2155 mscL- is depicted by the red line, error bars are the standard deviation calculated from the triplicate data. Panel C shows the analysis for *E. coli*. Data from *M. smegmatis* was analyzed on the logarithmic scale to emphasize changes happening at low growth densities, relative to the linear scale in panel A.



*Figure 6- Analysis of growth across dilution gradients of MC2155 and MC2155 mscL-.* Panels A and B show growth of MC2155 and MC2155 *mscL-* on a 7H9 medium plate containing 20 ug/mL spectinomycin. Panels C and D show the same cell lines in a non-selective 7H9 plate.

*Table of primers used in this study:*

Primer	Sequence	Purpose
pGK_F	tcggtcggcccgtagagaATGAGTCTGAAA GAAAAAA	Amplification of GalK
pGK_R	AGCAGGACAGTGCTGAttggcgatcccg	""
pNH01GK_F	ttggcgatcccgaccgcagcacc	Amplification of pNH01 for GalK insertion
pNH02GK_R	gtcgctcggcggcccgtagaga	""
pMscLU_F	atttgctagccatggGgctgatcgccagcga	Amplification of MscL upstream
pMscLU_R	atttgctagccatggGgctgatcgccagcga	""
pMscLD_F	aggacgaagcggatcctggcggagaacagca	Amplification of MscL downstream
pMscLD_R	cggccacgatgtacttcgctcaacaaggggct	""
pMtMscL_F	gtacttcagggcgccatgggcatgctcaaaggat tcaag	Amplification of MtMscL
pMtMscL_R	ccctgaaacaagactccaattgcgattctgtgctc gcgc	""
pMsMscL_F	atgttgaagggcttcaaggagtcc	Amplification of MsMscL
pMsMscL_R	ccctgaaacaagactccaaggaggtgcggtcgc cgctgg	""
pGFPMtMscL_F	gcgcgagcacagaatcgcaattggaagtctgtttc aggg	Amplification of GFP
pGFPMsMscL_F	ccagcggcgaccgcacctccttgaagctgtttc aggg	
pGFP_R	gcgatatcgaattcggatccttaaagctttttaga gct	""
pCPCR_F	ctgcctcaccggcctggtc	Unmarking verification
pCPCR_R	ggttcacaggggaagc	""

*Table of plasmids made for this study:*

Plasmid	Purpose
pNH01	unmarking template
pNH02	mscL unmarking template
pMsMscL_GFP	MsMscL expression
pMtMscL_GFP	MtMscL expression

#### 4.5 References

1. Almeida Da Silva, P. E., and Palomino, J. C. (2011) Molecular basis and mechanisms of drug resistance in *Mycobacterium tuberculosis*: classical and new drugs. *J Antimicrob Chemother* **66**, 1417-1430
2. Zumla, A., Nahid, P., and Cole, S. T. (2013) Advances in the development of new tuberculosis drugs and treatment regimens. *Nat Rev Drug Discov* **12**, 388-404
3. Shiloh, M. U., and Champion, P. A. (2010) To catch a killer. What can mycobacterial models teach us about *Mycobacterium tuberculosis* pathogenesis? *Curr Opin Microbiol* **13**, 86-92
4. van Kessel, J. C., and Hatfull, G. F. (2007) Recombineering in *Mycobacterium tuberculosis*. *Nat Methods* **4**, 147-152
5. Bashiri, G., and Baker, E. N. (2015) Production of recombinant proteins in *Mycobacterium smegmatis* for structural and functional studies. *Protein Sci* **24**, 1-10
6. Barkan, D., Stallings, C. L., and Glickman, M. S. (2011) An improved counterselectable marker system for mycobacterial recombination using *galK* and 2-deoxy-galactose. *Gene* **470**, 31-36
7. Iscla, I., Wray, R., Wei, S., Posner, B., and Blount, P. (2014) Streptomycin potency is dependent on MscL channel expression. *Nat Commun* **5**, 4891
8. Jones, D., Metzger, H. J., Schatz, A., and Waksman, S. A. (1944) Control of gram-negative bacteria in experimental animals by streptomycin. *Science* **100**, 103-105
9. Wassersug, J. D. (1946) Pulmonary tuberculosis. *N Engl J Med* **235**, 220-229
10. Taniguchi, H., Chang, B., Abe, C., Nikaido, Y., Mizuguchi, Y., and Yoshida, S. I. (1997) Molecular analysis of kanamycin and viomycin resistance in *Mycobacterium smegmatis* by use of the conjugation system. *J Bacteriol* **179**, 4795-4801
11. Sakamoto, K. (2012) The pathology of *Mycobacterium tuberculosis* infection. *Vet Pathol* **49**, 423-439

12. Griffin, J. E., Gawronski, J. D., Dejesus, M. A., Ioerger, T. R., Akerley, B. J., and Sassetti, C. M. (2011) High-resolution phenotypic profiling defines genes essential for mycobacterial growth and cholesterol catabolism. *PLoS Pathog* **7**, e1002251
13. Malen, H., Pathak, S., Softeland, T., de Souza, G. A., and Wiker, H. G. (2010) Definition of novel cell envelope associated proteins in Triton X-114 extracts of *Mycobacterium tuberculosis H37Rv*. *BMC Microbiol* **10**, 132
14. Anishkin, A., Gendel, V., Sharifi, N. A., Chiang, C. S., Shirinian, L., Guy, H. R., and Sukharev, S. (2003) On the conformation of the COOH-terminal domain of the large mechanosensitive channel MscL. *J Gen Physiol* **121**, 227-244
15. Stephan, J., Bender, J., Wolschendorf, F., Hoffmann, C., Roth, E., Mailander, C., Engelhardt, H., and Niederweis, M. (2005) The growth rate of *Mycobacterium smegmatis* depends on sufficient porin-mediated influx of nutrients. *Mol Microbiol* **58**, 714-730
16. Booth, I. R., and Blount, P. (2012) The MscS and MscL families of mechanosensitive channels act as microbial emergency release valves. *J Bacteriol* **194**, 4802-4809
17. Jain, P., Hsu, T., Arai, M., Biermann, K., Thaler, D. S., Nguyen, A., Gonzalez, P. A., Tufariello, J. M., Kriakov, J., Chen, B., Larsen, M. H., and Jacobs, W. R., Jr. (2014) Specialized transduction designed for precise high-throughput unmarked deletions in *Mycobacterium tuberculosis*. *MBio* **5**, e01245-01214
18. Marshall, S. S., Niesen, M. J. M., Muller, A., Tiemann, K., Saladi, S. M., Galimidi, R. P., Zhang, B., Clemons, W. M., and Miller, T. F. (2016) A link between integral membrane protein expression and simulated integration efficiency. *Cell Rep* **16**, 2169-2177
19. Chang, G., Spencer, R. H., Lee, A. T., Barclay, M. T., and Rees, D. C. (1998) Structure of the MscL homolog from *Mycobacterium tuberculosis*: a gated mechanosensitive ion channel. *Science* **282**, 2220-2226
20. Noens, E. E., Williams, C., Anandhakrishnan, M., Poulsen, C., Ehebauer, M. T., and Wilmanns, M. (2011) Improved mycobacterial protein production using a

- Mycobacterium smegmatis groEL1DeltaC* expression strain. *BMC Biotechnol* **11**, 27
21. Paul, T. R., and Beveridge, T. J. (1992) Reevaluation of envelope profiles and cytoplasmic ultrastructure of mycobacteria processed by conventional embedding and freeze-substitution protocols. *J Bacteriol* **174**, 6508-6517
  22. Nikaido, H., and Vaara, M. (1985) Molecular-basis of bacterial outer-membrane permeability. *Microbiol Rev* **49**, 1-32
  23. Jarlier, V., and Nikaido, H. (1990) Permeability barrier to hydrophilic solutes in *Mycobacterium chelonae*. *J Bacteriol* **172**, 1418-1423
  24. Harder, K. J., Nikaido, H., and Matsushashi, M. (1981) Mutants of *Escherichia-coli* that are resistant to certain beta-lactam compounds lack the ompf porin. *Antimicrob Agents Ch* **20**, 549-552
  25. Yoshimura, F., and Nikaido, H. (1985) Diffusion of beta-lactam antibiotics through the porin channels of *Escherichia-coli K-12*. *Antimicrob Agents Ch* **27**, 84-92
  26. Stephan, J., Mailaender, C., Etienne, G., Daffe, M., and Niederweis, M. (2004) Multidrug resistance of a porin deletion mutant of *Mycobacterium smegmatis*. *Antimicrob Agents Chemother* **48**, 4163-4170

## 5 Discussion and future directions

### 5.1 *Mycobacterium smegmatis*

#### 5.1.1 Developments on mycobacterial target study

Since the genome for *M. tuberculosis* H37Rv was sequenced, a large number of genes with unknown function have been discovered (1). To this day, studies of *M. tuberculosis* are often problematic, as expression by conventional means in *E. coli* render insoluble and unstable protein (2,3). Advances in the field have yielded two organisms for protein expression which are less pathogenic and allow for studies of *M. tuberculosis* pathogenesis, they are *Mycobacterium marinum* and *Mycobacterium smegmatis* (3-5). Of the two organisms, *M. smegmatis* requires the lowest level of biosafety requirements, and is therefore a suitable organism for expression of *M. tuberculosis* protein targets in a laboratory setting set up to study proteins in other low-level biosafety organisms, such as *E. coli* and *Saccharomyces cerevisiae*. Furthermore, in the interest of pursuing membrane bound protein targets, electron microscopy ultrastructure studies have revealed that the cell walls of both organisms are very similar in the characteristics in the layers that make up the cell wall of *M. tuberculosis* (6,7). Biochemical analysis of the cell wall characteristics of *M. smegmatis* and *M. tuberculosis* show that they have identical characteristics in their lipid and mycolic acid compositions (8). Mycobacteria membrane proteins present an intriguing target, given that only three structures of membrane proteins, MtMscL, the porin MspA, and the

regulatory protein CrgA from *Mycobacteria* are currently known (9-11). These structures represent a low fraction of the proteins that regulate mycobacterial function and antibiotic resistance.

### 5.1.2 Mycobacterial cell walls and proteins

The mycobacterial cell wall contains a large array of proteins which allow for the diffusion of hydrophobic molecules into the cell, as found in mass spectrometry studies of cell walls (12). In *M. smegmatis*, the porin MspA was first identified as a significant component of the solubilized membrane (13). Later, it was found that MspA was visible in isolated *M. smegmatis* membranes using electron microscopy (14). In the analysis of MspA, a porin network was identified as a set of homologous gene products in *M. smegmatis* with high sequence identity to MspA and named MspB, MspC, and MspD (15). A study published after the initial network establishment showed that MscL is in the same locus as MspC, suggesting it is expressed under the same regulator as MspC (16). Though extensive studies have been done on MspA and MscL, it is clear that even within the Msp porin network, there lies a breadth of targets where a structure could inform antibiotic entry into *Mycobacteria*.

### 5.1.3 Mechanosensitive channels in *Mycobacterium smegmatis*

In addition to a porin network, we have also identified a mechanosensitive channel network in *M. smegmatis*. Our analysis of the *M. smegmatis* genome pointed to four sequences which have high sequence identity to mechanosensitive channels of small conductance. We identified these by using EcMscS as a search sequence in the

National Center for Biotechnology Information Basic Logical Alignment Tool. The sequences we found have 20-24% identity to EcMscS and correspond to reference numbers YP\_885704.1 (MscS 1), YP\_006566057.1 (MscS 2), YP\_887882.1 (MscS 3), and YP\_886447.1 (MscS 4). MscS 1 and 2 have a 24% identity to EcMscL and have different start codon sites so that MscS 2 is 12 amino acids longer than MscS 1. These proteins are predicted both to lack the periplasmic domains of EcMscS, and to have longer TM1 and TM2 than found in EcMscS. The third channel found, MscS 3, has a sequence identity of 20% to EcMscL. This channel has the longest sequence and it includes a cyclic AMP (cAMP) receptor protein (CRP) domain in the C-terminal region. The CRP domain is a transcriptional regulator that binds DNA via an allosteric interaction with cAMP (17). Finally, MscS 4 is the shortest channel found, and also lacks a periplasmic domain and some of the TM domains, but it retains a 23% identity to EcMscS. The alignment for these proteins is found in Figure 1.

Considering the extensive network of channels in *M. smegmatis*, an osmoregulation pathway must be present in these cells. Current studies seeking to understand osmoregulation in *M. smegmatis* are focused on studying effects under high osmolarity conditions using high amounts of salt (18). When bacteria are grown in high salinity environments, they regulate the osmolarity difference by producing intracellular inorganic salts or small organic osmolytes. *M. smegmatis*, and *E. coli* have both been shown to respond to high osmolarity conditions by producing small organic osmolytes (18,19). Further studies show that upon osmotic upshock, *M. tuberculosis* generates a signaling cascade with a Ser/Thr protein kinase that results in cell wall remodeling, bacterial transcription regulation and virulence factor production (20). While the

response to osmotic upshock has been characterized, however, there are no studies studying the osmotic downshock response of *M. smegmatis* or *M. tuberculosis*. Our observations present an opportunity for studies on these topics in *Mycobacteria*.

## 5.2 MscL Structural Studies

### 5.2.1 MscL structures to date

In this work, we have highlighted the structures of MscL solved to date. The structures have highlighted two conformational states of MscL, closed, and expanded non-conducting (9,21,22). These states are distinguished by the helix crossing angles between the first transmembrane (TM) domains of adjacent monomers. The TM1 helix crossing angle undergoes significant change when the lining around the pore region changes, as in the shift from closed to expanded non-conducting states of MscL. The trend observed in our analysis is that closed states of MscL have a TM1 - TM1' crossing angle of 37° - 39°, while the corresponding angles in the expanded state are 56° - 62°. The crossing angles between TM1 and the second TM domain in the same subunit, TM2, also reveal details about the changes in the tilt that the channels are undergoing in that region. In the structures of MtMscL, MtMscL  $\Delta$ C, and MaMscL closed the TM1 - TM2 angle is 130°-137°, a relatively conserved value. On the other hand, the crossing angles for the intermediate states of MscL are 104° and 124° in SaMscL  $\Delta$ C and MaMscL expanded, respectively.

The difference in crossing angle is likely influenced by the change in oligomeric state and slight difference in the loop between TM1 and TM2 in SaMscL and MaMscL. A critical missing element of our understanding of the MscL gating mechanism remains the full-length structure of EcMscL. Most studies in MscL physiology have been done in *E. coli*, as it is a well-characterized bacterial species with highly developed tools for

addressing protein function. In X-ray crystallography studies, pitfalls for structure determination lie within a few parameters: protein expression, protein stability, the ability to crystallize the protein, and, finally, protein crystallization properties. Of these properties, EcMscL expresses and purifies very well. It has been reported, however, as having a dynamic oligomeric state (pentamer and hexamer), at least in detergent (23-25). A protein with a mixed oligomeric state is difficult to crystallize, as sample heterogeneity that stems from oligomerization of the protein results in the formation of disordered crystals, for which a structure cannot be solved. Despite extensive attempts by our group, only the C-terminal domain of EcMscL has been solved using X-ray crystallography (26). The C-terminal domain forms a pentameric state, mediated by a coiled-coil domain. While full-length of EcMscL crystallizes readily, the resulting crystals invariably diffract X-rays poorly. Recent advances in electron microscopy may provide promising approaches for obtaining the high-resolution structure of this protein. The use of direct electron detector cameras, and updated computational software to process the images collected from these cameras have driven a revolution in the ability of single particle electron microscopy methods to determine protein structures at high resolution (27). Advances in membrane protein preparation for these studies also present the tools necessary to prepare a suitable environment for the protein without introducing too much background into the specimen (28). The small size of the MscL pentamer (75 kDa) does present a significant challenge in this approach which currently requires systems with molecular weights  $>\sim 200$  kDa. An alternative approach would be to utilize a new crystallography technique, Micro Electron Diffraction (microED (29)). This technique has advantages over traditional X-ray crystallography because the crystal

needed for the experiment has to be very small (<1  $\mu\text{m}$ ). Small crystals can be generated in crystallization conditions that yield precipitate; this kind of condition is usually overlooked for traditional X-ray crystallography and crystals suitable for microED could be present in any given crystallization screen. Additionally, it is possible that tiny crystals could be better ordered than large crystals that have typically been produced for X-ray diffraction, and hence EcMscL might be a suitable system for high resolution structural analysis by microED.

### 5.2.2 Limitations of MtMscL $\Delta\text{C}$ Crystals

In our studies, we were able to obtain crystals diffracting to 5.5  $\text{\AA}$  resolution. The lower resolution (12 – 45  $\text{\AA}$ ) reflections were much stronger than those from the higher resolutions. Reflections at lower resolution are attributed the contrast between solvent and protein, which will be more pronounced in crystals of MtMscL  $\Delta\text{C}$  with a solvent content of 75%. Membrane protein crystals are notorious for containing high solvent content, making it challenging to work with these targets. In our experiments, we only observed improved diffraction after crosslinking our crystals with glutaraldehyde. Crystals which were not crosslinked typically had a diffraction limit of 6.5-7  $\text{\AA}$ . This observation indicates that crosslinking of these crystals likely improved our diffraction because it was making the crystal a bit more resistant to deterioration upon handling. It would be of interest to pursue methods of crystal preservation through decreased crystal handling. In recent studies, beamlines 103, 104-1, and 124 at the Diamond Light Source in the United Kingdom have been established for *in situ* crystal screening. This method is currently limited by the requirement to have the crystal at room temperature,

but it presents a promising development that can yield alternative ways of obtaining X-ray crystallography data from delicate crystals.

### 5.2.3 The open state of MscL

One of the questions that remain in the field of MscL is the diameter of the final open pore. As previously stated, pore diameter only has to be 9 Å to allow for the passage of water, and 13 Å for the passage of charged ions. Those, however, have not been the only molecules suspected of travelling through the MscL open pore. In *B. subtilis* and *E. coli*, MscL is able to release of small proteins upon osmotic downshock (30,31). A unique characteristic of MscL is its conductance of 3 nS (32). This conductance is much larger than that found in any other type of channel in bacteria. For instance, KscA, the most extensively studied ion channel in bacteria, has a conductance of around only 0.1 nS, whereas non-selective ion channels in the outer membrane, porins (OmpF), have a recorded conductance of 0.3 nS (33). Furthermore, the OmpF channel forms a tetramer, and the diameter of the pore it forms is 10 Å in diameter. Taken together, both observations lead to the conclusion that in order to accommodate gating of small proteins, and a pentameric organization with a large conductance, MscL likely renders a large pore when it is in the open fully gated state (34). To further validate the observations, a few groups conducted studies where they were able to correlate electrophysiological measurements and pore size.

Initially, the pore size was studied in EcMscL based on Hille calculations coupled with measurements from electrophysiological studies (35,36). In this study, the open

state of EcMscL is modeled as a uniform cylindrical opening in the membrane and yielded an open pore diameter that was estimated to be 42Å (36). Observations in this study were supplemented by experimenting with the passage of several poly-L-lysines (PLL) through the channel pore using proteoliposomes. Based on these measurements, the estimation for pore diameter was reduced, and estimated to be 37 Å. Another approach to this problem was to account for the geometrical features of a gated channel. By observing a patch clamp experiment under a light microscope, the curvature in the membrane upon patch formation is visible. Using these observations, it was possible to make a better measurement of the force on the channel under different pressures (37). The measurements allowed for calculations of the change in cross-sectional area upon MscL gating. The new calculation, however, did not vary much from the latter assumption in the Cruickshank study despite assumptions in the formulation of the experiment. In the structure of MtMscL, the channel adopts more a conical shape in the closed state (9). The conical shape may not endure throughout complete channel gating towards the open state; however, this caveat can be addressed by rendering calculations assuming different initial pore diameters, which was done (37). Further methods to validate these observations persisted, regardless.

These studies were the foundation which helped pioneer the subsequent type of MscL open pore diameter analysis. Other PLL molecules of varying lengths and sizes were used in a patch clamp electrophysiology experiment. In this setup, if a PLL was too bulky, it would inhibit conductance through the patch. A PLL with a 25 Å diameter was found to allow for MscL gating and patching in electrophysiological experiments; however, a PLL of 37 Å diameter no longer allowed for measurements to be recorded.

This implies that the channel allows for the passage of proteins that are 25 Å in diameter, and becomes blocked by molecules which are larger than 37 Å (37). To further refine this measurement, dual color fluorescence burst analysis (DCFBA) was used to observe the passage of fluorescently labeled proteins, with known structures, through the gated MscL (38,39). DCFBA studies concluded that proteins as large as 6.5 kDa, such as the bovine pancreatic trypsin inhibitor with dimensions of 21 x 23 x 31 Å, can pass through MscL. To confirm this observation, a wide array of techniques was used by many others in the field.

Disulfide cross-linking, electrophysiology, molecular dynamics (MD), Förster resonance energy transfer (FRET) and electron paramagnetic resonance spectroscopy (EPR) represent some of the techniques that have been utilized to analyze the open state of MscL (40-42). These studies were all based on the 1MSL X-ray crystallography structure solved in 1998; however, this structure contained a number of registry errors that might have generated issues in reliably designing the *in silico* models that these studies were based on. MD models by Sukharev and Guy reported an open state of MscL generating a pore diameter between 30 and 40 Å that is formed with an iris-like opening of the helices in the channel. Using cysteine point mutants along the TM regions of the channel, these studies measured EPR distances in the closed, intermediate, and open states of EcMscL; the open state was stabilized by utilization of lysophospholipids in the EcMscL proteoliposomes (41). The pore diameter calculated using this approach was about 25 Å, but due to limitations in the technique, spin-spin interactions cannot be recorded beyond 15 Å. More direct imaging studies of the matter

were conducted with atomic force microscopy (AFM) and Förster resonance energy transfer (FRET).

AFM analyses were done on an immobilized system of self-assembled lipid monolayers containing StMscL at varying tensions (43). The signal acquired from these measurements showed MscL as a protein with a height of 22 – 27 Å and a pore diameter of 110 -150 Å. These measurements are much larger than those observed in X-ray crystallography structures of MtMscL. AFM measurements and analysis suggested that the open pore size for StMscL ranged from 50 -60 Å. Moreover, FRET studies were undertaken using EcMscL incorporated into proteoliposomes (42). The TM regions of EcMscL were labeled stochastically with donor and acceptor dyes and dual labeled channels were used to analyze the proteins in a unanimous manner irrespective of whether they had been labeled with donor or acceptor dye. A pore diameter of 28 Å was reported in this study.

The use of various techniques to illuminate the question of pore diameter in the open state of MscL has sketched a preliminary understanding for the gating mechanism of this channel. The unifying theory in most of these studies, though, is the use of EcMscL as the model of study. Whereas this system is vastly informative, these studies are all based on estimations made on the sequence of EcMscL, based on the X-ray crystallography structure of MtMscL. To this date, however, only MtMscL has been observed in its entirety with a high-resolution method, X-ray crystallography. For this reason, it would be useful to study this homologue and analyze the correspondence in function accordingly. The barrier to studying MtMscL, however, has been the inability to

utilize this homologue of MscL in two of the techniques that are most widely used for studies; electrophysiology and osmotic downshock survivability assays.

#### 5.2.4 Means of studying the open state of MscL

The open state structure of MscL remains a critical objective in our structural depiction of the gating mechanism. Many studies have identified gain of function mutations, which yield a channel that gains function under different conditions. Those conditions consist of introducing a variety of molecules that can be modified post-purification. Modifications have been tested on EcMscL and consist of three approaches. The first approach consists of introduction of a cysteine at the constriction site of the channel which can then be linked to either a light sensitive compound that become protonated with the addition of UV, or an pH sensitive compound that becomes protonated at low pH (44). Another approach includes modification of the loop between TM2 and the C-terminal domain; in this approach histidine is introduced in this loop and coordinated using a  $ZnCl_2$  solution. This coordinates the histidine residues and effectively crosslinks the channel into a gain of function conformation (45). The third and final approach involves mutating the residues around the constriction site of the channel to histidine; by doing so, the channel can be opened by lowering the pH of the solution the protein is in, as to protonate the histidine side chain and cause a charge repulsion based gating (46). These approaches have all been tested and shown to produce gain of function channels in electrophysiology experiments. An alternative approach that has not been tested *in vitro*, but suggested *in silico* makes use of the preconception that the membrane thins around the channel once tension is applied (47). Given this

information, a screen of short-chain lipid and detergent mixtures that could mimic a thinning membrane can be made, then the protein can be introduced into these conditions through buffer exchange. Once purified, the protein/detergent/lipid mixture can be used for crystallization experiments where upon crystal formation, an alternate conformation of MscL can be possibly triggered. Collectively, many avenues exist for triggering the final conformation of MscL, leaving a challenging yet captivating goal in the field of MscL structural studies.

```

EcmscS/1-286      1 -----MEDLNVDVDSINGAGSWLVANQALLLSYAVNIVAAL-AIIIVG41
MsMscS_1/1-304  1 -----MDVYNVAFE-----WTDNRHWFIEVPIRITAYIVIVLIRAR36
MsMscS_2/1-316  1 MSG-----ARSGYADAIMDVYNVAFE-----WTDNRHWFIEVPIRITAYIVIVLIRAR48
MsMscS_3/1-464  1 MRSVLEANWFYWALSVAVGLPIGLVLLTELHNTLARHGSYLARPVSLLRNYILPLAALLIL-LVKG65
MsMscS_4/1-326  1 MTI-----SSAATVLAFSVADRW--HDFVHGEIGVWILTKGLRIALLLIG----G45

EcmscS/1-286    42 LIIARMISNAVNRLMISRKI-----DATVADFLSA71
MsMscS_1/1-304  37 YVLHRLIDRATTGRSHQEREEGKPPSRPPLLRRLRERAPAAASS-SQAKRRQQAQTIGSVLKS101
MsMscS_2/1-316  49 YVLHRLIDRATTGRSHQEREEGKPPSRPPLLRRLRERAPAAASS-SQAKRRQQAQTIGSVLKS113
MsMscS_3/1-464  66 ---SEISAEATPVRIVA--TGFGF-----VVIILLLSGLNATLFQGAPEGSWR----KRIPSIIFLD117
MsMscS_4/1-326  46 LLAARFISWAAQRVRRID-----AEYQES---DQLVR-SES AKHRQ----AVASVISW91

EcmscS/1-286    72 LVRYGIIAF-TLIAALGRVGVQTASVIAVLGAAGLAVGLALQGSLSNLAAGVLLVMFRPFRAGEYV136
MsMscS_1/1-304  402 TVSIVLLGW-MVLGVLVSLGVNIAPLIASAGVAGVAIGFGAQLVRDFVTGMFMLEDDQYGVGDTV166
MsMscS_2/1-316  14 TVSIVLLGW-MVLGVLVSLGVNIAPLIASAGVAGVAIGFGAQLVRDFVTGMFMLEDDQYGVGDTV178
MsMscS_3/1-464  18 VARFALIAVGVGMI MAYVWGAVGGLFTALGVTSIVLGLALQNAVQIISGLLLLEEQPFQLGDWL183
MsMscS_4/1-326  92 VSVALLFVI-VLVEVTDVLA VPVAVSLVAPAAVLGAALGFGAQRIVQDLLAGFFIITEKQYGFGLV156

EcmscS/1-286   137 DLG-----GVAGTVLSVQIFSTTMR TADGKIIVI PNGKI IAGNI INF SREPVR RNE-FIIGVAYDS196
MsMscS_1/1-304  467 DLG-----AAVGQVESVGLRITTLRDIDGTLWYVRNGE IARVGNM--SQDYA-VAR-VEVPVAVTT223
MsMscS_2/1-316  79 DLG-----AAVGQVESVGLRITTLRDIDGTLWYVRNGE IARVGNM--SQDYA-VAR-VEVPVAVTT235
MsMscS_3/1-464  84 DTP-----SARGRVVEVNWVRATHIDT-GGGLQIMPNSVLAGASFTNLSRPEAAHLSVTTTTFGVSD243
MsMscS_4/1-326  57 RLTIGASNEAECTVEDVTLRVTKLRSTEGEMYTVPNGQIVKSLNL--SKDWA-RAV-VDIPVSVSV218

EcmscS/1-286   197 DIDQVKQILTNIIQS--EDRILK DREM-----TVRLNELGASSINFVVRVWSNSGD-245
MsMscS_1/1-304  224 DLNRAEEIALQAA-----EEALADPKVSDKTLGE-----PEMLGVQDF S ADHVT LRMTV----KT-274
MsMscS_2/1-316  236 DLNRAEEIALQAA-----EEALADPKVSDKTLGE-----PEMLGVQDF S ADHVT LRMTV----KT-286
MsMscS_3/1-464  244 SPDAVCA LLTRVATQLPQRRAGAAPKAIPLGAGEYKTSIPLRTPADD SAARAVFLR-WLWYAARRA308
MsMscS_4/1-326  219 DLNVVNDV LNEVA-----ERATEDAELSKLVLDK-----PQLMGVESIGVDTVNLRMVA----RT-269

EcmscS/1-286   246 -----LQNVYWDVLERIKR---EFDAAGISFPYPQMDVNFKRVKEDKAA-----286
MsMscS_1/1-304  275 -----RPNAQWSVQRRLRREILRAYDEHEIYAPNA-----304
MsMscS_2/1-316  287 -----RPNAQWSVQRRLRREILRAYDEHEIYAPNA-----316
MsMscS_3/1-464  809 ELHLDGETDDFSTPERLT KAVRQMAPTLRLSHTEQQEVLNHSALVRFGADEI IQEAGEIPTRMSFI374
MsMscS_4/1-326  270 -----LPGKQFEVGRRLRVRVRRALRRAGVVTSDASVAAAGDI IHPAAAAAEVQIAPQEPKK----326

EcmscS/1-286    -----
MsMscS_1/1-304  -----
MsMscS_2/1-316  -----
MsMscS_3/1-464  875 VSGR VGVSVAGD GDAV I PVRTL TEND F LGQTAL TREGALASAHALTETT VLQI SREFLEELVAGNP440
MsMscS_4/1-326  -----

EcmscS/1-286    -----
MsMscS_1/1-304  -----
MsMscS_2/1-316  -----
MsMscS_3/1-464  441 L L L L E L S R I I D D R R S A A R A A L T A D
MsMscS_4/1-326  -----

```

464

Figure 1- Alignment of MscS sequences identified in *M. smegmatis*.

Conserved residues are highlighted in dark purple, residues that are not conserved in every sequence are highlighted in lighter shades of purple.

### 5.3 References

1. Cole, S. T., Brosch, R., Parkhill, J., Garnier, T., Churcher, C., Harris, D., Gordon, S. V., Eiglmeier, K., Gas, S., Barry, C. E., 3rd, Tekaiia, F., Badcock, K., Basham, D., Brown, D., Chillingworth, T., Connor, R., Davies, R., Devlin, K., Feltwell, T., Gentles, S., Hamlin, N., Holroyd, S., Hornsby, T., Jagels, K., Krogh, A., McLean, J., Moule, S., Murphy, L., Oliver, K., Osborne, J., Quail, M. A., Rajandream, M. A., Rogers, J., Rutter, S., Seeger, K., Skelton, J., Squares, R., Squares, S., Sulston, J. E., Taylor, K., Whitehead, S., and Barrell, B. G. (1998) Deciphering the biology of *Mycobacterium tuberculosis* from the complete genome sequence. *Nature* **393**, 537-544
2. Baneyx, F. (1999) Recombinant protein expression in *Escherichia coli*. *Curr Opin Biotechnol* **10**, 411-421
3. Goldstone, R. M., Moreland, N. J., Bashiri, G., Baker, E. N., and Shaun Lott, J. (2008) A new Gateway vector and expression protocol for fast and efficient recombinant protein expression in *Mycobacterium smegmatis*. *Protein Expr Purif* **57**, 81-87
4. Gall, K., and Barker, L. P. (2006) Differential green fluorescent protein expression from mycobacterial promoter constructs in *Escherichia coli* and *Mycobacterium marinum*. *Fems Microbiol Lett* **255**, 301-307
5. Noens, E. E., Williams, C., Anandhakrishnan, M., Poulsen, C., Ehebauer, M. T., and Wilmanns, M. (2011) Improved mycobacterial protein production using a *Mycobacterium smegmatis groEL1DeltaC* expression strain. *BMC Biotechnol* **11**, 27
6. Wang, L., Slayden, R. A., Barry, C. E., 3rd, and Liu, J. (2000) Cell wall structure of a mutant of *Mycobacterium smegmatis* defective in the biosynthesis of mycolic acids. *J Biol Chem* **275**, 7224-7229
7. Bardou, F., Quemard, A., Dupont, M. A., Horn, C., Marchal, G., and Daffe, M. (1996) Effects of isoniazid on ultrastructure of *Mycobacterium aurum* and *Mycobacterium tuberculosis* and on production of secreted proteins. *Antimicrob Agents Chemother* **40**, 2459-2467

8. Bansal-Mutalik, R., and Nikaido, H. (2014) Mycobacterial outer membrane is a lipid bilayer and the inner membrane is unusually rich in diacyl phosphatidylinositol dimannosides. *Proc Natl Acad Sci U S A* **111**, 4958-4963
9. Chang, G., Spencer, R. H., Lee, A. T., Barclay, M. T., and Rees, D. C. (1998) Structure of the MscL homolog from *Mycobacterium tuberculosis*: a gated mechanosensitive ion channel. *Science* **282**, 2220-2226
10. Das, N., Dai, J., Hung, I., Rajagopalan, M. R., Zhou, H. X., and Cross, T. A. (2015) Structure of CrgA, a cell division structural and regulatory protein from *Mycobacterium tuberculosis*, in lipid bilayers. *Proc Natl Acad Sci U S A* **112**, E119-126
11. Faller, M., Niederweis, M., and Schulz, G. E. (2004) The structure of a mycobacterial outer-membrane channel. *Science* **303**, 1189-1192
12. Gu, S., Chen, J., Dobos, K. M., Bradbury, E. M., Belisle, J. T., and Chen, X. (2003) Comprehensive proteomic profiling of the membrane constituents of a *Mycobacterium tuberculosis* strain. *Mol Cell Proteomics* **2**, 1284-1296
13. Trias, J., and Benz, R. (1994) Permeability of the cell wall of *Mycobacterium smegmatis*. *Mol Microbiol* **14**, 283-290
14. Stephan, J., Bender, J., Wolschendorf, F., Hoffmann, C., Roth, E., Mailander, C., Engelhardt, H., and Niederweis, M. (2005) The growth rate of *Mycobacterium smegmatis* depends on sufficient porin-mediated influx of nutrients. *Mol Microbiol* **58**, 714-730
15. Stahl, C., Kubetzko, S., Kaps, I., Seeber, S., Engelhardt, H., and Niederweis, M. (2001) MspA provides the main hydrophilic pathway through the cell wall of *Mycobacterium smegmatis*. *Mol Microbiol* **40**, 451-464
16. Iscla, I., Wray, R., Wei, S., Posner, B., and Blount, P. (2014) Streptomycin potency is dependent on MscL channel expression. *Nat Commun* **5**, 4891
17. Lawson, C. L., Swigon, D., Murakami, K. S., Darst, S. A., Berman, H. M., and Ebright, R. H. (2004) Catabolite activator protein: DNA binding and transcription activation. *Curr Opin Struct Biol* **14**, 10-20

18. Ofer, N., Wishkautzan, M., Meijler, M., Wang, Y., Speer, A., Niederweis, M., and Gur, E. (2012) Ectoine biosynthesis in *Mycobacterium smegmatis*. *Appl Environ Microbiol* **78**, 7483-7486
19. Larsen, P. I., Sydnes, L. K., Landfald, B., and Strøm, A. R. (1987) Osmoregulation in *Escherichia coli* by accumulation of organic osmolytes: betaines, glutamic acid, and trehalose. *Archives of Microbiology* **147**, 1-7
20. Hatzios, S. K., Baer, C. E., Rustad, T. R., Siegrist, M. S., Pang, J. M., Ortega, C., Alber, T., Grundner, C., Sherman, D. R., and Bertozzi, C. R. (2013) Osmosensory signaling in *Mycobacterium tuberculosis* mediated by a eukaryotic-like Ser/Thr protein kinase. *Proc Natl Acad Sci U S A* **110**, E5069-5077
21. Liu, Z., Gandhi, C. S., and Rees, D. C. (2009) Structure of a tetrameric MscL in an expanded intermediate state. *Nature* **461**, 120-124
22. Li, J., Guo, J., Ou, X., Zhang, M., Li, Y., and Liu, Z. (2015) Mechanical coupling of the multiple structural elements of the large-conductance mechanosensitive channel during expansion. *Proc Natl Acad Sci U S A* **112**, 10726-10731
23. Gandhi, C. S., Walton, T. A., and Rees, D. C. (2011) OCAM: a new tool for studying the oligomeric diversity of MscL channels. *Protein Sci* **20**, 313-326
24. Reading, E., Walton, T. A., Liko, I., Marty, M. T., Laganowsky, A., Rees, D. C., and Robinson, C. V. (2015) The effect of detergent, temperature, and lipid on the oligomeric state of MscL constructs: insights from mass spectrometry. *Chem Biol* **22**, 593-603
25. Walton, T. A., Idigo, C. A., Herrera, N., and Rees, D. C. (2015) MscL: channeling membrane tension. *Pflugers Arch* **467**, 15-25
26. Walton, T. A., and Rees, D. C. (2013) Structure and stability of the C-terminal helical bundle of the *E. coli* mechanosensitive channel of large conductance. *Protein Sci* **22**, 1592-1601
27. Cheng, Y., Grigorieff, N., Penczek, P. A., and Walz, T. (2015) A primer to single-particle cryo-electron microscopy. *Cell* **161**, 438-449
28. De Zorzi, R., Mi, W., Liao, M., and Walz, T. (2016) Single-particle electron microscopy in the study of membrane protein structure. *Microscopy (Oxf)* **65**, 81-96

29. Shi, D., Nannenga, B. L., de la Cruz, M. J., Liu, J., Sawtelle, S., Calero, G., Reyes, F. E., Hattne, J., and Gonen, T. (2016) The collection of MicroED data for macromolecular crystallography. *Nat Protoc* **11**, 895-904
30. Ajouz, B., Berrier, C., Garrigues, A., Besnard, M., and Ghazi, A. (1998) Release of thioredoxin via the mechanosensitive channel MscL during osmotic downshock of *Escherichia coli* cells. *J Biol Chem* **273**, 26670-26674
31. Kouwen, T. R., Antelmann, H., van der Ploeg, R., Denham, E. L., Hecker, M., and van Dijl, J. M. (2009) MscL of *Bacillus subtilis* prevents selective release of cytoplasmic proteins in a hypotonic environment. *Proteomics* **9**, 1033-1043
32. Booth, I. R., and Blount, P. (2012) The MscS and MscL families of mechanosensitive channels act as microbial emergency release valves. *J Bacteriol* **194**, 4802-4809
33. Basle, A., Iyer, R., and Delcour, A. H. (2004) Subconductance states in OmpF gating. *Biochim Biophys Acta* **1664**, 100-107
34. Cowan, S. W., Schirmer, T., Rummel, G., Steiert, M., Ghosh, R., Pauptit, R. A., Jansonius, J. N., and Rosenbusch, J. P. (1992) Crystal structures explain functional properties of two *E. coli* porins. *Nature* **358**, 727-733
35. Hille, B. (1968) Pharmacological modifications of the sodium channels of frog nerve. *J Gen Physiol* **51**, 199-219
36. Cruickshank, C. C., Minchin, R. F., Le Dain, A. C., and Martinac, B. (1997) Estimation of the pore size of the large-conductance mechanosensitive ion channel of *Escherichia coli*. *Biophys J* **73**, 1925-1931
37. Sukharev, S. I., Sigurdson, W. J., Kung, C., and Sachs, F. (1999) Energetic and spatial parameters for gating of the bacterial large conductance mechanosensitive channel, MscL. *J Gen Physiol* **113**, 525-540
38. van den Bogaart, G., Krasnikov, V., and Poolman, B. (2007) Dual-color fluorescence-burst analysis to probe protein efflux through the mechanosensitive channel MscL. *Biophys J* **92**, 1233-1240
39. Mika, J. T., Birkner, J. P., Poolman, B., and Kocer, A. (2013) On the role of individual subunits in MscL gating: "all for one, one for all?". *Faseb J* **27**, 882-892

40. Sukharev, S., Durell, S. R., and Guy, H. R. (2001) Structural models of the MscL gating mechanism. *Biophys J* **81**, 917-936
41. Perozo, E., Cortes, D. M., Sompornpisut, P., Kloda, A., and Martinac, B. (2002) Open channel structure of MscL and the gating mechanism of mechanosensitive channels. *Nature* **418**, 942-948
42. Wang, Y., Liu, Y., Deberg, H. A., Nomura, T., Hoffman, M. T., Rohde, P. R., Schulten, K., Martinac, B., and Selvin, P. R. (2014) Single molecule FRET reveals pore size and opening mechanism of a mechano-sensitive ion channel. *Elife* **3**, e01834
43. Ornatska, M., Jones, S. E., Naik, R. R., Stone, M. O., and Tsukruk, V. V. (2003) Biomolecular stress-sensitive gauges: surface-mediated immobilization of mechanosensitive membrane protein. *J Am Chem Soc* **125**, 12722-12723
44. Iscla, I., Eaton, C., Parker, J., Wray, R., Kovács, Z., and Blount, P. (2013) Improving the design of a MscL-based triggered nanovalve. *Biosensors* **3**, 171-184
45. Yang, L. M., Wray, R., Parker, J., Wilson, D., Duran, R. S., and Blount, P. (2012) Three routes to modulate the pore size of the MscL channel/nanovalve. *ACS Nano* **6**, 1134-1141
46. Iscla, I., Levin, G., Wray, R., Reynolds, R., and Blount, P. (2004) Defining the physical gate of a mechanosensitive channel, MscL, by engineering metal-binding sites. *Biophys J* **87**, 3172-3180
47. Vanegas, J. M., and Arroyo, M. (2014) Force transduction and lipid binding in MscL: a continuum-molecular approach. *PLoS One* **9**, e113947